Available online at www.sciencedirect.com
ScienceDirect
Physics Reports 457 (2008) 217–283
PHYSICS REPORTS
www.elsevier.com/locate/physrep

Helioseismology and solar abundances

Sarbani Basu[a,*], H.M. Antia[b]

[a] *Department of Astronomy, Yale University, P.O. Box 208121, New Haven, CT 06520-8101, USA*
[b] *Tata Institute of Fundamental Research, Homi Bhabha Road, Mumbai 400 005, India*

Accepted 13 December 2007
Available online 23 December 2007

editor: M.P. Kamionkowski

Abstract

Helioseismology has allowed us to study the structure of the Sun in unprecedented detail. One of the triumphs of the theory of stellar evolution was that helioseismic studies had shown that the structure of solar models is very similar to that of the Sun. However, this agreement has been spoiled by recent revisions of the solar heavy-element abundances. Heavy-element abundances determine the opacity of the stellar material and hence, are an important input to stellar model calculations. The models with the new, low abundances do not satisfy helioseismic constraints. We review here how heavy-element abundances affect solar models, how these models are tested with helioseismology, and the impact of the new abundances on standard solar models. We also discuss the attempts made to improve the agreement of the low-abundance models with the Sun and discuss how helioseismology is being used to determine the solar heavy-element abundances. A review of current literature shows that attempts to improve agreement between solar models with low heavy-element abundances and seismic inference have been unsuccessful so far. The low-metallicity models that have the least disagreement with seismic data require changing all input physics to stellar models beyond their acceptable ranges. Seismic determinations of the solar heavy-element abundances yield results that are consistent with the older, higher values of the solar abundance, and hence, no major changes to the inputs to solar models are required to make higher-metallicity solar models consistent with the helioseismic data.
© 2007 Elsevier B.V. All rights reserved.

PACS: 96.60.Jw; 96.60.Ly; 96.60.Fs

Keywords: Solar interior; Helioseismology; Abundances

Contents

* Corresponding author.
E-mail address: sarbani.basu@yale.edu (S. Basu).

0370-1573/$ - see front matter © 2007 Elsevier B.V. All rights reserved.
doi:10.1016/j.physrep.2007.12.002

1. Introduction

Arthur Eddington began his book "The Internal Constitution of the Stars" saying that *"At first sight it would seem that the deep interior of the sun and stars is less accessible to scientific investigation than any other region of the universe. Our telescopes may probe farther and farther into the depths of space; but how can we ever obtain certain knowledge of that which is hidden behind substantial barriers? What appliance can pierce through the outer layers of a star and test the conditions within?"* (Eddington, 1926). Eddington went on to say that perhaps we should not aspire to directly "probe" the interiors of the Sun and stars, but instead use our knowledge of basic physics to determine what the structure of a star should be. This is still the predominant approach in studying stars today. However, we now also have the "appliance" that can pierce through the outer layers of the Sun and give us detailed knowledge of what the internal structure of the Sun is. This "appliance" is helioseismology, the study of the interior of the Sun using solar oscillations. While solar neutrinos can probe the solar core, helioseismology provides us a much more detailed and nuanced picture of the entire Sun.

The first definite observations of solar oscillations were made by Leighton et al. (1962), who detected roughly periodic oscillations in Doppler velocity with periods of about 5 min. Evans and Michard (1962) confirmed the initial observations. The early observations were of limited duration, and the oscillations were generally interpreted as phenomena in the solar atmosphere. Later observations that resulted in power spectra as a function of wave-number (e.g., Frazier (1968)) indicated that the oscillations may not be mere surface phenomena. The first major theoretical advance in the field came when Ulrich (1970) and Leibacher and Stein (1971) proposed that the oscillations were

standing acoustic waves in the Sun, and predicted that power should be concentrated along ridges in a wave-number v/s frequency diagram. Wolff (1972) and Ando and Osaki (1975) strengthened the hypothesis of standing waves by showing that oscillations in the observed frequency and wave-number range may be linearly unstable and hence, can be excited. Acceptance of this interpretation of the observations as normal modes of solar oscillations was the result of the observations of Deubner (1975), which first showed ridges in the wave-number v/s frequency diagram. Rhodes et al. (1977) reported similar observations. These observations did not, however, resolve the individual modes of solar oscillations, despite that, these data were used to draw initial inferences about solar structure and dynamics. Claverie et al. (1979) using Doppler-velocity observations, integrated over the solar disk were able to resolve the individual modes of oscillations corresponding to the largest horizontal wavelength. They found a series of almost equidistant peaks in the power spectrum just as was expected from theoretical models. However, helioseismology as we know it today did not begin till Duvall and Harvey (1983) determined frequencies of a reasonably large number of solar oscillation modes covering a wide range of horizontal wavelengths. Since then many sets of solar-oscillation frequencies have been published. A lot of early helioseismic analysis was based on frequencies determined by Libbrecht et al. (1990) from observations made at the Big Bear Solar Observatory in the period 1986–1990. Accurate determination of solar oscillations frequencies requires long, uninterrupted observations of the Sun, that are possible only with a network of ground based instruments or from an instrument in space. The Birmingham Solar Oscillation Network (BiSON; Elsworth et al., 1991; Chaplin et al., 2007a) was one of the first such networks. BiSON, however, observes the Sun in integrated light and hence is capable of observing only very large horizontal-wavelength modes. The Global Oscillation Network Group (GONG), a ground based network of telescopes, and the Michelson Doppler Imager (MDI) on board the Solar and Heliospheric Observatory (SOHO) have now collected data for more than a decade and have given us an unprecedented opportunity to determine the structure and dynamics of the Sun in great detail. Data from these instruments have also allowed us to probe whether or not the Sun changes on the time-scale of a solar activity cycle.

Helioseismology has proved to be an extremely important tool in studying the Sun. Thanks to helioseismology, we know the most important features of the structure of the Sun extremely well. We know what the sound-speed and density profiles are (see e.g., Christensen-Dalsgaard et al. (1985, 1989), Dziembowski et al. (1990), Däppen et al. (1991), Antia and Basu (1994a), Gough et al. (1996), Kosovichev et al. (1997) and Basu et al. (1997, 2000) etc.), which in turn means that we can determine the radial distribution of pressure. We can also determine the profile of the adiabatic index (e.g., Antia and Basu (1994a), Elliott (1996) and Elliott and Kosovichev (1998)). Inversions of solar-oscillation frequencies have allowed us to determine a number of other fundamental facts about the Sun. We know, for instance, that the position of base of the solar convection zone can be determined precisely (Christensen-Dalsgaard et al., 1991; Basu and Antia, 1997; Basu, 1998). Similarly, we can determine the helium abundance in the solar convection zone (Däppen and Gough, 1986; Christensen-Dalsgaard and Pérez Hernández, 1991; Kosovichev et al., 1992; Antia and Basu, 1994b). In addition to these structural parameters, helioseismology has also revealed what the rotational profile of the Sun is like. It had been known for a long time that the rotation rate at the solar surface depends strongly on latitude, with rotation being fastest at the equator and slowest at the poles. Only with helioseismic data however, we have been able to probe the rotation of the Sun as a function of depth (Duvall et al. (1986); Thompson et al. (1996); Schou et al. (1998b) etc.).

The ability of helioseismology to probe the solar interior in such detail has allowed us to use the Sun as a laboratory to test different inputs that are used to construct solar models. For instance, helioseismic inversions have allowed us to study the equation of state of stellar material (Lubow et al., 1980; Ulrich, 1982; Christensen-Dalsgaard and Däppen, 1992; Basu and Christensen-Dalsgaard, 1997; Elliott and Kosovichev, 1998; Basu et al., 1999) and to test opacity calculations (Korzennik and Ulrich, 1989; Basu and Antia, 1997; Tripathy and Christensen-Dalsgaard, 1998). Assuming that opacities, equation of state, and nuclear energy generation rates are known, one can also infer the temperature and hydrogen-abundance profiles of the Sun (Gough and Kosovichev (1988), Shibahashi (1993), Antia and Chitre (1995, 1998), Shibahashi and Takata (1996) and Kosovichev (1996) etc.). These studies also provide a test for nuclear reaction rates (e.g., Antia and Chitre (1998) and Brun et al. (2002)) and the heavy-element abundances in the convection zone (e.g., Basu and Antia (1997) and Basu (1998)) and the core (e.g., Antia and Chitre (2002)).

One of the major inputs into solar models is the abundance of heavy elements. The heavy-element abundance, Z, affects solar structure by affecting radiative opacities. The abundance of some specific elements, such as oxygen, carbon, and nitrogen can also affect the energy generation rates through the CNO cycle. The effect of Z on opacities changes the boundary between the radiative and convective zones, as well as the structure of radiative region; the

effect of Z on energy generation rates can change the structure of the core. The heavy-element abundance of the Sun is believed to be known to a much better accuracy than that of other stars, however, there is still a lot of uncertainty and that results in uncertainties in solar models. It is not only the total Z that affects structure, the relative abundance of different elements has an effect as well. Elements that affect core opacity are, in the order of importance, iron, sulfur, silicon and oxygen. The elements that contribute to opacity in the region near the base of the convection zone and thereby affect the position of the base of the solar convection zone are, again in the order of importance, oxygen, iron and neon. Although, the main effect of heavy-element abundances is through opacity, these abundances also affect the equation of state. In particular, the adiabatic index Γ_1 is affected in regions where these elements undergo ionization. This effect is generally small, but in the convection zone where the stratification is adiabatic and hence the structure is determined by equation of state rather than opacity, this effect can be significant.

The importance of the solar heavy-element abundance does not merely lie in being able to model the Sun correctly, it is often used as the standard against which heavy-element abundances of other stars are measured. Thus the predicted structure of those stars too become uncertain if the solar heavy-element abundance is uncertain. Given that for most stars other than the Sun, we usually only know the position on the HR diagram, an error in the solar abundance could lead to errors in the predicted mass and age of the stars. Stellar evolution calculations are used throughout astronomy to classify, date, and interpret the spectra of individual stars and of galaxies, and hence errors in metallicity affect age determinations, and other derived parameters of stars and star clusters. The exact value of the solar heavy-element abundance determines the amount of heavy elements that had been present in the solar neighborhood when the Sun was formed. This, therefore, determines the chemical evolution history of galaxies.

Solar models in the 1990's were generally constructed with the solar heavy-element mixture of Grevesse and Noels (1993). The ratio of the mass fraction of heavy elements to hydrogen in the Sun was determined to be $Z/X = 0.0245$. Grevesse and Sauval (1998, henceforth GS98) revised the abundances of oxygen, nitrogen, carbon and some other elements, and that resulted in $Z/X = 0.023$. In a series of papers Allende Prieto et al. (2001, 2002) and Asplund et al. (2004, 2005a) have revised the spectroscopic determinations of the solar photospheric composition. In particular, their results indicate that carbon, nitrogen and oxygen abundances are lower by about 35%–45% than those listed by GS98. The revision of the oxygen abundance leads to a comparable change in the abundances of neon and argon since these abundances are generally measured through the abundances ratio for Ne/O and Ar/O. Additionally, Asplund (2000) also determined a somewhat lower value (by about 10%) for the photospheric abundance of silicon compared with the GS98 value. As a result, all the elements for which abundances are obtained from meteoritic measurements have seen their abundances reduced by a similar amount. These measurements have been summarized by Asplund et al. (2005b, henceforth AGS05). The net result of these changes is that Z/X for the Sun is reduced to 0.0165 (or $Z = 0.0122$), about 28% lower than the previous value of GS98 and almost 40% lower than the old value of Anders and Grevesse (1989). The change in solar abundances implies large changes in solar structure as well as changes in quantities derived using solar and stellar models, and therefore, warrants a detailed discussion of the consequence of the changes, and how one can test the new abundances. In this paper we review the effects of solar abundances on solar models and how the models with lower abundances stand up against helioseismic tests.

The review is written in a pedagogical style with detailed explanations of how the analysis is done. However, the review is organized in such a manner that not all readers need to read all sections unless they want to. We start with a description of how solar models are constructed (Section 2), this section also describes the sources of uncertainties in solar models (Section 2.4). In Section 3 we describe how helioseismology is used to test solar models as well as how helioseismology can be used to determine solar parameters like the convection-zone helium abundance, the depth of the convection zone and how input physics, like the equation of state, can be tested. In Section 4 we describe what helioseismology has taught us about the Sun and inputs to solar model thus far. Thus readers who are more interested in helioseismic results rather than techniques can go directly to this section. In Section 5 we give a short review of how solar abundances are determined and the results obtained so far. The consequences of the new abundances are described in Section 6. This section also includes a brief summary of the changes in the solar neutrino outputs (Section 6.3) and some consequences of the new abundances on models of stars other than the Sun (Section 6.5), though the latter discussion is by no means complete and comprehensive. Readers who are only interested in how the lower solar abundances affect the models would perhaps wish to go straight to this section. The next section, Section 7, is devoted to reviewing the numerous attempts that have been made to reconcile the low-metallicity solar models with the Sun by changing different physical inputs. In Section 8 we describe attempts that have been made to determine solar metallicity using helioseismic techniques. In Section 9 we discuss some possible reasons for the discrepancy

Table 1
Global parameters of the Sun

Quantity	Estimate	Reference
Mass ($M_\odot$)[a]	$1.98892(1 \pm 0.00013) \times 10^{33}$ g	Cohen and Taylor (1987)
Radius ($R_\odot$)[b]	$6.9599(1 \pm 0.0001) \times 10^{10}$ cm	Allen (1973)
Luminosity ($L_\odot$)	$3.8418(1 \pm 0.004) \times 10^{33}$ ergs s^{-1}	Fröhlich and Lean (1998), Bahcall et al. (1995)
Age	$4.57(1 \pm 0.0044) \times 10^9$ yr	Bahcall et al. (1995)

[a] Derived from the values of G and $GM_\odot$.
[b] See Schou et al. (1997), Antia (1998) and Brown and Christensen-Dalsgaard (1998) for a more recent discussion about the exact value of the solar radius.

between helioseismically determined abundances and the new spectroscopic abundances and we present some final thoughts in Section 10.

2. Making solar models

The Sun is essentially similar to other stars. The internal structure of the Sun and other stars obey the same principles, and hence we use the theory of stellar structure and evolution to make models of the Sun. However, since we have more observational constraints on the Sun, these constraints have to be met before we can call a model a solar model. Otherwise, the result is simply a model of a star that has the same mass as the Sun. As in the case of other stars, we know the effective temperature and luminosity of the Sun, but unlike most stars, we also have independent estimates of the age and radius of the Sun. Thus to be called a solar model, a $1M_\odot$ model must have the correct radius and luminosity at its current age. This makes modelling the Sun somewhat different from modelling other stars. The commonly adopted values of solar mass, radius, luminosity and age of the Sun are listed in Table 1.

There are many excellent textbooks on stellar structure and evolution. The equations governing stellar structure and evolution have been discussed in detail by Kippenhahn and Weigert (1990), Huang and Wu (1998), Hansen et al. (2004) and Weiss et al. (2004), etc. We, therefore, only give a quick overview.

2.1. Equations of stellar structure and evolution

The most common assumption involved in making solar and stellar models is that stars are not merely spherical, but that they are also spherically symmetric, i.e., their internal structure is only a function of radius and not of latitude or longitude. This assumption implies that rotation and magnetic fields do not unduly change stellar structure. This is a good approximation for most stars and can be applied to the Sun too. The measured oblateness of the Sun is about a part in 10^5 (Kuhn et al., 1998). The latitudinal dependence of solar structure is also small (Antia et al., 2001). This assumption allows us to express the properties of a star with a set of one-dimensional (1D) equations, rather than a full set of three-dimensional (3D) equations. These equations can be derived from very basic physical principles.

The first equation is a result of conservation of mass and can be written as

$$\frac{\mathrm{d}m}{\mathrm{d}r} = 4\pi r^2 \rho, \tag{1}$$

where ρ is the density, and m is the mass enclosed in radius r. Since stars expand or contract over their lifetime, it is generally easier to use equations with mass m as the independent variable since for most stars the total mass does not change much during their lifetimes. The Sun for instance, loses about 10^{-14} of its mass per year. Thus in its expected main-sequence lifetime of about 10 Gyr, the Sun will lose only about 0.01% of its mass. The radius on the other hand is expected to change significantly. Thus Eq. (1) is usually re-written as

$$\frac{\mathrm{d}r}{\mathrm{d}m} = \frac{1}{4\pi r^2 \rho}. \tag{2}$$

The next equation is a result of conservation of momentum. In the stellar context it implies that any acceleration of a mass shell is caused by a mismatch between outwardly acting pressure and inwardly acting gravity. However, pressure and gravity balance each other throughout most of a star's life, and under these conditions we can write the so-called equation of *hydrostatic equilibrium*, i.e.,

$$\frac{\mathrm{d}P}{\mathrm{d}m} = -\frac{Gm}{4\pi r^4}. \tag{3}$$

The third equation is conservation of energy. Since stars are not just passive spheres of gas, but produce energy through nuclear reactions in the core, the energy equation needs to be considered. In a stationary state, energy l flows through a shell of radius r per unit time as a result of nuclear reactions in the interior. If ϵ be the energy released per unit mass per second by nuclear reactions, and ϵ_ν the energy lost by the star because of neutrinos streaming out of the star without depositing their energy, then,

$$\frac{\mathrm{d}l}{\mathrm{d}m} = \epsilon - \epsilon_\nu. \tag{4}$$

Since stars expand (or contract) at certain phases of their lives, the equation needs to be re-written to include the energy used (or released) due to expansion (or contraction). Thus:

$$\frac{\mathrm{d}l}{\mathrm{d}m} = \epsilon - \epsilon_\nu - C_P\frac{\mathrm{d}T}{\mathrm{d}t} + \frac{\delta}{\rho}\frac{\mathrm{d}P}{\mathrm{d}t}, \tag{5}$$

where C_P is the specific heat at constant pressure, t is time, and δ, given by the equation of state, is defined as

$$\delta = -\left(\frac{\partial \ln \rho}{\partial \ln T}\right)_{P,X_i}, \tag{6}$$

where X_i denotes composition. The last two terms on the right-hand side of Eq. (5) are often referred to together as ϵ_g, g for gravity, because they denote the gravitational release of energy. The next is the equation of energy transport which determines the temperature at any point. In general terms, and with the help of Eq. (3), this equation can be written quite trivially as

$$\frac{\mathrm{d}T}{\mathrm{d}m} = -\frac{GmT}{4\pi r^4 P}\nabla, \tag{7}$$

where ∇ is the dimensionless "temperature gradient" $\mathrm{d}\ln T/\mathrm{d}\ln P$. The difficulty lies in determining what ∇ is. In the radiative zones, under the approximation of diffusive radiative transfer, ∇ is given by

$$\nabla = \nabla_{\mathrm{rad}} = \frac{3}{64\pi\sigma G}\frac{\kappa l P}{mT^4}, \tag{8}$$

where, σ is the Stefan–Boltzmann constant and κ is the opacity.

The situation is more complicated if energy is transported by convection. Deep inside the star, ∇ is usually the adiabatic temperature gradient $\nabla_{\mathrm{ad}} \equiv (\partial \ln T/\partial \ln P)_s$ (s being the specific entropy), which is determined by the equation of state. In the outer layers, one has to use some approximate formalism, since there is no "theory" of stellar convection as such. Convection can be described by solving the Navier–Stokes equations. However the mismatch between time-scales involved with convective transport of energy (minutes to hours to days) and time-scales of stellar evolution (millions to billions of years) makes solving the Navier–Stokes equations along with the equations of stellar evolution computationally impossible today. As a result, several approximations are used to describe convection in stellar models. One of the most common formulations used in the calculation of convective flux in stellar models is the so-called "mixing length theory" (MLT). The mixing length theory was first proposed by Prandtl (1925). His model of convection was analogous to heat transfer by particles; the transporting particles are the macroscopic eddies and their mean free path is the "mixing length". This was applied to stars by Biermann (1951), Vitense (1953), and Böhm-Vitense (1958). Different mixing length formalisms have slightly different assumptions about what the mixing length is. The main assumption in the usual mixing length formalism is that the size of the convective eddies at any radius is the mixing length l_m, where $l_m = \alpha H_P$, and α, a constant, is the so-called "mixing length parameter", and

H_P is the pressure-scale height given by $-\mathrm{d}r/\mathrm{d}\ln P$. Details of how under these assumptions ∇ is calculated can be found in any standard textbook, such as Kippenhahn and Weigert (1990). There is no *a priori* way to determine α, and it is one of the free parameters in stellar models. A different prescription for calculating convective flux based on a treatment of turbulence was given by Canuto and Mazzitelli (1991). These are the so-called "local" prescriptions, as the convective flux at any depth is determined by the local values of T, P, ρ, etc. There have been attempts to formulate nonlocal treatments for calculating convective flux (e.g., Xiong and Chen (1992) and Balmforth (1992)), but these treatments introduce free parameters to quantify the nonlocal effects and there are no standard ways of determining those parameters.

Whether energy is transported by radiation or by convection depends on the value of ∇_{rad}. For any given material there is a maximum value of ∇ above which the material is convectively unstable. This maximum is ∇_{ad}. If ∇_{rad} obtained from Eq. (8) exceeds ∇_{ad}, convection sets in. This is usually referred to as the "Schwarzschild Criterion". Regions where energy is transported by radiation are usually referred to as radiative zones, and regions where a part of the energy is transported by convection are referred to as convection zones.

The last important equation concerns the change of chemical composition with time. There are three main reasons for the change in chemical composition at any point in the star. These are: (1) nuclear reactions; (2) the changing boundaries of convection zones; and (3) Diffusion and gravitational settling (usually simply referred to as diffusion) of helium and heavy elements.

If X_i is the mass fraction of any isotope i, then the change in X_i with time because of nuclear reactions can be written as

$$\frac{\partial X_i}{\partial t} = \frac{m_i}{\rho}\left[\sum_j r_{ji} - \sum_k r_{ik}\right], \tag{9}$$

where m_i is the mass of the nucleus of each isotope i, r_{ji} is the rate at which isotope i is formed from isotope j, and r_{ik} is the rate at which isotope i is lost because it turns into a different isotope k. The rates r_{ik} are inputs to models.

Convection zones are chemically homogeneous since eddies of matter move carrying their composition with them and when they break-up, the material gets mixed with the surrounding. They become chemically homogeneous over very short time-scales compared to the time-scale of a star's evolution. If a convection zone exists in the region between two spherical shells of masses m_1 and m_2, the average abundance of any species i in the convection zone is:

$$\bar{X}_i = \frac{1}{m_2 - m_1}\int_{m_1}^{m_2} X_i \,\mathrm{d}m. \tag{10}$$

Thus the rate at which $\bar{X}_i$ changes will depend on nuclear reactions in the convection zone, as well as the rate at which the mass limits m_1 and m_2 change. One can therefore write:

$$\begin{aligned}\frac{\partial \bar{X}_i}{\partial t} &= \frac{\partial}{\partial t}\left(\frac{1}{m_2 - m_1}\int_{m_1}^{m_2} X_i \,\mathrm{d}m\right)\\ &= \frac{1}{m_2 - m_1}\left[\int_{m_1}^{m_2}\frac{\partial X_i}{\partial t}\,\mathrm{d}m + \frac{\partial m_2}{\partial t}(X_{i,2} - \bar{X}_i) - \frac{\partial m_1}{\partial t}(X_{i,1} - \bar{X}_i)\right],\end{aligned} \tag{11}$$

where $X_{i,1}$ and $X_{i,2}$ is the mass fraction of element i at m_1 and m_2 respectively.

The gravitational settling of helium and heavy elements can be described by the process of diffusion and the change in abundance can be found with the help of the diffusion equation:

$$\frac{\partial X_i}{\partial t} = D\nabla^2 X_i, \tag{12}$$

where D is the diffusion coefficient, and ∇^2 is the Laplacian operator. The diffusion coefficient hides the complexity of the process and includes, in addition to gravitational settling, diffusion due to composition and temperature gradients. All three processes are generally simply called "diffusion". The coefficient D depends on the isotope under consideration. Typically, D is an input to stellar model calculations and is not calculated from first principles in the stellar evolution code. Among the more commonly used prescriptions for calculating diffusion coefficients are those of Thoul et al. (1994) and Proffitt and Michaud (1991).

Eqs. (2), (3), (5) and (7) together with the equations relating to change in abundances, form the full set of equations that govern stellar structure and evolution. In the most general case, Eqs. (2), (3), (5) and (7) are solved for a given X_i at a given time t. Time is then advanced, Eqs. (9), (11) and (12) are solved to give new X_i, and Eqs. (2), (3), (5) and (7) are solved again. Thus we consider two independent variables, mass m and time t, and we look for solutions in the interval $0 \leq m \leq M$ (stellar structure) and $t \geq t_0$ (stellar evolution).

Four boundary conditions are required to solve the stellar structure equations. Two (on radius and luminosity) can be applied quite trivially at the center. The remaining conditions (on temperature and pressure) need to be applied at the surface. The boundary conditions at the surface are much more complex than the central boundary conditions and are usually determined with the aid of simple stellar-atmosphere models. It is very common to define the surface using the Eddington approximation. The initial conditions needed to start evolving a star depend on where we start the evolution. If the evolution begins at the pre-main-sequence phase, i.e., while the star is still collapsing, the initial structure is quite simple. Temperatures are low enough to make the star fully convective and hence chemically homogeneous. If evolution is begun at the ZAMS, i.e., the Zero Age Main Sequence, which is the point at which hydrogen fusion begins, a ZAMS model must be used.

2.2. Input microphysics

Eqs. (2), (3), (5) and (7) and the equation for abundance changes are simple, but hide their complexity in the form of the external inputs (usually referred to as "microphysics") needed to solve the equations. We discuss these below:

2.2.1. The equation of state

There are five equations in six unknowns, r, P, l, T, X_i, and ρ. None of the equations tells us how density, ρ, changes with time or mass. Thus we need a relation connecting density to the other quantities. This is given by the equation of state which specifies the relation between density, pressure, temperature and composition. Although the ideal gas equation of state is good enough for making simple models, it does not apply in all regions of stars. In particular, the ideal-gas law does not include effects of ionization, radiation pressure, pressure ionization, degeneracy, etc. Modern equations of state are usually given in tabular form as functions of T, P (or ρ) and composition, and interpolations are done to obtain the thermodynamic quantities needed to solve the equations. Among the popular equations of state used to construct solar models are the OPAL equation of state (Rogers et al., 1996; Rogers and Nayfonov, 2002), the so-called MHD (i.e., Mihalas, Hummer and Däppen) equation of state (Däppen et al., 1987, 1988a; Hummer and Mihalas, 1988; Mihalas et al., 1988) and the CEFF equation of state (Guenther et al., 1992; Christensen-Dalsgaard and Däppen, 1992). CEFF stands for Coulomb corrected Eggleton, Faulker and Flannery equation of state, and is basically the equation of state described by Eggleton et al. (1973), along with the correction for Coulomb screening.

2.2.2. Opacity

In order to calculate $\nabla_{\rm rad}$ (Eq. (8)), we need to know the opacity. The opacity, κ, is a measure of how opaque a material is to photons. Like the modern equations of state, Rosseland mean opacities are given in tabular form as a function of density, temperature and composition. Among the tables used to model the Sun are the OPAL tables (Iglesias and Rogers, 1996), and the OP tables (Badnell et al., 2005; Mendoza et al., 2007). The OPAL opacity tables include contributions from 19 heavy elements whose relative abundances (by numbers) with respect to hydrogen are larger than about 10^{-7}. The OP opacity calculations include only 15 of these heavy elements, as P, Cl, K and Ti are not included. These tables do not properly include all contributions from molecules, and hence these tables are usually supplemented with more accurate low-temperature opacity tables. For solar models, opacity tables by Kurucz (1991) or Ferguson et al. (2005) are often used at low temperatures.

2.2.3. Nuclear reaction rates

Nuclear reaction rates are required to compute energy generation, neutrino fluxes and composition changes. Two major sources of reaction rates for solar model construction are the compilations of Adelberger et al. (1998) and Angulo et al. (1999). The rates of most relevant nuclear reactions are obtained by extrapolation from laboratory measurements, but in some cases the reaction rates are based on theoretical calculations. These reaction rates need to be corrected for electron screening in the solar plasma. Solar models generally use the weak (Salpeter, 1954) or intermediate (Mitler, 1977) screening approximations to treat electron screening.

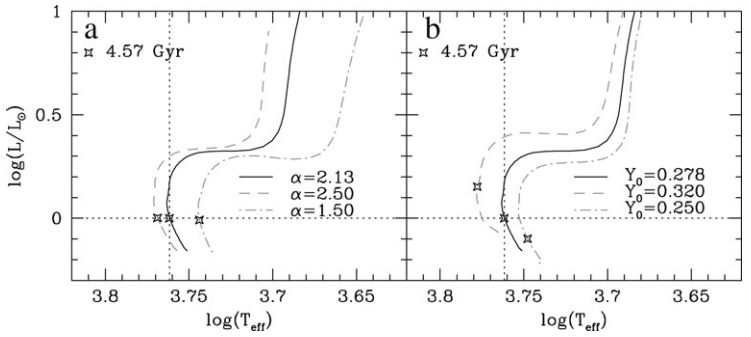

Fig. 1. Panel (a): The effect of the mixing length parameter on the evolution of a $1M_\odot$ star. All models have $Y_0 = 0.278$. Panel (b): The effect of the initial helium abundance Y_0 on the evolution of a $1M_\odot$ star. All models have $\alpha = 2.13$. In both panels the intersection of the dotted lines mark the position of the Sun. The star on each curve marks 4.57 Gyr, the current age of the Sun.

2.3. Constructing standard solar models

The mass of a star is the most fundamental quantity needed to model a star. Once the mass is known, one can, in principle, begin making models of the star and determine how it will evolve. In reality, several other quantities are required. These include Z_0, the initial heavy-element abundance of the star, as well as the initial helium abundance Y_0. Both these quantities affect evolution since they affect the equation of state and opacities. Also required is an estimate of the mixing length parameter α. Once these quantities are known, or chosen by some means, the model is evolved by solving the equations. For most stars, the models are evolved till they reach a given temperature and luminosity. The age of the star is assumed to be the age of the model, and the radius of the star is assumed to be the radius of the model.

The Sun is modeled in a slightly different manner since the age, luminosity and radius are known independently. Thus to be called a solar model, a $1M_\odot$ model must have a luminosity of $1L_\odot$ and a radius of $1R_\odot$ at the age of 4.57 Gyr. The way we ensure that we get a solar model is to vary the mixing length parameter α and the initial helium abundance Y_0 till we get a model with the required characteristics. Mathematically speaking, we have two unknown parameters (α and Y_0) and two constraints (radius and luminosity) at 4.57 Gyr, and hence this is a well-defined problem. However, since the equations are non-linear, we need an iterative method to determine α and Y_0. The value of α obtained in this manner for the Sun is often used to model other stars. In addition to α and Y_0, very often initial Z is adjusted to get the observed Z/X in the solar envelope. The solar model so obtained does not have any free parameters, since the two unknowns, α and Y_0, are determined to match solar constraints.

Fig. 1(a) shows a series of evolutionary tracks for a $1M_\odot$ model constructed using different values of α. All models have the same Y_0 (0.278). All models have been constructed with YREC, the Yale Rotating Evolutionary Code in its non-rotating configuration (Guenther et al., 1992). They were constructed using the OPAL equation of state (Rogers and Nayfonov, 2002) and OPAL opacities (Iglesias and Rogers, 1996). The models were constructed to have $Z/X = 0.023$ (i.e., the GS98 value) at the age of the current Sun. As can be seen from the figure, only one of the models (with $\alpha = 2.13$) satisfies solar constraints at 4.57 Gyr. Fig. 1(b) shows models with different Y_0 but the same α (2.13). Again, only one model (with $Y_0 = 0.278$) satisfies solar constraints, and thus is the only solar model of the three models shown.

The concept of standard solar models (SSM) is very important in solar physics. Standard solar models are models where only standard input physics such as equations of state, opacity, nuclear reaction rates, diffusion coefficients etc., are used. The parameters α and Y_0 (and sometime Z_0) are adjusted to match the current solar radius and luminosity (and surface Z/X). No other input is adjusted to get a better agreement with the Sun. Thus a standard solar model does not have any free parameters. By comparing standard solar models constructed with different input physics with the Sun we can put constraints on the input physics. One can use helioseismology to test whether or not the structure of the model agrees with that of the Sun. The model in Fig. 1 that satisfies current solar constraints on luminosity, radius and age is a standard solar model.

A solar model turns out to be quite simple. Like all stars of similar (and lower) masses, it has an outer convection zone and an inner radiative zone. In the case of the Sun, the convection zone occupies the outer 30% by radius. The outer convection zone is a result of large opacities caused by relatively low temperatures. The temperature

gradient required to transport energy by radiation in this region exceeds the adiabatic temperature gradient resulting in a convectively unstable layer. Convective eddies ensure that the convection zone is chemically homogeneous. In models that incorporate the diffusion and gravitational settling of helium and heavy elements, the abundances of these elements build up below the convection-zone base.

2.4. Sources of uncertainty in standard solar models

Standard solar models constructed by different groups are usually not identical, and are only as good as the input physics. The models depend on nuclear reaction rates, radiative opacities, equation of state, diffusion coefficients, surface boundary conditions. Uncertainties in any of these inputs result in uncertainties in solar models. Even the numerical scheme used to construct a model can introduce some uncertainties. There have been many investigations of the effect of uncertainties in inputs on standard solar models.

Boothroyd and Sackmann (2003) did a systematic investigation on the effect of some of the uncertainties in input physics on standard solar models. They also investigated the effect of the number of mass zones and time steps used to calculate the models. They found that models with 2000 spatial zones, about what is usually used to calculate solar models, did only marginally worse than a model with 10,000 zones. Their coarse-zoned models agreed with the adopted solar radius to a part in 10^5 and with Z/X to a part in 10^4. Their fine-zoned models were better than a part in 10^5 in radius and a few parts in 10^5 in Z/X. They found that the rms relative difference in sound speed and density of the coarse-zoned models relative to the fine-zoned models was 0.0001 and 0.0008 respectively, but that the difference in the number of zones had no effect on the adiabatic index Γ_1.

Bahcall et al. (2001) tested the effects of 2σ changes in $L_\odot$ and found negligible effects on most quantities, though there were minor effects on neutrino fluxes. Boothroyd and Sackmann (2003) found that a shift of 0.8% in $L_\odot$ produces a fractional change in the sound speed of less than three parts in 10^4 that drops to one part in 10^4 for $r > 0.3R_\odot$. Uncertainties in solar radius have a much larger effect. Basu (1998) showed that using a solar radius different from the standard value of $R_\odot = 695.99$ Mm causes a small, but significant, change in the sound-speed and density profiles of the models. If the radius is reduced to 695.78 Mm (Antia, 1998), then in the regions that can be successfully probed with helioseismology, the rms relative sound-speed difference between this and a model with the standard radius is 0.00014 with a maximum difference of 0.0002. The rms relative density difference is 0.0015 and the maximum difference is 0.0019. The effect of uncertainties in solar age are minor (Morel et al., 1997; Boothroyd and Sackmann, 2003). A change of 0.02 Gyr in the solar age of 4.57 Gyr yield small effects according to Boothroyd and Sackmann (2003), with rms relative sound-speed differences of about 0.0001 and rms relative density differences of 0.001. The effect of changing the value of solar mass is more subtle since the product $GM_\odot$ is known very accurately. Any change in the value of solar mass has to be compensated by an opposite change in the value of G in order to keep $GM_\odot$ the same. The effect of a change in the value of the gravitational constant G will be similar — compensated by the need to change the value of $M_\odot$. It turns out that the solar models are not very sensitive to these changes. Christensen-Dalsgaard et al. (2005) found that changing G by 0.1%, changes the position of the base of the convection zone by $0.00005R_\odot$ and the helium abundance at the surface by 0.0003. Similarly, the relative change in sound speed is less than 10^{-4}, while that in the density is less than 0.002.

Uncertainties and changes in nuclear reaction rates predominantly affect the core. However, the effect is not completely limited to the core and can be felt in the solar envelope too, and results in the change in the position of the convection-zone base. Boothroyd and Sackmann (2003) found that a change of 5% in the p–p reaction rate results in rms relative sound-speed changes of 0.0009 and rms relative density changes of 0.018. The relative sound-speed change in the core can be as much as 0.003, but only 0.0014 in the regions that can be successfully probed by helioseismology. Brun et al. (2002) found that changing the ^{3}He–^{3}He and ^{3}He–^{4}He reaction rates by 10% results in less than 0.1% change in sound speed and less than 0.6% in density. Recently, the cross section of the $^{14}\mathrm{N}(p,\gamma)^{15}\mathrm{O}$ reaction rate was reduced (Formicola et al., 2004). This changes the core structure, and even changes the position of the base of the convection zone by $0.0007R_\odot$ (Bahcall et al., 2005c).

It is difficult to quantify the uncertainties in input physics like the equation of state and opacities since these depend on a number of quantities such as temperature, density, composition, etc. A measure of the uncertainties can be obtained by using two independent estimates. Basu et al. (1996) found that changing the input equation of state from OPAL to MHD changes the position of the base of convection zone in the model by $0.0009R_\odot$. Guzik and Swenson (1997) tested a number of different equations of state and also found that OPAL and MHD models differ

significantly and that the use of the MHD equation of state gives rise to higher pressure in parts of the solar envelope. This was confirmed by Boothroyd and Sackmann (2003).

One of the largest effects on a solar model is that of radiative opacity. Opacities determine the structure of the radiative interior, and in particular, the position of the base of the convection zone. Neuforge-Verheecke et al. (2001a) compared models using the 1995 OPAL opacities with LEDCOP opacities from Los Alamos to find fractional sound-speed difference as large as 0.003. Boothroyd and Sackmann (2003) found that the differences can be much larger, depending on how much the opacities are changed. Opacities are often given in tabular form and require interpolation when used in stellar models, and interpolation errors can also play a role. Neuforge-Verheecke et al. (2001a) suggest that T and ρ interpolation errors in the opacity can be as much as a few percent. Bahcall et al. (2004) found that different state-of-the-art interpolation schemes used to interpolate between existing OPAL tables yield opacity values that differ by up to 4%. Interpolation errors also play a role in defining the position of the base of the convection zone in solar models. Bahcall et al. (2004) did a detailed study of how accurately one could calculate the depth of the convection zone in a model, and concluded that radiative opacities need to be known to an accuracy of 1% in order to get an accuracy of 0.14% in the position of the convection-zone base.

Another input whose uncertainties affect solar structure is the diffusion coefficient. Boothroyd and Sackmann (2003) showed that a 20% change in the helium diffusion rate leads to an rms relative sound-speed difference of 0.0008 and rms relative density difference of 0.007. The effect on the rms differences, of changing the heavy-element diffusion coefficients was found to be smaller, with a 40% change causing an rms relative sound-speed difference of 0.0004 and density of 0.004. Increasing diffusion coefficients also change the position of the base of the convection zone and the convection-zone helium abundance. Montalbán et al. (2004) found that increasing the heavy-element diffusion coefficients by 50% changes the position of the convection-zone base by $0.006R_\odot$ and the convection-zone helium abundance by 0.009.

The formulation used to calculate convective flux in the convection zone also affects solar models. However, since the temperature gradient in most of the convection zone is close to the adiabatic value the formulation used for calculating convective flux does not play much of a role in those parts of the convection zone. Differences arise only in regions close to the solar surface where convection is inefficient. If the prescription of Canuto and Mazzitelli (1991) is used instead of Mixing length theory, the difference is confined to outer 5% of solar radius (Basu and Antia, 1994), with maximum relative difference in sound speed of 6% close to the solar surface, though the difference is less than 1% below $0.99R_\odot$ and less than 0.15% below $r = 0.95R_\odot$. Similarly, the maximum relative difference in density can exceed 10% near the surface, but is less than 2% below $0.99R_\odot$ and less than 0.2% below $r = 0.95R_\odot$. Both these differences fall-off rapidly with depth.

Since helioseismology allows us to determine the position of the base of the convection zone as well as the convection-zone helium abundance, Delahaye and Pinsonneault (2006) have presented a table listing the theoretical errors on the position of the convection-zone base and helium abundance, and we refer the reader to that as a convenient reference. The effect of these uncertainties on neutrino fluxes has been discussed by Bahcall and Peña-Garay (2004), and Bahcall et al. (2006).

In addition to all the sources of uncertainty discussed above, the solar heavy-element abundance Z plays an important role in the structure of solar models, and that is the subject of this review. This is probably the largest source of uncertainty in current solar models.

There are many physical processes not included in "standard" solar models since there are no standard formulations derived from first principles that can be used to model the processes. Models that include these effects rely on simple formulations with free parameters and hence are not regarded as standard solar models, which by definition have no free parameters (since the mixing length parameter and the initial helium abundance are fixed from known solar constraints). Among the missing processes are the effects of rotation on structure and of mixing induced by rotation. There are other proposed mechanisms for mixing in the radiative layers of the Sun, such as mixing caused by waves generated at the convection-zone base (e.g., Kumar et al. (1999)). These processes also affect the structure of the model. For example, Turck-Chièze et al. (2004) found that mixing below the convection-zone base can change both the position of the convection-zone base (gets shallower) and the helium abundance (abundance increases). Accretion and mass-loss at some stage of solar evolution can also affect the solar models. Castro et al. (2007) have investigated the effects of accretion.

Another non-standard input is the effect of magnetic fields. Magnetic fields are extremely important in the Sun, but standard solar models do not include magnetic fields. Part of the reason, of course, is that we do not know the

configuration of magnetic fields inside the Sun. However, given that we know that the solar cycle exists means that there are changes in the Sun that take place on much shorter time-scales than the evolutionary time-scale of the Sun. There are attempts to include convection and magnetic fields in solar models (e.g., Li et al. (2006)), however, the effort is extremely computationally intensive, and it is not likely that such models will become the norm anytime soon.

3. Helioseismology

As mentioned in the previous section one can put constraints on the inputs that go into constructing the model by comparing the structure of standard solar models with that of the Sun. Helioseismology gives us the means to do such a detailed comparison. In order to do so, oscillation frequencies of solar models need to be calculated first. In this section, we describe the basic equations used to describe solar oscillations and indicate how frequencies of solar models can be calculated. We then outline how helioseismic techniques are used to determine the structure of the Sun and compare solar models with the Sun.

3.1. The basic equations

To a good approximation, solar oscillations can be described as linear and adiabatic. Each solar-oscillation mode has a velocity amplitude of the order of 10 cm/s at the surface, which is very small compared to the sound speed at the surface as determined from solar models. Except in the regions close to the solar surface, the oscillations are very nearly adiabatic since the thermal time-scale is much larger than the oscillation period. Although the adiabatic approximation breaks down near the surface, non-adiabatic effects are generally ignored because there are many other uncertainties associated with the treatment of these near-surface layers. As explained later, the effect of these uncertainties can be filtered out by other means. It is reasonably straightforward to calculate the frequencies of a solar model. The equations are written in spherical polar coordinates and the variables are separated by writing the solution in terms of spherical harmonics. The resulting set of equations form an eigenvalue problem, with the frequencies being the eigenvalues. Details of the equations, how they are solved, and the properties of the oscillation have been described by Cox (1980), Unno et al. (1989), Christensen-Dalsgaard and Berthomieu (1991), Gough (1993) and Christensen-Dalsgaard (2002) etc. Here we give a short overview of the basic equations.

The basic equations of fluid dynamics, i.e., the continuity equation, the momentum equation and the energy equation (in the adiabatic approximation) and the Poisson's equation to describe the gravitational field, can be applied to the solar interior. These equations are:

$$\frac{\partial \rho}{\partial t} + \nabla \cdot (\rho \mathbf{v}) = 0, \tag{13}$$

$$\rho \left(\frac{\partial v}{\partial t} + \mathbf{v} \cdot \nabla \mathbf{v} \right) = -\nabla P - \rho \nabla \Phi, \tag{14}$$

$$\frac{\partial P}{\partial t} + \mathbf{v} \cdot \nabla P = c^2 \left(\frac{\partial \rho}{\partial t} + \mathbf{v} \cdot \nabla \rho \right), \tag{15}$$

$$\nabla^2 \Phi = 4\pi G \rho, \tag{16}$$

where $\mathbf{v}$ is the velocity of the fluid element, $c = \sqrt{\Gamma_1 P/\rho}$ is the sound speed, Φ is the gravitational potential, and G the gravitational constant. The equations describing solar oscillations are obtained by a linear perturbation analysis of Eqs. (13)–(16). Since time does not appear explicitly in the equations, the time dependence of the different perturbed quantities can be assumed to have an oscillatory form and separated out. Thus we can write the perturbation to pressure as:

$$P(r, \theta, \phi, t) = P_0(r) + P_1(r, \theta, \phi) \mathrm{e}^{-\mathrm{i}\omega t}, \tag{17}$$

where the subscript 0 denotes the equilibrium, spherically symmetric, quantity which by definition does not depend on time, and the subscript 1 denotes the perturbation. As is customary, we have used spherical polar coordinates centered at the solar center with r being the radial distance, θ the colatitude, and ϕ the longitude. Here, ω is the frequency of the oscillation. Perturbations to other quantities, such as density, can be expressed in the same form. These are the

Eulerian perturbations, which are evaluated at a specified point. Velocity is given by as $\mathbf{v} = \partial\vec{\xi}/\partial t$, where $\vec{\xi}$ is the displacement from equilibrium position. Substituting the perturbed quantities in the basic Eqs. (13)–(16), and keeping only linear terms in the perturbations, we get:

$$\rho_1 + \nabla\cdot(\rho_0\vec{\xi}) = 0, \tag{18}$$

$$-\omega^2\rho\vec{\xi} = -\nabla P_1 - \rho_0\nabla\Phi_1 - \rho_1\nabla\Phi_0, \tag{19}$$

$$P_1 + \vec{\xi}\cdot\nabla P_0 = c_0^2\left(\rho_1 + \vec{\xi}\cdot\nabla\rho_0\right), \tag{20}$$

$$\nabla^2\Phi_1 = 4\pi G\rho_1. \tag{21}$$

Eliminating P_1 and ρ_1, and expressing the gravitational potential as an integral, we can combine Eqs. (18)–(21) to get one equation to describe linear, adiabatic oscillations:

$$-\omega^2\rho\vec{\xi} = \rho\mathcal{L}\vec{\xi} = \nabla(c^2\rho\nabla\cdot\vec{\xi} + \nabla P\cdot\vec{\xi}) - \vec{g}\nabla\cdot(\rho\vec{\xi}) - G\rho\nabla\left(\int_V \frac{\nabla\cdot(\rho\vec{\xi})\,\mathrm{d}V}{|\vec{r}-\vec{r}'|}\right). \tag{22}$$

Here for convenience we have dropped the subscript 0 from the equilibrium quantities since the perturbations, ρ_1, P_1 etc., do not occur in this equation. This equation, supplemented by appropriate boundary conditions at the center and the solar surface, defines an eigenvalue problem for the operator $\mathcal{L}$, with frequency ω as the eigenvalue. The different modes are uncoupled in the linear approximation, and hence, the equations can be solved for each mode separately. Furthermore, it can be shown that the radial and angular dependencies can be separated by expressing the perturbations in terms of spherical harmonics. Thus the perturbation to any scalar quantity can be written as:

$$P(r,\theta,\phi,t) = P_0(r) + P_1(r)Y_\ell^m(\theta,\phi)\mathrm{e}^{-\mathrm{i}\omega t}. \tag{23}$$

The displacement vector can be expressed as:

$$\vec{\xi} = \left(\xi_r(r)Y_\ell^m(\theta,\phi), \xi_h(r)\frac{\partial Y_\ell^m}{\partial\theta}, \frac{\xi_h(r)}{\sin\theta}\frac{\partial Y_\ell^m}{\partial\phi}\right)\mathrm{e}^{-\mathrm{i}\omega t}, \tag{24}$$

where ξ_r and ξ_h are respectively the radial and horizontal components of the displacement. A detailed discussion of properties of the different oscillation modes is given by Unno et al. (1989), Gough (1993) and Christensen-Dalsgaard (2002).

The different modes of solar oscillations are described by three numbers that characterize the perturbations that define the effect of the mode. These are: (1) the radial order n which is related to the number of nodes in the radial direction, (2) the degree ℓ which is related to the horizontal wavelength of the mode and is approximately the number of nodes on the solar surface, and (3) the azimuthal order m which defines the number of nodes along the equator. The radial order, n, can have any integral value. Positive values of n are used to denote acoustic modes, i.e., the so-called p-modes (p for pressure, since the dominant restoring force for these modes is provided by the pressure gradient). Negative values of n are used to denote modes for which buoyancy provides the main restoring force. These are usually referred to as g-modes (g for gravity). Modes with $n = 0$ are the so-called fundamental or f-modes. For large ℓ, f-modes are essentially surface gravity modes whose frequencies are largely independent of the stratification of the solar interior. As a result, f-mode frequencies are normally not used for determining the structure of the Sun, however, these have been used to draw inferences about the solar radius (e.g., Schou et al. (1997), Antia (1998) and Lefebvre et al. (2007)). Only p- and f-modes have been reliably detected in the Sun and we shall confine our discussion to these modes. The degree ℓ and the azimuthal order m describe the angular dependence of the mode as determined by $Y_\ell^m(\theta,\phi)$. The degree ℓ is either 0 (the radial mode) or positive (non-radial modes). The azimuthal order m can have $2\ell+1$ values with $-\ell \le m \le \ell$. While ℓ and m can be determined by spherical harmonic transform of Doppler or intensity images of the solar surface, n can only be determined from the power spectrum of the spherical harmonic transforms by counting the ridges in the power spectra. The positions of the peaks in the power spectrum, when compared with the asymptotic expressions or frequencies of solar models, can also give an estimate of n. The frequencies of solar oscillations are usually expressed as the cyclic frequency $\nu = \omega/(2\pi)$.

If the Sun were spherically symmetric, the frequencies would be independent of m. Rotation and magnetic fields lift the $(2\ell+1)$-fold degeneracy of modes with the same n and ℓ, giving rise to the so-called frequency splittings. The

frequencies $\nu_{n\ell m}$ of the modes within a multiplet are usually expressed in terms of the splitting coefficients

$$\nu_{n\ell m} = \nu_{n\ell} + \sum_{j=1}^{J_{\max}} a_j^{n\ell} \mathcal{P}_j^{\ell}(m). \tag{25}$$

Here, $\nu_{n\ell}$ is the mean frequency of a given (n, ℓ) multiplet and $a_j^{n\ell}$ are the "splitting coefficients", often referred to as "a-coefficients". In this expression, $\mathcal{P}_j^{\ell}(m)$ are orthogonal polynomials in m of degree j. The orthogonality of these polynomials is defined over the discrete values of m. In the expansion, $J_{\max}$ is generally much less than 2ℓ. Although this expansion reduces the number of data points that are available for use, the splitting coefficients can be determined to much higher precision than the individual frequencies $\nu_{n\ell m}$. Unfortunately, different workers have used different normalizations of $\mathcal{P}_j^{\ell}(m)$ (e.g., Ritzwoller and Lavely (1991) and Schou et al. (1994)) and there is no unique definition of splitting coefficients either. Early investigators (e.g., Duvall et al. (1986)) commonly used Legendre polynomials, whereas now it is common to use the Ritzwoller–Lavely formulation (Ritzwoller and Lavely, 1991) where the basis functions are orthogonal polynomials related to Clebsch–Gordan coefficients. The readers are referred to Pijpers (1997) for details on how the different polynomials and splitting coefficients are related.

The mean frequency, $\nu_{n\ell}$, in Eq. (25) is determined by the spherically symmetric structure of the Sun, and hence can be used to determine the solar structure. The odd-order coefficients $a_1, a_3, \ldots$ depend principally on the rotation rate (Durney et al., 1988; Ritzwoller and Lavely, 1991) and reflect the advective, latitudinally symmetric part of the perturbations caused by rotation. Hence, these are used to determine the rotation rate inside the Sun. The even order a coefficients on the other hand, result from a number of different causes, such as magnetic fields (Gough and Thompson, 1990; Dziembowski and Goode, 1991), asphericities in solar structure (Gough and Thompson, 1990), and the second order effects of rotation (Gough and Thompson, 1990; Dziembowski and Goode, 1992). In this review we shall only concentrate on the spherically symmetric part of the solar structure and hence, only the mean frequencies $\nu_{n\ell}$ are relevant.

As mentioned earlier, most of the observed oscillations are acoustic or p-modes, which are essentially sound waves. These modes are stochastically excited by convection in the very shallow layers of the Sun (Goldreich and Keeley, 1977; Goldreich et al., 1994). As these waves travel inwards from the solar surface, they pass through regions of increasing sound speed, a result of increasing temperatures. This causes the waves to be refracted away from the vertical direction until they undergo a total internal reflection. The depth at which this happens is called the "lower turning point" of the mode, and is approximately the position at which $\omega^2 = \ell(\ell+1)c^2(r)/r^2$, where $c(r)$ is the sound speed at radial distance r from the center. Thus, low-degree modes penetrate to the deep interior, but high-degree modes are trapped in the near-surface regions. Each solar-oscillation mode is trapped in a different region inside the Sun and the frequency of the mode is determined by the structure variables, like sound speed and density, in the trapping region. By considering different modes it is possible to determine the solar structure in the region that is covered by the observed set of modes, which includes almost the entire Sun. This is done by solving the inverse problem (Gough and Thompson, 1991; Christensen-Dalsgaard, 2002).

There are a number of projects that provide readily available solar-oscillation frequencies, the chief among these are the ground-based Global Oscillation Network Group (GONG) project (Hill et al., 1996)[1] and the Michelson Doppler Imager (MDI) instrument on board the Solar and Heliospheric Observatory (SOHO) (Scherrer et al., 1995).[2] These projects determine frequencies of both low- and intermediate-degree modes, and typical sets include 3000 modes for different values of n and ℓ, with ℓ up to ≈ 200 and $\nu_{n\ell}$ in the range 1–4.5 mHz. Most of the frequencies are determined to a precision of about 1 part in 10^5 which allows one to make stringent tests of solar models. The most precise sets of low-degree data ($\ell = 0$, 1, 2 and 3), i.e., data that probe the solar core, are however, obtained from unresolved observations of the solar disc such as those made by the Birmingham Solar Oscillation Network (BiSON; (Elsworth et al., 1991; Chaplin et al., 2007a)) or the Global Oscillations at Low Frequencies (GOLF) instrument (Gabriel et al., 1995a) on board SOHO. Fig. 2 shows the frequencies of one set of solar-oscillation data plotted as a function of the degree ℓ for different radial orders n. This figure also plots the frequencies of a solar model. On the scale of the figure there is very good agreement between the two, which essentially confirms the mode identification and also gives us confidence in the model.

[1] GONG frequencies can be downloaded from http://gong.nso.edu/data/.

[2] MDI frequencies are available at http://quake.stanford.edu/~schou/anavw72z/.

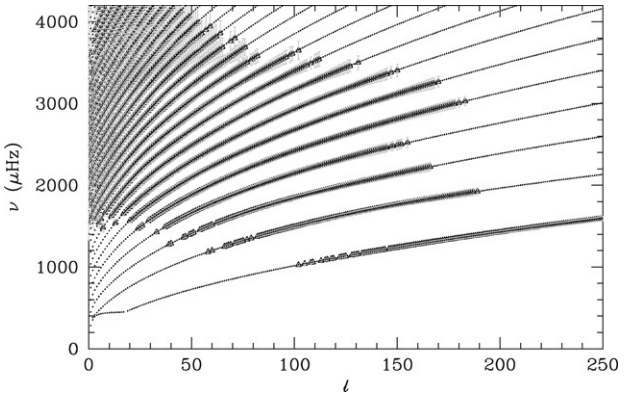

Fig. 2. The frequencies of a solar model plotted as a function of degree ℓ are shown by dots which have merged into lines which can be identified with ridges in power spectrum. The triangles with error-bars are the observed frequencies obtained from the first 360 days of observations by the MDI instrument. The error-bars represent 5000σ errors. The lowermost ridge corresponds to f-modes.

3.2. Determining the solar structure from seismic data

To determine solar structure from solar-oscillation frequencies one begins with the equation for solar oscillations as given by Eq. (22). In Eq. (22), ω is the observed quantity and we would like to determine sound speed c and density ρ (and hence pressure P assuming hydrostatic equilibrium). However, the displacement eigenfunction $\vec{\xi}_{n,\ell}$ can only be observed at the solar surface and therefore the equations cannot be inverted directly. The way out of this is to recognize that Eq. (22) defines an eigenvalue problem of the form

$$\mathcal{L}\vec{\xi}_{n,\ell} = -\omega_{n,\ell}^2 \vec{\xi}_{n,\ell}, \tag{26}$$

$\mathcal{L}$ being a differential operator in Eq. (22). Under specific boundary conditions, namely $\rho = P = 0$ at the outer boundary, the eigenvalue problem defined by Eq. (22) is Hermitian (Chandrasekhar, 1964) and hence, the variational principle can be used to linearize Eq. (22) around a known solar model (called the "reference model") to obtain

$$\delta\omega_{n,\ell}^2 = -\frac{\int_V \rho \vec{\xi}^{\star}_{n,\ell} \cdot \delta\mathcal{L}\vec{\xi}_{n,\ell}\, \mathrm{d}V}{\int_V \rho \vec{\xi}^{\star}_{n,\ell} \cdot \vec{\xi}_{n,\ell}\, \mathrm{d}V}, \tag{27}$$

where $\delta\omega_{n,\ell}^2$ is the difference in the squared frequency of an oscillation mode of the reference model and the Sun, $\delta\mathcal{L}$ is the perturbation to the operator $\mathcal{L}$ (defined by Eq. (22)) as a result of the differences between the reference model and the Sun, and $\vec{\xi}_{n,\ell}$ is the displacement eigenfunction for the known solar model (and thus can be calculated). One such equation can be written for each mode of oscillation characterized by (n, ℓ), and the set of equations can be used to calculate the difference in structure between the solar model and the Sun, and thus determine the structure of the Sun. The denominator on the right-hand side of Eq. (27) is usually denoted as $I_{n,\ell}$, and is often called the mode inertia since it can be shown that the time-averaged kinetic energy of a mode is proportional to $\omega_{n,\ell}^2 I_{n,\ell}$.

Eq. (27) implies that for a given difference in structure, the resulting differences in frequencies of modes with a high inertia are less than those of modes with lower inertia. For modes of a given frequency, lower degree (i.e., deeply penetrating) modes have higher mode inertias than higher-degree (i.e., shallow) modes. The mode inertia therefore, is a convenient weighing factor to quantify the effect of any perturbation on the frequency of a mode. Since computed eigenfunctions of a solar model are arbitrary to a constant multiple, it is customary to use $I_{n,\ell}$ normalized by the value at the surface, sometimes referred to as $E_{n,\ell}$. When modes are represented as spherical harmonics, $E_{n,\ell}$ can be shown to be

$$E_{n\ell} = \frac{4\pi \int_0^R \left[|\xi_r(r)|^2 + \ell(\ell+1)|\xi_h(r)|^2\right] \rho_0 r^2\, \mathrm{d}r}{M\left[|\xi_r(R_\odot)|^2 + \ell(\ell+1)|\xi_h(R_\odot)|^2\right]}, \tag{28}$$

where ξ_r and ξ_h are the radial and horizontal components of the displacement eigenfunction, M the total mass and $\rho_0(r)$ the density profile of the model. It is convenient to define another measure of inertia, denoted by $Q_{n\ell}$, which is

defined as

$$Q_{n\ell} = \frac{E_{n\ell}}{E_0(\nu_{n\ell})}, \tag{29}$$

where $E_0(\nu)$ is $E_{n\ell}$ for $\ell = 0$ modes interpolated to the frequency ν. Thus $Q_{n\ell} = 1$ for $\ell = 0$ modes and less than one for modes with higher ℓ. Multiplying frequency differences with $Q_{n\ell}$ is equivalent to inversely scaling the frequency differences with mode inertia.

Linearizing Eq. (22) around a known solar model by applying the variational principle results in an equation that relate the frequency differences between the Sun and the solar model to the differences in structure between the Sun and the model:

$$\frac{\delta\nu_{n\ell}}{\nu_{n\ell}} = \int_0^R \mathcal{K}^{n\ell}_{c^2,\rho}(r)\frac{\delta c^2}{c^2}(r)\,\mathrm{d}r + \int_0^R \mathcal{K}^{n\ell}_{\rho,c^2}(r)\frac{\delta\rho}{\rho}(r)\,\mathrm{d}r, \tag{30}$$

where, $\delta c^2/c^2$ and $\delta\rho/\rho$ are the relative differences in the squared sound speed and density between the Sun and the model. The functions $\mathcal{K}^{n\ell}_{c^2,\rho}(r)$ and $\mathcal{K}^{n\ell}_{\rho,c^2}(r)$ are the kernels of the inversion that relate the changes in frequency to the changes in c^2 and ρ respectively. These are known functions of the reference solar model.

Eq. (30), unfortunately, is not enough to represent the differences between the Sun and the models. There is an additional complication that arises due to uncertainties in modelling layers just below the solar surface. Eq. (27) implies that we can invert the solar frequencies provided we know how to model the Sun properly, and if the frequencies can be described by the equations for adiabatic oscillations. Neither of these two assumptions is completely correct. For example, our treatment of convection in surface layers is known to be approximate. Simulations of convection seem to indicate that there are significant departures between the temperature gradients obtained from the mixing length approximation and that from a full treatment of convection. The deviations mainly occur close to the solar surface (see e.g., Robinson et al. (2003) and references therein). This results in differences in the density and pressure profiles. Not using a full treatment of convection also means that several physical effects, such as turbulent pressure and turbulent kinetic energy, are missing from the models. Another source of error is the fact that the adiabatic approximation that is used to calculate the frequencies of the models breaks down near the surface where the thermal time-scale is comparable to the period of oscillations. This implies that the right-hand side of Eq. (30) does not fully account for the frequency difference $\delta\nu/\nu$ between the Sun and the model. Fortunately, all these uncertainties are localized in a thin layer near the solar surface. For modes which are not of very high degree ($\ell \simeq 200$ and lower), the structure of the wavefront near the surface is almost independent of the degree, the wave-vector being almost completely radial. This implies that any additional difference in frequency due to errors in the surface structure has to be a function of frequency alone once mode inertia has been taken into account. It can also be shown (e.g., Gough (1990)) that surface perturbations cause the difference in frequency to be a slowly varying function of frequency which can be modeled as a sum of low degree polynomials. This effect is shown in Fig. 3 which shows the frequency differences, scaled inversely by their mode inertia, between two models which differ only near the surface due to differences in their convection formalisms. It can be seen that all points tend to fall on a curve which is a function of frequency. Thus Eq. (30) is modified to represent the difference between the model and the Sun and is re-written as

$$\frac{\delta\nu_{n\ell}}{\nu_{n\ell}} = \int_0^R \mathcal{K}^{n\ell}_{c^2,\rho}(r)\frac{\delta c^2}{c^2}(r)\,\mathrm{d}r + \int_0^R \mathcal{K}^{n\ell}_{\rho,c^2}(r)\frac{\delta\rho}{\rho}(r)\,\mathrm{d}r + \frac{F(\nu_{n\ell})}{E_{n\ell}}, \tag{31}$$

where $F(\nu_{n\ell})$ is a slowly varying function of frequency that arises due to the errors in modelling the near-surface regions (Dziembowski et al., 1990; Antia and Basu, 1994a). In addition to satisfying Eq. (31), the differences in density should integrate to zero since otherwise the total solar mass will be modified. This is ensured by putting an additional constraint on $\delta\rho$.

Instead of sound speed and density we can write Eq. (31) in terms of other pairs of independent structure variables, such as the adiabatic index Γ_1 and density, or Γ_1 and P/ρ. It can be shown that once sound speed and density are known, other structure variables that are required for the adiabatic oscillation equations can be calculated. For example, pressure can be calculated from the equation of hydrostatic equilibrium. The equation of state is not required for this purpose, since the only thermodynamic index that occurs in the oscillation equations is the adiabatic index,

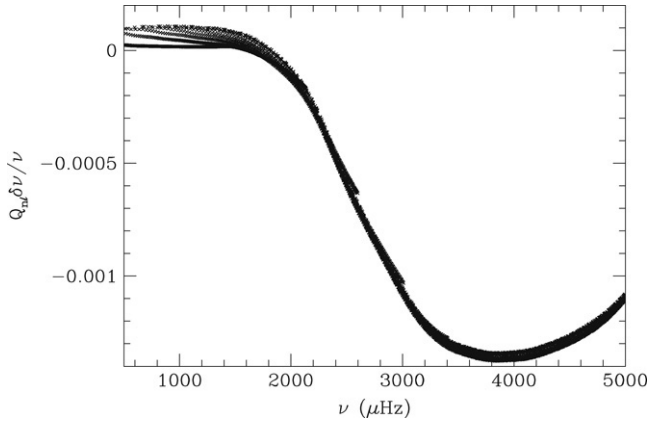

Fig. 3. The scaled, relative differences between the frequencies of two solar models constructed using different formulations of convective flux. Other input physics is the same for both models. One of the models was constructed using the mixing length theory and the other using the Canuto and Mazzitelli (1991) formulation for calculating convective flux.

$\Gamma_1 = (\partial \ln P/\partial \ln \rho)_S = c^2\rho/P$, which can be directly calculated once ρ, P and c are known. However, other thermodynamic quantities like temperature, composition etc., do not occur in the equations of adiabatic oscillations, and hence, these cannot be obtained directly through inversions. In order to estimate temperature and composition one has to assume that input physics such as the equation of state, opacities and nuclear energy generation rate are known exactly. Additionally, the equations of thermal equilibrium are needed to relate temperature to the other quantities (see e.g., Gough and Kosovichev (1990), Shibahashi and Takata (1996), and Antia and Chitre (1998)).

It turns out that most of the difference in frequencies between the Sun and modern solar models are a result of uncertainties in the near-surface layers. This makes it difficult to test the internal structure of these models by directly comparing the frequencies of the models with those of the Sun. The frequency differences caused by the near-surface errors are often larger than the frequency differences caused by differences in the structure of the inner regions, making the comparison ineffective. As a result, one resorts to inverting the frequency differences in order to determine the differences between solar models and the Sun as a function of radius. A number of techniques have been developed for solving the inverse problem (Gough and Thompson (1991), Christensen-Dalsgaard (2002) and references therein). Inverse problems are generally ill-conditioned since it is not possible to infer a function like sound speed in the solar interior using only a finite and discrete set of observed modes. Thus additional assumptions have to be made (e.g., solar sound speed or density are positive quantities and that the profiles are not discontinuous and do not vary sharply) in order to determine the structure of the Sun. There are two classes of methods to determine $\delta c^2/c^2$ and $\delta\rho/\rho$ from Eq. (31): the regularized least-squares (RLS) method, and the method of optimally localized averages (OLA).

In the RLS technique the unknown functions $\delta c^2/c^2$, $\delta\rho/\rho$ and $F(\nu)$ are expanded in terms of a suitable set of basis functions and the coefficients of expansion are determined by fitting the given data. Noise in the data can cause the solution to be highly oscillatory unless the result is smoothed by applying regularization (e.g., Craig and Brown (1986)). Regularization is usually applied by ensuring that either the first or the second derivative of the solution is also small. It is common to assume that the second derivative is small, and this is achieved by minimizing the function

$$\chi^2 = \sum_{n,\ell}\left(\frac{d_{n,\ell}}{\sigma_{n,\ell}}\right)^2 + \lambda_{c^2}\int_0^R\left(\frac{\mathrm{d}^2(\delta c^2/c^2)}{\mathrm{d}r^2}\right)^2\mathrm{d}r + \lambda_\rho\int_0^R\left(\frac{\mathrm{d}^2(\delta\rho/\rho)}{\mathrm{d}r^2}\right)^2\mathrm{d}r, \tag{32}$$

where $d_{n,\ell}$ is the difference between the left-hand side and right-hand side in Eq. (31) and $\sigma_{n,\ell}$ is the estimated error in the observed relative frequency difference. The smoothness is controlled by the regularization parameters λ_{c^2} and λ_ρ which are adjusted to get the required smoothness of the solutions for $\delta c^2/c^2$ and $\delta\rho/\rho$. If these parameters are zero, then the solution reduces to normal least-squares approximation and the solution is highly oscillatory, while for very large values of these parameters, the solution will approach a linear function in r. Details of how the regularization parameters can be determined in general has been described by Hansen (1992). A description of how these parameters can be chosen for helioseismic inversions is given in Antia and Basu (1994a) and Basu and Thompson (1996).

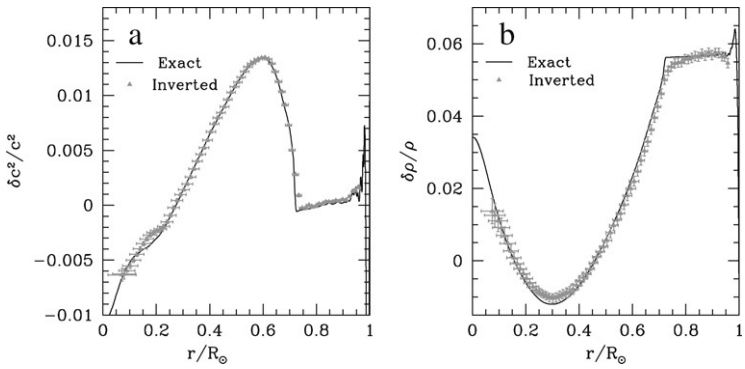

Fig. 4. The exact and inverted relative sound-speed (panel a) and density (panel b) differences between two models. The mode set corresponding to the first 360 days of MDI data (Schou et al., 1998a) was used for the inversion. Random errors were added to the frequencies of the test model prior to the inversions. The vertical error-bars show the formal 1σ errors on the inversion results caused by errors in the MDI data. The horizontal error-bars are a measure of the width of the averaging kernels and hence, of the resolution of the inversions.

In the OLA technique (Backus and Gilbert, 1968), a linear combination of the kernels is obtained such that the combination is localized in space. The linear combination is called the resolution kernel or the averaging kernel. The solution obtained is then an average of the true solution weighted by the averaging kernel. Very often a variant of the OLA method called "Subtractive" Optimally Localized Averages (SOLA; (Pijpers and Thompson, 1992, 1994)) is used. In either case, if $\mathcal{K}_{\rm av}$ is an averaging kernel for an inversion, then

$$\langle f\rangle = \int \mathcal{K}_{\rm av} f(r){\rm d}r \tag{33}$$

represents the average of the quantity f over a sufficiently narrow range in r. Thus if

$$\mathcal{K}_{\rm av} = \sum_{n,\ell} c_{n,\ell} K^{n\ell}_{c^2,\rho}, \quad \text{then, } \left\langle \frac{\delta c^2}{c^2}\right\rangle = \sum_{n,\ell} c_{n,\ell} \frac{\delta\nu_{n\ell}}{\nu_{n\ell}}. \tag{34}$$

From Eq. (31) we can see that this is possible only if $\int \mathcal{K}_{\rm av}{\rm d}r = 1$, and if $\mathcal{C} = \sum_{n,\ell} c_{n,\ell} K^{n\ell}_{\rho,c^2}$ and $\mathcal{F} = \sum_{n,\ell} c_{n,\ell} F(\nu_{n\ell})$ are small. Details of how this is done for solar structure inversions has been described by Rabello-Soares et al. (1999). Fig. 4 shows the result of inverting the frequency differences between two models. As can be seen from the figure, we are able to invert for the differences in structure very well.

It is difficult to determine precisely the structure of the solar core through inversions because of the dearth of low-degree modes. The inversion results often have large errors and poor resolution. As a result, it is also customary to compare the cores of solar models and that of the Sun using combinations of frequencies that are sensitive to the structure of the core (e.g., Elsworth et al. (1990) and Chaplin et al. (1997)). For example, the so-called small frequency spacings of low-degree modes (Tassoul, 1980; Gough, 1986) is sensitive to the sound-speed gradient in the core. The small frequency spacing (or separation) is given by

$$\delta\nu_{n,\ell} = \nu_{n,\ell} - \nu_{n-1,\ell+2} \approx -(4\ell+6)\frac{\Delta\nu_{n,\ell}}{4\pi^2\nu_{n,\ell}} \int_0^R \frac{{\rm d}c}{{\rm d}r}\frac{{\rm d}r}{c}, \tag{35}$$

where $\Delta\nu_{n,\ell} = \nu_{n+1,\ell} - \nu_{n,\ell}$ is the large frequency spacing. The approximation given in Eq. (35) is obtained from an asymptotic analysis of solar-oscillation frequencies and is valid for $n \gg \ell$. The large frequency spacing is determined by the sound-travel time from center to surface and hence has large contribution from near-surface layers where sound speed is low. As a result, the large frequency spacing for models is affected by our inability to model the near-surface layers correctly. One way of reducing the effects of the near-surface errors is to use the so-called frequency separation ratios. The frequency separation ratios (Roxburgh and Vorontsov, 2003; Otí Floranes et al., 2005; Roxburgh, 2005) formed from the small frequency and large frequency spacings of the modes are given by

$$r_{0,2}(n) = \frac{\delta\nu_{n,0}}{\Delta\nu_{n,1}}, \qquad r_{1,3}(n) = \frac{\delta\nu_{n,1}}{\Delta\nu_{n+1,0}}. \tag{36}$$

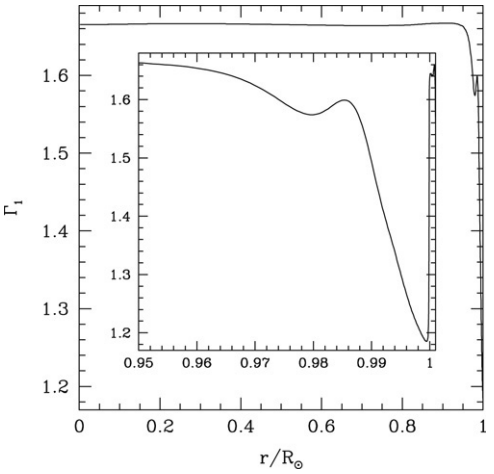

Fig. 5. The adiabatic index, Γ_1 in a solar model plotted as a function of radial distance. The inset shows a blow-up of the outer regions.

3.3. Determining the solar helium abundance

If one assumes that the equation of state of solar material is known well and that it is the same as that used in solar models, Eq. (31) can be modified to determine the helium abundance in the solar convection zone. Since helium does not form lines at photospheric temperatures, it is difficult to determine its abundance spectroscopically. Helioseismic techniques are the most accurate way to determine the solar helium abundance. Helium abundance determinations are usually done through the adiabatic index Γ_1. Although Γ_1 is generally close to the ideal-gas value of $5/3$ in most of the solar interior, it deviates significantly from this value in regions where elements undergo ionization. The adiabatic index is smaller than $5/3$ in the ionization zones, and the extent of reduction depends on the abundance of the element undergoing ionization as well as the equation of state. Thus Γ_1 is sensitive to the helium abundance in the layers where helium ionizes, and this is exploited in several different ways to determine Y in those regions. Since the helium ionization zone lies in solar convection zone, and since the convection zone is well mixed, the helium abundance determined from Γ_1 is the abundance throughout the solar convection zone. Fig. 5 shows Γ_1 in a solar model as a function of radius. The dip near $r = 0.98R_\odot$ is due to the He II ionization zone, while the bigger dip closer to the surface is due to the ionization of H I and He I.

Däppen et al. (1991) and Dziembowski et al. (1990, 1991) showed that Eq. (31) written in terms of Γ_1 and ρ differences can be modified to determine the helium abundance in the Sun because

$$\frac{\delta\Gamma_1}{\Gamma_1} = \left(\frac{\partial \ln \Gamma_1}{\partial \ln P}\right)_{Y,\rho} \frac{\delta P}{P} + \left(\frac{\partial \ln \Gamma_1}{\partial \ln \rho}\right)_{Y,P} \frac{\delta\rho}{\rho} + \left(\frac{\partial \ln \Gamma_1}{\partial Y}\right)_{P,\rho} \delta Y, \tag{37}$$

where the partial derivatives can be determined from the equation of state. This equation ignores contributions of differences in the equation of state and heavy-element abundances to $\delta\Gamma_1$ between the models and the Sun. Eq. (37) was then used by Dziembowski et al. (1991) to rewrite Eq. (31) as

$$\frac{\delta\nu_{n\ell}}{\nu_{n\ell}} = \int_0^R \mathcal{K}^{n\ell}_{u,Y}(r)\frac{\delta u}{u}(r)\,\mathrm{d}r + \int_0^R \mathcal{K}^{n\ell}_{Y,u}(r)\delta Y\,\mathrm{d}r + \frac{F(\nu_{n\ell})}{E_{n\ell}}, \tag{38}$$

where $u \equiv P/\rho$. They further assumed that since δY is constant in the convection zone, and if one were only using modes trapped in the convection zone, δY could be brought out of the integral sign. This method has been used quite extensively to determine solar helium abundance (e.g., Dziembowski et al. (1991) and Kosovichev et al. (1992)), but suffers from extreme sensitivity to the equation of state of the reference model.

There are other methods to determine the solar helium abundance that appear to be somewhat less sensitive to the equation of state. This is done by calibrating the dip in Γ_1 in the helium abundance zone (see Fig. 5). The reduction in Γ_1 in the ionization zones also affects the sound speed, but since sound speed increases very rapidly with depth, the variation may not be detectable in the sound-speed profile itself. Gough (1984) suggested that this variation can

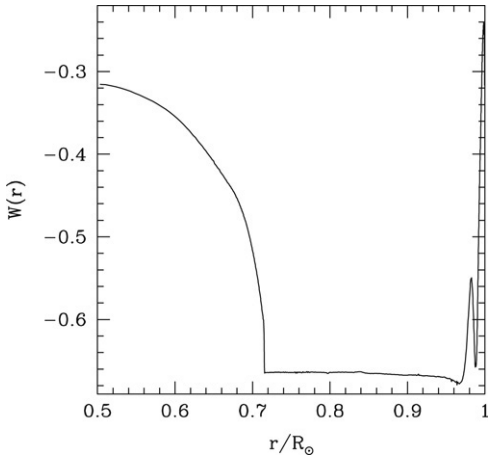

Fig. 6. The dimensionless gradient of sound speed, $W(r)$, of a solar model plotted as a function of radius.

be found in the dimensionless gradient of the sound speed, $W(r)$, where

$$W(r) = \frac{1}{g}\frac{\mathrm{d}c^2}{\mathrm{d}r}, \tag{39}$$

and g is the acceleration due to gravity. In the lower part of the convection zone, $\Gamma_1 \approx 5/3$ and $W(r) \approx -2/3$. Fig. 6 shows $W(r)$ for a solar model. The peak around $r = 0.98R_\odot$ in this figure is due to the He II ionization zone. This peak can be calibrated to find the helium abundance (Gough, 1984; Däppen et al., 1991; Antia and Basu, 1994b). The prominent peak in $W(r)$ near the surface that can be seen from Fig. 6, is due to the hydrogen and He I ionization zones. Since this peak occurs in a region where inversions are not very reliable, it is difficult to use this for any diagnostic purpose. The solar helium abundance can also be determined by directly calibrating the sound-speed difference between the Sun and solar models with known Y (Antia and Basu, 1994b) around the He II ionization zone.

The solar helium abundance can also be determined by examining the surface term $F(\nu)$. The helium ionization zone is relatively deep, but it is close enough to the surface to leave its signature on that term. Although, $F(\nu)$ is a "smooth" function of frequency mainly determined by surface effects, it is also influenced by discontinuities or sharp variations in the sound-speed profile in deeper regions. In general, these discontinuities introduce a small oscillatory term in frequencies as a function of n and the scale of the oscillation is determined by the acoustic depth (i.e., the sound-travel time) of the perturbation (Gough, 1990), and its amplitude depends on the extent of variation around the discontinuity. The oscillatory signature in the frequencies caused by the helium ionization zone translates into a similar oscillatory signature in $F(\nu)$. This signature of the helium ionization zone has been used in different ways by Pérez Hernández and Christensen-Dalsgaard (1994) and Antia and Basu (1994b) etc., to determine the solar helium abundance.

3.4. Determining the depth of the solar convection zone

Solar-oscillation frequencies can be used to determine r_b, the position of the convection-zone base. The function $W(r)$ (Eq. (39)) obtained by inverting solar-oscillation frequencies can be used for this purpose. At the base of the convection zone, the temperature gradient switches from the adiabatic value inside the convection zone to the radiative value below the convection zone. This introduces a discontinuity in the second derivative of the temperature and hence, the sound speed. This results in a discontinuity in the gradient of $W(r)$, which is clearly visible in Fig. 6. The position of this discontinuity can be determined to estimate the convection-zone depth (Christensen-Dalsgaard et al., 1991). The frequencies of solar oscillations are very sensitive to this depth and hence, r_b can be determined very accurately from the observed solar oscillation frequencies. However, there is a more precise method to determine the base of the convection zone, and that is by looking at the sound-speed difference between the Sun and models with different position of the convection-zone base. The shift between radiative and adiabatic temperature gradients at the

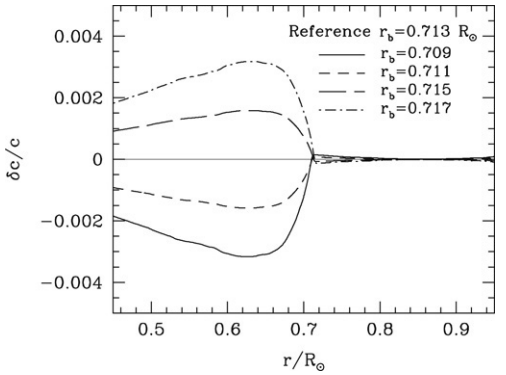

Fig. 7. The relative sound-speed difference between a model with a convection-zone base at $r_b = 0.713R_\odot$ and models with convection-zone bases at different positions.

convection-zone base results in a large sound-speed difference between two models or a model and the Sun when the depths of the convection zones do not match, as can be seen in Fig. 7. This difference can be calibrated to determine the position of the solar convection-zone base (Basu and Antia (1997), Basu (1998) and Basu and Antia (2004) etc.).

3.5. Testing equations of state

Eq. (38) had been used extensively to determine both δY and $\delta u/u$. The equation, written in terms of $\delta\rho/\rho$ and δY was used to determine density ρ. Basu and Christensen-Dalsgaard (1997) however, noticed that determining $\delta u/u$ and $\delta\rho/\rho$ using that equation gives rise to systematic errors, which they found were related to differences in the equation of state. The problem lies in the fact that Eq. (37) ignores the effect of equation of state on Γ_1. Thus an extra term, $\delta\Gamma_{1,\mathrm{int}}/\Gamma_1$, needs to be added to Eq. (37) to account for the differences in Γ_1 at fixed pressure, temperature, and density. This term is often referred to as the "intrinsic" difference in Γ_1. This quantity can be obtained from the frequencies by rewriting the inversion equation as:

$$\frac{\delta\nu_{n\ell}}{\nu_{n\ell}} = \int_0^R \mathcal{K}^{n\ell}_{u,Y}(r)\frac{\delta u}{u}(r)\mathrm{d}r + \int_0^R \mathcal{K}^{n\ell}_{Y,u}(r)\delta Y(r)\mathrm{d}r + \int_0^R \mathcal{K}^{n\ell}_{\Gamma_1,\rho}(r)\frac{\delta\Gamma_{1,\mathrm{int}}}{\Gamma_1}(r)\mathrm{d}r + \frac{F(\nu_{n\ell})}{E_{n\ell}}. \tag{40}$$

A non-zero $\delta\Gamma_{1,\mathrm{int}}/\Gamma_1$ would imply differences between the equation of state used to construct a solar model and that of the Sun, and hence can be used to test different equations of state.

4. Helioseismic results

Early observations of high-degree modes had provided significant constraints on the solar interior, however, detailed results had to wait for the availability of reliable frequencies of low- and intermediate-degree modes, as well as development of inversion techniques. In this section we describe what we have learned about solar structure. We also discuss the results of some tests of different inputs to solar models. The discussion is mainly restricted to results that are relevant for this review.

4.1. Results about solar structure

One of the most important results obtained from the inversion of solar-oscillation frequencies is the detailed knowledge of solar structure, in particular the solar sound-speed and density profiles (Christensen-Dalsgaard et al. (1989), Dziembowski et al. (1990), Däppen et al. (1991), Antia and Basu (1994a), Gough et al. (1996), Kosovichev et al. (1997) and Basu et al. (1997, 2000) etc.). With current frequency sets, such as those from GONG or MDI, the sound-speed, density and Γ_1 profiles of the Sun can be reliably determined from as close to the center as $0.05R_\odot$ to about $0.95R_\odot$. The dearth of low-degree modes make it difficult to go deeper, while the lack of reliable high-degree mode frequencies makes it difficult to investigate layers shallower than about $0.95R_\odot$. A table listing solar sound speed and density as a function of radius can be found in the online material accompanying this review. Sound speed

is known in most of the solar interior with a precision of better than 0.01%, while Γ_1 is known to a precision of better than 0.1%. The density profile is known less precisely, but nonetheless with a precision of 0.6% in the core and better (0.2%) in the envelope. The basic inversion techniques are described in Section 3.2. Basu et al. (2000) showed that the inferred solar structure depends minimally on the reference model used for inversion, thereby justifying the linearization used to obtain Eq. (31).

The position of the base of the solar convection zone is another important structural parameter that has been determined. Comparisons of early helioseismic data with models had shown that the convection zone was deeper than what had been assumed (Ulrich and Rhodes, 1977), and Rhodes et al. (1977) showed that the base of the convection zone was between 0.62 and $0.75 R_\odot$. By comparing the frequencies of a solar model with observed ridges in the power spectrum Berthomieu et al. (1980) estimated the depth of the convection zone to be about 200 Mm. More precise determinations had to wait for inversions to determine the solar sound-speed profile. As explained in Section 3.4, the solar sound-speed profile can be used to measure the depth of the solar convection zone. Christensen-Dalsgaard et al. (1991) found that the base of the convection zone is located at $r_b = (0.713 \pm 0.003) R_\odot$. Similar results were also obtained by Kosovichev and Fedorova (1991). Basu and Antia (1997) made a detailed study of systematic errors involved in this measurement, and with better data from the GONG project determined the base of the solar convection zone to be at $r_b = (0.713 \pm 0.001) R_\odot$. Basu (1998) studied the effect of small errors in the value of the solar radius in estimating the position of the solar convection-zone base, and found that the effect was within current error-bars. Using data from both GONG and MDI projects she determined the base to be at $r_b = (0.7133 \pm 0.0005) R_\odot$. Basu and Antia (2004) studied the influence of the heavy-element abundance on the seismically estimated position of the convection-zone base and found the results to be insensitive to Z/X, and using GONG data they determined the convection-zone base to be at $r_b = (0.7133 \pm 0.0005) R_\odot$. Furthermore, Basu and Antia (2001) found that, within errors, the position of the base of convection zone is independent of latitude. Analyses of observed solar frequencies have also been used to show that the extent of overshoot below the convection zone is very small, at least, when a simple model of the thermal structure of the overshoot layer is assumed (Basu et al., 1994; Monteiro et al., 1994; Roxburgh and Vorontsov, 1994; Basu and Antia, 1994; Basu, 1997).

Another important solar property that has been determined successfully using helioseismology is Y_s, the helium abundance in the solar convection zone. Various techniques discussed in Section 3.3 have been used. The first attempts to determine the solar helium abundance were made by Däppen and Gough (1986) and Däppen et al. (1988b). They were, however, hampered by the lack of high-precision datasets. Däppen et al. (1991), using a full inversion technique (Eq. (38)), found $Y_s = 0.268 \pm 0.01$. Using a similar technique Dziembowski et al. (1991) found $Y_s = 0.234 \pm 0.005$. Kosovichev et al. (1992), again through inversion of Eq. (38), found $Y_s = 0.232 \pm 0.006$. They did a thorough analysis to determine the cause of the variation between different results about Y_s obtained through inversions and found that the major source of systematic error is the equation of state. The problem with the spread of results remained even when better data were available. Richard et al. (1998) found $Y_s = 0.248 \pm 0.002$ using reference models constructed with the MHD equation of state, and Di Mauro et al. (2002) found $Y_s = 0.2457 \pm 0.0005$ using reference models with the MHD equation of state and $Y_s = 0.2539 \pm 0.0005$ using models with the OPAL equation of state.

There are of course other ways to determine the helium abundance and some have been described in Section 3.3. Vorontsov et al. (1992) using a different technique found $Y_s = 0.25 \pm 0.01$. Guzik and Cox (1992), by comparing frequencies of models with different Y_s with observations, found $Y_s = 0.24 \pm 0.005$ in the solar envelope. Antia and Basu (1994b) studied the sensitivity of the estimated Y_s to the equation of state for techniques based on calibrating $W(r)$ (Eq. (39)) or other equivalent functions. When using the function $W(r)$ to determine Y_s, they found that models constructed with equations of state such as EFF were inadequate to determine the solar helium abundance, while models using the MHD equation of state yielded better results giving $Y_s = 0.252 \pm 0.003$ for the Sun. The OPAL equation of state was not available at that time. Basu and Antia (1995) used both MHD and OPAL equations of state, and found that the calibration methods of finding Y_s were less sensitive to the differences between the two equations of state than results obtained by inverting Eq. (38). They obtained $Y_s = 0.246$ using calibration models constructed with MHD equation of state and $Y_s = 0.249$ for models with OPAL equation of state. This work used frequencies from the Big Bear Solar Observatory (Libbrecht et al., 1990). The errors due to errors in frequencies in each case was very small, but taking into account systematic errors in the calibration technique and some uncertainty from the equation of state, they estimated the solar helium abundance to be $Y_s = 0.249 \pm 0.003$. Using better data from both GONG and MDI projects, Basu (1998) found $Y_s = 0.248$.

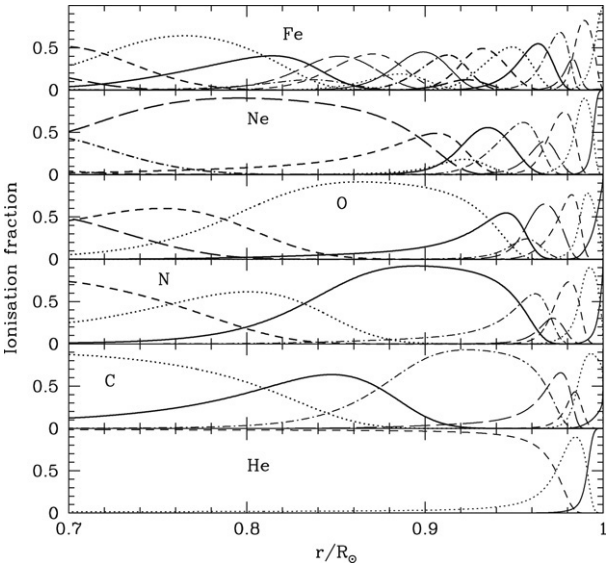

Fig. 8. The fractional abundances of different ionization states of some elements in a solar model plotted as a function of radius. The elements are marked in each panel. Different lines represent the fractional abundance of different ionization states, and the states can be identified by the fact that the peak in the abundance shifts inwards for each successive ionization state. The CEFF equation of state was used in these calculations.

Basu and Antia (2004) studied the effects of heavy-element abundances on the estimated Y_s to find that Y_s is not very sensitive to the value of Z in the calibration models. They estimated $Y_s = 0.2485 \pm 0.0034$ using calibration models with $Z/X = 0.0171$. This is remarkably close to the estimate Basu and Antia (1995) obtained using calibration models with $Z/X = 0.0245$. This may be a coincidence since there is a small change in the value of Y_s caused by improvements in input physics and also because of the availability of better seismic data from GONG and MDI during the intervening years. It turns out that the estimated value of hydrogen abundance X is remarkably insensitive to Z. This would imply that $Y = 1 - X - Z$ will increase slightly when Z decreases. Thus a decrease of the solar-envelope Z by 0.0048 between the GS98 and AGS05 values will lead to an increase in Y_s by 0.0048. Trampedach et al. (2006), while doing a detailed comparison of the effects of OPAL and MHD equations of state on solar models, have pointed out that He II ionization zone also coincides with the O III ionization zone (see Fig. 8). Because of this the estimated helium abundance is affected and the effect is to increase estimated Y_s when Z is reduced. Using the MHD equation of state they estimate that Y_s should increase by 0.0039 when Z is reduced from 0.018 to 0.011. This is slightly less than the effect seen by Basu and Antia (2004). The differences could be due to differences in the equation of state — Basu and Antia (2004) used the OPAL equation of state. Alternately, the difference could be due to the ionization zones of other elements, not accounted for by Trampedach et al. (2006), that also coincide with the He II ionization zone. These other overlapping ionization zones can also be seen in Fig. 8. The OPAL equation of state used in this study includes only the heavy elements C, N, O and Ne in proportions that are different from the AGS05 mixture. This introduces some systematic error in the seismic estimate of Y_s. Basu and Antia (2004) calculated X using calibration models constructed with different values of X with fixed Z. By trying different heavy-element mixtures and Z values, they found that the estimated X for the Sun appears to be fairly independent of Z. When models with reduced Z are used for calibration they will have less contribution from heavy elements and as a result the solar value of Y_s could be slightly overestimated, as discussed by Trampedach et al. (2006). Thus it would be preferable to use the seismic results for X_s, the surface value of X, which are less sensitive to Z. Using MDI and GONG data, Basu and Antia (2004) found $X_s = 0.7389 \pm 0.0034$ using calibration models that had $Z/X = 0.0171$.

4.2. Seismic tests of input physics

As Eq. (31) shows, inverting the frequency differences between models and the Sun immediately tells us how different the models are compared with the Sun. This allows us to test different solar models. Additional tests of solar models are the position of the base of convection zone and the abundance of helium in the convection zone. By

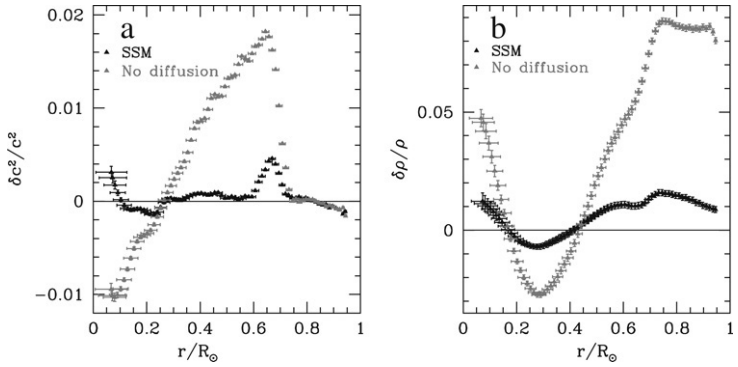

Fig. 9. The relative sound-speed (panel a) and density (panel b) differences between the Sun and two solar models as obtained by inverting the MDI 360-day data set. One model is a standard solar model and includes diffusion, the other does not. Other physics inputs are the same. The models have $Z/X = 0.0245$ and are from Basu et al. (2000).

examining differences between the Sun and solar models constructed with different input physics like the treatment of diffusion, equation of state, opacity, nuclear energy generation rates, etc., one can test these inputs.

The analysis of the solar sound-speed profile just below the base of the convection zone demonstrated the need to include gravitational settling of helium and heavy elements below the convection zone (Christensen-Dalsgaard et al., 1993). The need for diffusion had earlier been discussed by Michaud et al. (1984) as a means to solve the problem of lithium abundance in stars. Vauclair and Vauclair (1982) proposed diffusion as the explanation for the large abundance variations in main sequence and horizontal branch stars, as well as in white dwarfs. Demarque and Guenther (1988) and Cox et al. (1989) constructed solar models that included diffusion to find that the mode-frequencies of models with diffusion match observed solar frequencies better than those of models without diffusion. Incorporation of diffusion of helium and heavy elements in solar models led to significantly better agreement with seismic inversions. The main reason for the improvement is that models with diffusion have a deeper convection zone than models without diffusion — for models with the Grevesse and Noels (1993) and GS98 values of Z/X, the position of the base of the convection zone almost matches that of the Sun when diffusion is included. Diffusion causes a buildup of helium and metals at the base of the convection zone and this in turn results in an increase in opacity at relatively high temperatures, resulting in a deeper convection zone in models with diffusion. Incorporating diffusion also leads to a better agreement between the convection-zone helium abundance of the models and the Sun. Models without diffusion have helium abundances of about 0.27–0.28, much larger than the seismically derived value of 0.24–0.25. The enormous improvements in solar models caused by the inclusion of diffusion has resulted in diffusion being considered as one of the standard ingredients in the construction of solar models. All modern standard solar models, such as those of Christensen-Dalsgaard et al. (1996), Guzik and Swenson (1997), Guenther and Demarque (1997), Brun et al. (1998), Neuforge-Verheecke et al. (2001a,b), Couvidat et al. (2003) and Bahcall et al. (2005a,b,c), etc., incorporate diffusion of helium and heavy elements.

Since diffusion plays a major role in the Sun, it must be important in other stars too. Diffusion moves helium from the outer layers to the core, which decreases the hydrogen abundance in the core, thereby decreasing the main-sequence lifetime of stars (Stringfellow et al., 1983). Proffitt and Vandenberg (1991) found that including helium diffusion reduces globular cluster ages as determined from the main-sequence turn-off by 10%. However, ages determined from the difference in luminosity between the main-sequence turn-off and the zero-age horizontal branch are less affected (Chaboyer et al., 1992a,b) except at very low metallicities. Not accounting for diffusion can also lead to errors when determining the ages of individual stars by matching their positions on the HR diagram (Weiss and Schlattl, 1998). The settling of heavy elements, such as lithium, below the convection zone also means that diffusion must be taken into account while deriving the primordial abundance of such elements (see e.g., Vauclair (1998)).

Modern solar models agree very well with the Sun. Fig. 9 shows the relative difference in sound speed and density between the Sun and a standard solar model as obtained by inverting Eq. (31). The model includes diffusion. For contrast, also shown in the figure is the result for a model without diffusion which has the same physics as the model with diffusion. It is clear that in most of the interior, the sound speed in a solar model is within about 0.1% of that in the Sun. With the data set used, the surface layers cannot be resolved, but for the rest we can see that the maximum

difference in sound speed occurs just below the base of the convection zone. Although, we show only one standard solar model, all others give qualitatively similar results and differ only in detail. The strong peak in the relative sound-speed difference has been identified to be the result of the sharp gradient in the helium abundance just below the base of the convection zone in solar models with diffusion (e.g., Basu and Antia (1995) and Christensen-Dalsgaard et al. (1996)). This discrepancy can be alleviated if some mixing is included in the region just below the convection-zone base. Helioseismic tests show that the increase in Y below the solar convection-zone base is not as steep as in the models (Antia and Chitre, 1998). Inversions to obtain the rotation rate in the solar interior (e.g., Thompson et al. (1996) and Schou et al. (1998b)) show the presence of a strong shear-layer around the base of the convection zone, referred to as the tachocline (Spiegel and Zahn, 1992). The strong shear in the tachocline may lead to turbulence, which could mix these layers and smooth out the composition profiles in this region. Models which incorporate mixing in the tachocline region do show better agreement with the Sun (Richard et al. (1996), Brun et al. (1999) and Basu et al. (2000); etc.).

The small difference between the Sun and the solar models, particularly in the core, led helioseismologists to believe that the solar neutrino problem was not caused by deficiencies in the solar models but by deficiencies in the standard model of particle physics which postulates mass-less neutrinos (e.g., Bahcall et al. (1997), Antia and Chitre (1997), Takata and Shibahashi (1998), Watanabe and Shibahashi (2001); etc.). Bahcall et al. (1998) showed that if a solar model that satisfied the observed solar neutrino constraints provided by the Chlorine experiment was constructed, the sound-speed difference between the Sun and the model will be about 10% in the core — much worse than that for a standard solar model. Therefore, they claimed, the problem must be with our knowledge of neutrino physics. Similar inferences were obtained by comparing observed neutrino fluxes from different experiments (e.g., Hata et al. (1994), Haxton (1995), Castellani et al. (1997) and Heeger and Robertson (1996)) without involving solar models. The helioseismic inference about solution of the solar neutrino problem has since been confirmed by results from the Sudbury Neutrino Observatory (Ahmad et al., 2002). With this, the role of helioseismology in the study of solar neutrinos has been reversed since now the Sun can be used as a well-calibrated source of neutrinos. The observed neutrino fluxes at Earth are now used to study the properties of neutrinos, such as mass differences and mixing angles between different neutrino eigenstates (e.g., Bandyopadhyay et al. (2002) and Bahcall and Peña-Garay (2004); etc.).

Except for a small region near the surface, the convection zone is almost adiabatically stratified and hence its structure is determined by the equation of state and composition. As discussed in Section 3.5, several methods can be used to test the equation of state used in constructing solar models. By comparing frequencies of models with those of the Sun, Christensen-Dalsgaard and Däppen (1992) concluded that the older, simpler EFF equation of state needed corrections for Coulomb effects. Antia and Basu (1994b) compared the function $W(r)$ (cf., Eq. (39)) for the Sun and different models and concluded that the MHD equation of state was better than older equations of state such as the EFF equation of state. Using the same function, Antia and Basu (2006) also concluded that the CEFF equation of state, i.e., the EFF equation of state with Coulomb corrections is almost as good as the OPAL equation of state throughout most of the convection zone. Similarly, Christensen-Dalsgaard and Däppen (1992) also found that CEFF equation of state gives a satisfactory agreement with the seismic data. Basu and Antia (1995, 1997) examined the details of the sound-speed difference between models and the Sun in layers just below the He II ionization zone to conclude that the OPAL equation of state was a better description of the solar equation of state than the MHD equation of state. Basu et al. (1996) examined the sound-speed difference between models constructed with MHD and OPAL equations of state throughout the Sun to find that OPAL models were in better agreement with the Sun at all radii compared to models with MHD equation of state. This led them to conclude that the OPAL is better than MHD for the Sun.

There have also been studies on the equation of state using the Γ_1 differences between the models and the Sun. By looking at the Γ_1 differences in the core, Elliott and Kosovichev (1998) showed that both OPAL and MHD equations of state used in the construction of models of solar-type stars were deficient at high-temperature and high-density regimes. The cause of the discrepancy was identified as the use of the non-relativistic approximation to describe partially degenerate electrons instead of the relativistic Fermi–Dirac integrals. The deficiency has since been corrected in both the OPAL equation of state (Rogers and Nayfonov, 2002) and the MHD equation of state (Gong et al., 2001). Since Γ_1 in the outer layers depends on the structure in addition to the equation of state, Basu and Christensen-Dalsgaard (1997) used the so-called "intrinsic Γ_1" difference (cf., Eq. (40)). They found that the EFF equation of state was very obviously deficient, and that the CEFF, MHD, and OPAL were reasonably similar, except that the MHD equation of state had problems just below the He II ionization zone. Basu et al. (1999) did a more detailed study of

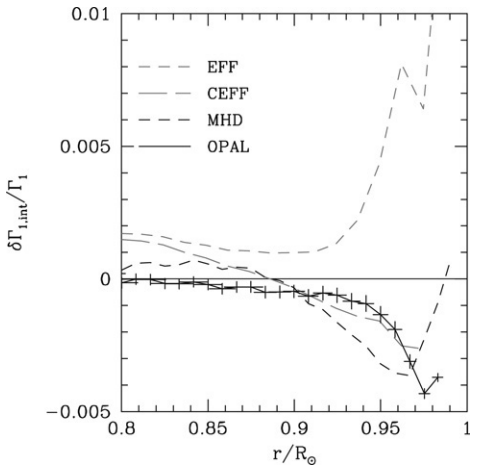

Fig. 10. The intrinsic Γ_1 difference between the Sun and solar models constructed with different equations of state. All models have $Z/X = 0.0245$.

the differences between the MHD and OPAL equations of state and found that while indeed the MHD equation of state fared poorly compared to the OPAL below the He II ionization zone, it did better than OPAL much closer to the surface. The intrinsic Γ_1 differences between the Sun and the models constructed with different equations of state are shown in Fig. 10.

Opacities used in constructing solar models can also be tested. Guzik and Cox (1991) compared frequencies of models with those of the Sun and suggested that the then used solar opacities (Cox and Tabor, 1976) were too low. Somewhat more quantitative results can be obtained by comparing the structure of models with that of the Sun. Saio (1992), assuming that the the sound-speed difference between models and the Sun were completely due to opacity errors, found that the discrepancy between models and the Sun can be reduced below the convection zone if the Los Alamos opacities (Weiss et al., 1990) were increased by 20%–50%. The publication of the OPAL opacity tables by Rogers and Iglesias (1992) resolved this problem and confirmed that opacities needed to be increased substantially in region near the base of the convection zone. The Cox–Tabor and Los Alamos opacities are not in use these days, but similar methods can be used to determine changes to OPAL opacities used today. Tripathy and Christensen-Dalsgaard (1998), using the same assumption as that of Saio (1992), calculated kernels linking the opacity changes to sound-speed changes. Tripathy and Christensen-Dalsgaard (1998) also used these kernels to determine the opacity changes needed to explain the sound-speed differences between the Sun and Model S of Christensen-Dalsgaard et al. (1996). Basu and Antia (1997) found that the relative density differences between models and the Sun were much more sensitive to opacities than the sound-speed differences were, and using solar-envelope models with the correct position of the convection-zone base concluded that the OPAL opacities were indeed consistent with seismic constraints. Of course the result were based on models that had the then accepted value of Z/X, i.e., 0.0245.

Assuming that opacities, equation of state, and nuclear energy generation rates are known, one can also infer the temperature and hydrogen-abundance profiles of the Sun. For this one uses the equations of thermal equilibrium coupled with the sound-speed and density profiles inferred through primary inversions, and a specified heavy-element abundance profile. Once all these profiles are calculated, it is possible to calculate the total energy generated through nuclear reactions. In general, this computed energy does not agree with the observed solar luminosity, and the difference between the two provides a test of the input physics as well as the heavy-element abundance profile used in the calculations. The nuclear energy generation rate in the solar interior is primarily controlled by the reaction rate for the p–p reaction, which has not been measured in laboratories. This reaction rate is computed theoretically and seismic data allow us to test these calculations (Antia and Chitre, 1998, 1999, 2002; Degl'Innocenti et al., 1998; Schlattl et al., 1999). The current seismic estimate for this reaction rate $S_{11} = (4.07 \pm 0.07) \times 10^{-25}$ MeV barns (Antia and Chitre, 2002; Brun et al., 2002), is consistent with the latest theoretical estimate of $S_{11} = (4.00 \pm 0.03) \times 10^{-25}$ MeV barns (Adelberger et al., 1998).

5. Solar abundances

The Sun is unique among stars in that there are multiple ways to determine its heavy-element abundance. Spectroscopy allows us to determine the heavy-element abundance of the solar photosphere, chromosphere and corona, and sometimes in sunspots. Solar abundances can also be determined from solar winds (cf., Bochsler (2007a)) and solar energetic particles (cf., Stone (1989) and Reames (1994, 1998)). And another important source of solar abundance information are C1 chondrites — i.e., meteorites that have never been heated to melting temperatures. These meteorites are expected to have preserved the original composition of the solar nebula, except for the most volatile elements like, H, C, N, O and the noble gases. Meteoritic abundances are usually given relative to silicon, which is used as a bridge to determine the photospheric abundances of meteoritic elements. For most of the non-volatile elements, the agreement between meteoritic and photospheric abundances determined through spectroscopy is fairly good. The meteoritic abundances may be expected to represent the initial solar abundance, which is different from the current photospheric abundances because of the diffusion of helium and heavy elements below the convection zone. If the diffusion rates of various heavy elements are different, their relative abundance could also be different in the meteorites compared to the present-day solar photosphere. The accuracy of current photospheric abundance determinations is probably not sufficient to detect these small differences. The abundances of elements is usually expressed in a logarithmic-scale. This scale is normalized with respect to the hydrogen abundance, which is assumed to have a logarithmic abundance of 12. Thus if N_A/N_H is the ratio of the number densities of element A and hydrogen respectively, then the "abundance" of A is written as $\log_{10}(N_A/N_H) + 12$ dex, this is often denoted by $\log \epsilon(A)$.

The method of determining solar abundances from spectroscopy is the same as that for other stars and can be broken down into four steps: (i) identifying the lines to be used to measure the abundance, (ii) construction of a model atmosphere, (iii) use the model atmosphere to do a line-formation calculation, and (iv) determine the abundance either using a curve-of-growth analysis or through spectral synthesis. In principle, this process is iterative since the model atmosphere in step (ii) also depends on abundances obtained in step (iv). Hence, ideally these steps should be repeated till model becomes self-consistent, though in practice this is often not done. Techniques to analyze stellar spectra are described by Gray (2005). The calculations are usually done under the assumption of local thermodynamic equilibrium (LTE), though non-LTE calculations are gaining ground since departures from LTE affect many lines. Usually, a 1D photospheric model with a given T–τ relation is used. Since these models lack dynamical information, free parameters are used to represent the line-broadening effects of turbulence on the spectral lines in either the form of micro-turbulence or macro-turbulence. The micro-turbulence parameters are supposed to account for the effects of turbulent elements that are smaller than unit optical depth. Macro-turbulence is the effect of turbulent elements larger than unit optical depth. Micro-turbulence is brought into the radiative-transfer calculations by increasing the thermal velocity in the absorption coefficients. Calculations to estimate the effect of macro-turbulence on lines bypass radiative-transfer calculations altogether. These effects are usually determined by convolving the line intensity function calculated without macro-turbulence to the velocity distribution of the macro-turbulent cells. In either case only kinematic effects are included. These effects, however, cannot reproduce the line-bisectors of stellar spectral lines and hence, cannot reproduce the spectral lines accurately.

Modern solar abundance calculations usually rely on semi-empirical photospheric models such as those by Vernazza et al. (1973), Holweger and Müller (1974) and Maltby et al. (1986), or on photospheric models obtained from ab initio calculations, such as those obtained by using the MARCS code (Gustafsson et al., 1975) and the atmospheric model of Kurucz[3] (Kurucz (1970), Sbordone et al. (2004) and Kurucz (2005a,b), etc.). The semi-empirical atmospheric models rely on some form of inversion procedure to infer the stratification of the solar atmosphere using spectral lines formed at different heights. The atmospheric models keep improving with advances in input physics. In addition to the model atmosphere, there is one important input to the whole process of determining abundances from spectroscopy, and that is the transition probability (or alternately the oscillator strength) of the line. Improvements in the measurement of oscillator strengths can lead to sudden changes in the estimated abundance, an interesting case being that of the abundance of iron in the late 1960s and early 1970s. Garz and Kock (1969) measured the oscillator strengths of thirty iron lines leading to a downward revision of the oscillator strength. This led to a nearly ten-fold increase in the estimated solar iron abundance (Garz et al., 1969; Baschek et al., 1970); etc.). In

[3] Atmospheric models of Kurucz can be downloaded from http://kurucz.harvard.edu.

addition, including line-broadening effects (other than turbulence already mentioned earlier) is important. Errors and uncertainties in spectroscopic techniques to determine stellar abundances have been discussed by Johnson (2002).

Solar abundance determinations started with spectroscopy. Russell (1929) estimated the line intensities of several lines by eye and derived the abundances of more than fifty elements. An important conclusion from his work was that the Sun was largely made of hydrogen. The abundance of helium was not known at that time. Unsöld (1948) had much better data and techniques at his disposal and determined the abundances of twenty five elements. Surprisingly, Russell's estimates were not very different from those of Unsöld (1948). Perhaps the first "modern" abundance analysis is that by Goldberg et al. (1960). They did a careful curve-of-growth analysis with improved photospheric models and oscillator strengths to determine the abundances of more than forty elements. Since the work of Goldberg et al. (1960), many groups have been engaged in determining solar abundances through spectroscopy. The abundance of carbon, nitrogen and oxygen, elements that are important for solar structure, are usually derived from photospheric lines.

The solar photospheric spectrum however, does not contain lines of the noble gases. As a result, the abundances of these elements are determined from coronal lines, solar energetic particles or solar wind. This includes determining the abundances of helium and neon. Helium, of course, is the second most abundant element, and its abundance determines the evolution of the Sun, and neon is an important source of opacity in the solar interior. Owing to their very low abundances, other noble gases do not affect solar structure or evolution significantly. Initial estimates of the solar helium abundance were obtained through theoretical solar models (e.g., Strömgren (1938) and Schwarzschild (1946)) as explained in Section 2.3. This continued to be the most reliable technique until seismic techniques were developed (cf., Section 3.3). Although helium was discovered in a prominence spectrum, it is difficult to use prominence spectra for abundance determinations because these regions are more difficult to model than the photosphere and equilibrium conditions do not apply. Values of $N_{\rm He}/N_{\rm H}$ ranging from 0.065 to 0.16 were obtained from prominence and flare spectra (e.g., Hirayama (1979), Heasley and Milkey (1978) and Feldman et al. (2005)). Observations made in 1985 by the Coronal Helium Abundance Spacelab Experiment (CHASE) on the space shuttle Challenger yielded an abundance of 0.070 ± 0.011 (Gabriel et al., 1995b). Similar results were obtained from solar winds and solar energetic particles. Furthermore, the helium abundance found in the slow solar wind was found to vary with solar cycle. It varies from 0.02 during minimum activity to 0.04 during maximum activity (Aellig et al., 2001). Owing to these difficulties, attempts were made to measure the helium abundance in giant planets that may be expected to preserve the abundances at the time of formation of solar system. The Voyager spacecraft was used to measure the abundance ratio of helium to hydrogen in Jupiter and Saturn and it was found to be 0.057 ± 0.013 and 0.016 ± 0.013 respectively (Gautier et al., 1981; Conrath et al., 1984), lower than the expected value. Uranus and Neptune, however, yielded a value of 0.092 ± 0.017 (Conrath et al., 1987) which is close to the now accepted value. Later measurements by the Galileo spacecraft have resulted in a higher value, 0.078, for Jupiter (von Zahn and Hunten, 1996), while a reanalysis of Voyager data for Saturn (Conrath and Gautier, 2000) has also yielded higher value of $Y = 0.18$–0.25 (by mass). As a result of these discrepant results, most of the early estimates of the solar helium abundance were obtained from extrasolar sources, such as planetary nebulae, H II regions, or hot stars in solar neighborhood (e.g., Bowen (1935)).

The major problem in determining the abundance of elements using coronal lines or solar wind is that the abundances in the outer layers of the Sun show evidence of fractionation. This occurs at low-chromospheric levels leading to the so-called FIP (first ionization potential) effect. Elements with low first ionization potential ($\leq$10 eV) show much higher abundances in the corona than in the photosphere. The FIP effect also varies strongly with coronal structure (e.g., Reames (1999)). Abundances in the solar wind also vary tremendously. Elements with a low FIP are overabundant by a factor of 3–5 relative to high-FIP elements in the slow solar wind, but only by a factor of 1.5–2 in the fast streams that emanate from coronal holes (e.g., von Steiger et al. (1995)). Thus these sources are not very useful for determining abundances required for modelling the solar interior. An estimate of the extent of fractionation can be obtained by studying elements which have both photospheric and coronal lines. However, these elements have comparative low first ionization potential compared to the noble gases, e.g., the FIP of C, N and O are 11.3, 14.5 and 13.6 eV, respectively, while those for He and Ne are 24.6 and 21.6 eV respectively. Thus it is difficult to get a direct calibration of fractionation for noble gases because of the lack of elements with comparable first ionization potentials. Even if the normal correction for fractionation is applied, the estimated helium abundance from coronal studies is about 0.2 dex lower than the currently accepted value (Anders and Grevesse, 1989). It turns out that currently the most precise method for determining the solar helium abundance is through helioseismology as has been discussed in Sections 3.3 and 4.1. While the issue of the solar helium abundance has been resolved, Neon poses a difficulty:

because there are no independent estimates on the solar neon abundance, it is difficult to estimate the systematic error in its abundance determined from coronal lines. The abundance of neon is still determined from the outer layers of the Sun and hence uncertainties are large. These are generally based on the relative abundance of neon with respect to either oxygen or magnesium. From the ratio Ne/O or Ne/Mg one can determine the absolute abundance of neon by using the photospheric value of O or Mg abundances. Appropriate corrections need to be applied for the FIP effect, particularly for Ne/Mg since Mg is a low-FIP element. In view of the FIP effect, it is not clear if this gives the correct photospheric abundance of neon, and it should be noted that the same technique failed to give reliable abundance estimates of helium. Recently Drake and Ercolano (2007) have suggested that the solar neon abundance can be measured by observing the Ne Kα line that is fluoresced by coronal X-rays and is emitted near the temperature minimum region of the solar atmosphere. They have done Monte Carlo simulations to show that it would be feasible to use this line if good quality spectra of the relevant spectral region are available. This uncertainty in neon abundance plays a role in the current controversy about solar abundances and is discussed later in Section 7.3.

For many elements, particularly refractory elements, meteoritic abundances are more precise than spectroscopic abundances. Meteoritic abundances have been measured extensively since the 1920s and 1930s. Early meteoritic-abundance estimates were systematically tabulated by Goldschmidt (1937). Brown (1949) and Suess and Urey (1956) put together tables of "cosmic abundances" by choosing among different source of data. Among the more recent tables of meteoritic abundances are those by Cameron (1982) who based it on his previous works, and those of Anders and Ebihara (1982), Palme and Beer (1993), and Lodders (2003). The abundance of refractory elements in the C1 chondrites and the Sun is now believed to be the same (Grevesse and Noels, 1993; Palme and Jones, 2005), and even abundances of moderately volatile elements, such as sodium, zinc and sulfur, are in agreement with the Sun (Palme and Jones, 2005).

There have been significant improvements in abundance determinations during the last few decades. Solar photospheric spectra with very high resolution and very high signal-to-noise ratio, covering a large wavelength range from ultraviolet to far infrared, have been obtained from the ground and from space (e.g., Kurucz (1995)). Solar atmospheric models have also improved significantly. Finally, accurate atomic and molecular data including the transition probabilities have been obtained. As a result of all these improvements, discrepancies between the photospheric abundances determined spectroscopically and the abundances in C1 meteorites has steadily decreased.

Solar structure calculations during the last two decades have generally been done using solar abundance tables compiled by Anders and Grevesse (1989) and the updates to that by Grevesse and Noels (1993). This was later superseded by the compilation of GS98. The default OPAL opacity tables are calculated for Grevesse and Noels (1993) mixture, though recently it has become possible to calculate OPAL opacity tables for any specified mixture of 19 heavy elements listed in Table 2.[4] The abundance table of Anders and Grevesse (1989) was an update of the meteoritic data of Anders and Ebihara (1982) and Grevesse (1984a,b). They obtain $Z/X = 0.0274$ for the Sun and C, N, O abundances of $\log\epsilon(\mathrm{C}) = 8.56 \pm 0.04$ dex, $\log\epsilon(\mathrm{N}) = 8.05 \pm 0.04$, and $\log\epsilon(\mathrm{O}) = 8.93 \pm 0.035$. They have a photospheric Fe abundance of $\log\epsilon(\mathrm{Fe}) = 7.67 \pm 0.03$, and Ne abundance of $\log\epsilon(\mathrm{Ne}) = 8.09 \pm 0.10$ dex. Grevesse and Noels (1993) updated these abundances. In the process, abundances of C, N, O, Ne and Fe were lowered to 8.55 ± 0.05, 7.97 ± 0.07, 8.87 ± 0.07, 8.07 ± 0.06 and 7.51 ± 0.01 respectively. This lowered the total Z to give $Z/X = 0.0245$. The photospheric Fe abundance was lowered because of work by different groups with more accurate transition probabilities. This photospheric Fe abundance matches the meteoritic abundance, while the earlier values did not. The updates for C, N and O were a result of new infrared data observed by the Atmospheric Trace Molecule Spectroscopy (ATMOS) experiment, new transition probabilities for C I, N I and O I lines, and the change in the gas and electron pressures in the Holweger–Müller model atmosphere caused by the change in the Fe abundance. The new neon abundance was a weighted mean of the abundance derived from the analysis of impulsive flare spectra and from solar energetic particles.

The next revision of this table was that by GS98. This revision lowered solar Z further to $Z/X = 0.023$. GS98 redid some of the computations for C, N and O abundances with different photospheric models based on the empirical photospheric model of Grevesse and Sauval (1999). The abundances of C, N and O in their table are 8.52 ± 0.06, 7.92 ± 0.06 and 8.83 ± 0.06 respectively. The iron abundance was lowered slightly to 7.50 ± 0.05, and they changed the neon-abundance estimate to 8.08 ± 0.06 based on the measurements of the Ne/Mg ratio by Widing (1997).

[4] http://www-pat.llnl.gov/Research/OPAL/.

Table 2
A comparison of solar abundances of some elements in tables of Anders and Grevesse (1989, AG89), Grevesse and Noels (1993, GN93), Grevesse and Sauval (1998, GS98) and Asplund et al. (2005b, AGS05)

Element	Z	AG89	GN93	GS98	AGS05
C	6	8.56 ± 0.04	8.55 ± 0.05	8.52 ± 0.06	8.39 ± 0.05
N	7	8.05 ± 0.04	7.97 ± 0.05	7.92 ± 0.06	7.78 ± 0.06
O	8	8.93 ± 0.04	8.87 ± 0.04	8.83 ± 0.06	8.66 ± 0.05
Ne	10	8.09 ± 0.10	8.07 ± 0.06	8.08 ± 0.06	7.84 ± 0.06
Na	11	6.33 ± 0.03	6.33 ± 0.03	6.33 ± 0.03	6.17 ± 0.04
Mg	12	7.58 ± 0.05	7.58 ± 0.05	7.58 ± 0.05	7.53 ± 0.09
Al	13	6.47 ± 0.07	6.47 ± 0.07	6.47 ± 0.07	6.37 ± 0.06
Si	14	7.55 ± 0.05	7.55 ± 0.05	7.55 ± 0.05	7.51 ± 0.04
P	15	5.45 ± 0.04	5.45 ± 0.04	5.45 ± 0.04	5.36 ± 0.04
S	16	7.21 ± 0.06	7.21 ± 0.06	7.33 ± 0.11	7.14 ± 0.05
Cl	17	5.50 ± 0.30	5.50 ± 0.30	5.50 ± 0.30	5.50 ± 0.30
Ar	18	6.56 ± 0.10	6.60 ± 0.14	6.40 ± 0.06	6.18 ± 0.08
K	19	5.12 ± 0.13	5.12 ± 0.13	5.12 ± 0.13	5.08 ± 0.07
Ca	20	6.36 ± 0.02	6.36 ± 0.02	6.36 ± 0.02	6.31 ± 0.04
Ti	22	4.99 ± 0.02	5.04 ± 0.02	5.02 ± 0.06	4.90 ± 0.06
Cr	24	5.67 ± 0.03	5.67 ± 0.03	5.67 ± 0.03	5.64 ± 0.10
Mn	25	5.39 ± 0.03	5.39 ± 0.03	5.39 ± 0.03	5.39 ± 0.03
Fe	26	7.67 ± 0.03	7.51 ± 0.01	7.50 ± 0.05	7.45 ± 0.05
Ni	28	6.25 ± 0.04	6.25 ± 0.04	6.25 ± 0.04	6.23 ± 0.04
Z/X		$.0274 \pm .0016$	$.0244 \pm .0014$	$.0231 \pm .0018$	$.0165 \pm .0011$

Abundances are in units of $\log_{10}(A/\mathrm{H}) + 12$.

The compilations of GS98 were changed dramatically by AGS05. Most of the updates were a results of the new abundance determinations by Allende Prieto et al. (2001, 2002) and Asplund et al. (2004, 2005a). All these calculations were based on 3D atmospheric models obtained from simulations of the upper convection zone and lower photosphere of the Sun. Since this change is the main effect responsible in decreasing the total heavy-element abundances of the Sun, we discuss these works, and others that followed, in some detail. A comparison of the abundances of some of the elements in the GS98, AGS05 and earlier tables is given in Table 2. This table includes all elements used in OPAL opacity calculations.

Although oxygen is the most abundant of all heavy elements, determining its abundance spectroscopically is problematic since the relevant spectral lines are difficult to model. The forbidden lines at 630 nm and 636.3 nm are affected by blends, while the O I triplets at 777.3 nm and 844.6 nm require extensive NLTE corrections. Additionally, OH and CO lines are also difficult to model and are very sensitive to atmospheric models. As a result, the solar oxygen abundance determined from various lines do not generally agree with each other (e.g., Reetz (1999)). It should be noted that 1D atmospheric model can only represent an average atmospheric structure. Such models cannot represent thermal inhomogeneities and velocity fields that are present in the solar atmosphere. Kiselman and Nordlund (1995) attempted to determine the solar oxygen abundance using a 3D model with NLTE treatment. Although, they found some improvement in the sense that the abundances determined from different lines were somewhat closer to each other, the differences were still significant. They pointed out that an oxygen abundance of less than 8.8 dex may be justified from their studies.

Asplund et al. (1999, 2000b) started a systematic investigation using 3D radiative-hydrodynamical simulations of solar convection instead of 1D model atmospheres to determine solar abundances from spectroscopy. They first applied the 3D models to some Fe I and Fe II lines. These model atmospheres include dynamic information and hence free parameters for turbulence are not required to fit spectral lines. These models are, however, the result of a simulation, and hence, whether or not they really represent the solar atmosphere depends on the input physics and correct treatment of radiative transfer in the simulation. The 3D simulation used by Asplund et al. (2000b) was obtained with the 3D compressible, radiative-hydrodynamic code developed to study solar surface convection and granulation developed by Nordlund and Stein (1990), and Stein and Nordlund (1989, 1998). This is a large eddy simulation (LES) code. The equations of mass, momentum, and energy conservation coupled to the radiative-transfer equation along a ray are solved. The simulations have periodic boundary conditions in the horizontal direction and

transmitting boundary conditions at the top and bottom. The simulation covers a small part of the solar atmosphere and the convection zone with a horizontal extent of 6×6 Mm and a vertical extent of 3.8 Mm of which about 1.0 Mm is above the level at which optical depth for the continuum is unity. They had $200 \times 200 \times 82$ grid points in their simulations which typically covered 2 solar hours. The code uses the hyper-viscosity diffusion algorithm described by Stein and Nordlund (1998) for numerical viscosity. Radiative transfer is assumed to happen in LTE. The 3D equation of radiative transfer is solved along 8 inclined rays using the opacity binning technique (Nordlund, 1982), and four bins were used. The code used the MHD equation of state. Continuum opacities of Gustafsson et al. (1975, and updates) were used, and line opacities were privately obtained from Kurucz. The simulations were done using the GS98 solar heavy-element abundances. The simulation was then used as the model atmosphere to do line-formation calculations using a spectral line-formation code. To do the spectral line calculation, a 50 min subset of the simulations was chosen with snapshots stored at every 30 s. They were also interpolated to a finer depth-scale to improve vertical sampling. Asplund et al. (2000b) showed that they could get better fits to the Fe lines than conventional 1D calculations even without using free parameters for micro- and macro-turbulence, and also that they could fit the line-bisectors. They did not need any adjustable parameters to fit the lines.

Allende Prieto et al. (2001) used the same simulation to determine the solar oxygen abundance. They analyzed the forbidden [O I] line at 630 nm. Since this being a forbidden line, it is not affected by non-LTE effects, however, this line is blended with a Ni I line. Allende Prieto et al. (2001) used the Uppsala synthesis package of Gustafsson et al. (1975, and updates) for inputs needed for the line-formation calculation, and included natural broadening using data from the Vienna Atomic Line Database (Kupka et al., 1999), and solar line fluxes from Kurucz et al. (1984). The oscillator strength of the Ni I line was not well known and was considered to be a free parameter. Allende Prieto et al. (2001) got a very good fit to the [O I] line for an abundance of $\log \epsilon(\mathrm{O}) = 8.69 \pm 0.05$. However, since this work, the oscillator strength of the Ni I has been measured (Johansson et al., 2003) and the fit to the line is not as good if that value is used (Koesterke et al., 2007). Asplund et al. (2004) investigated the solar oxygen abundance further using the same simulation as the Asplund et al. (2000b) work. They used a mixture of [O I], O I, OH vibration–rotation and OH pure rotation lines. They used the MULTI3D code (Botnen, 1997; Botnen and Carlsson, 1999; Asplund et al., 2003) to do the non-LTE calculations. Instead of the 50 snapshots from the simulations, as was used by Asplund et al. (2000b) and Allende Prieto et al. (2001), they used two. They derived an oxygen abundance of $\log \epsilon(\mathrm{O}) = 8.66 \pm 0.05$, again much smaller than the GS98 value of 8.83 ± 0.06.

Allende Prieto et al. (2002) examined the solar carbon abundance using the [C I] line at 872.7 nm, again using the 3D simulation of Asplund et al. (2000b), and did a calculation similar to what Allende Prieto et al. (2001) did for the [O I] line at 630 nm. They find $\log \epsilon(\mathrm{C}) = 8.39 \pm 0.04$ dex, which is lower than the GS98 value of 8.52 ± 0.05. Asplund et al. (2005a) investigated the solar photospheric carbon abundance using [C I], C I, CH vibration–rotation, CH A-X electronic and C_2 Swan electronic lines using the same simulations and a non-LTE line calculation using the code MULTI (Carlsson, 1986). They get the same abundance as that of Allende Prieto et al. (2002).

AGS05 used the same simulation to study the solar nitrogen abundance using N I and NH vibration–rotation lines. They obtained an abundance of $\log \epsilon(\mathrm{N}) = 7.88 \pm 0.08$ using LTE analysis of N I lines. Since there is no NLTE study of these lines for 3D models they applied the NLTE corrections from Rentzsch-Holm (1996) to get an abundance of 7.85 ± 0.08. They argue that this may require a small downward correction. The NH vibration–rotation lines are more difficult to treat as they are very sensitive to temperature and hence there is a large difference between results obtained from 1D and 3D models. They obtain an abundance of $\log \epsilon(\mathrm{N}) = 7.73 \pm 0.05$ from these lines, which is significantly lower than the value obtained from N I lines.

Earlier, Asplund (2000) used the same 3D simulations to get $\log \epsilon(\mathrm{Si}) = 7.51 \pm 0.04$. This is slightly smaller than the GS98 value of 7.55 ± 0.04 and led AGS05 to the lower abundances of meteoritic elements listed in Lodders (2003). AGS05 have also applied the 3D model to study abundances of other elements and in all cases the abundances are lower than those obtained using 1D models. The Na abundance is obtained using six weak Na I lines to get a value of 6.17 ± 0.04, which is about 0.1 dex lower than the meteoritic value and also lower than the GS98 value. The cause of this discrepancy is not understood. The Al, P and S abundances are also reduced by about 0.1 dex when 3D models are used.

The investigations mentioned in this section resulted in a net lowering of the solar heavy-element abundance to $Z/X = 0.0165$ as compiled by AGS05. The largest effects are due to C, N, O and Ne abundances, these are elements that play important roles in determining solar structure. Since Ne and Ar abundances cannot be determined from photospheric spectra due to the lack of spectral lines, their values were estimated by AGS05 using measured abundance

ratios in the solar corona and solar energetic particles along with the photospheric abundance for oxygen. Thus the reduction in the O abundance, along with refined coronal-abundance ratio from Reames (1999), led to the reduction in the abundances of Ne and Ar. If the Ne/Mg ratio from Feldman and Widing (2003) were used instead, a much higher Ne abundance of 8.06 ± 0.10, a value similar to the GS98 one, would be obtained. Before the AGS05 revision, the two ratios (Ne/O or Mg/O) gave mutually consistent results. This is also true for the abundance of argon. Other changes in abundances, predominantly caused by the lowering of the Si abundance, have been smaller. It should be noted however, that the underlying 3D photospheric model used in each case had the higher GS98 abundances, and the calculations have not been repeated with simulations that have the AGS05 background abundances. Nor have the investigations been re-done with other simulations with different input physics (such as equation of state or opacities), or even different numerical viscosity parameters to check for the sensitivity of the results to the background 3D model.

The main reason for confidence in the abundances obtained using these 3D models is the good agreement with observed line profiles and line-bisectors, and the fact that different lines give similar abundances. While this is true for oxygen, the nitrogen abundance obtained using N I and NH lines are significantly different even when 3D models are used. Another argument in favor of the reduced abundances is that old abundances suggested that the Sun has much higher metallicity as compared to galactic neighborhood and Magellanic clouds (Meyer, 1989; Turck-Chièze et al., 1993, 2004). With the reduced heavy-element abundances the Sun now appears to be naturally enriched in oxygen in comparison with extragalactic H II regions, Magellanic clouds, other clusters and neighbors. One measure of enrichment is the ratio $\Delta Y/\Delta \mathrm{O}$, when ΔY and $\Delta \mathrm{O}$ are respectively the increase in the helium and oxygen abundances over the same epoch. The starting epoch is assumed to be just after the Big Bang nucleosynthesis. Peimbert et al. (2007) estimate the ratio to be 3.3 ± 0.7. Using the primordial helium abundance, $Y_p = 0.2482 \pm 0.0004$ from WMAP (Spergel et al., 2007) we find the ratio of the helium to oxygen enrichment to be 2.78 for a solar model with GS98 abundances and 1.90 for a model with AGS05 abundance. Of course, if a lower primordial helium abundance is used the numbers may change in favor of the AGS05 model. It is not clear if these arguments can be used to constrain solar abundances. Cunha and Lambert (1992) found that the mean oxygen abundance in 18 B type stars in Orion association is $\log \epsilon(\mathrm{O}) = 8.65 \pm 0.12$, which is consistent with the AGS05 value. However, Edvardsson et al. (1993) had done a detailed study of abundances of various elements in 189 F and G type nearby stars, and concluded that solar abundances are consistent with those in other similar stars after accounting for the dispersion in abundances between different stars. Similar conclusions have been drawn by Gustafsson (1998). Furthermore, there is evidence that stars with planetary systems have higher heavy-element abundances as compared to stars without planets (e.g., Santos et al. (2003, 2005)). Thus we would expect the Sun to have a higher metallicity compared to other, average, stars. It should also be kept in mind that comparison of solar abundances with interstellar medium and H II region abundances is affected by dust formation, which traps some elements. Additionally, comparison of solar abundances with that of nearby stars needs to account for diffusion of elements below the outer convection zone. The amount of depletion caused by diffusion depends on the star's age and the thickness of its outer convection zone, and hence a proper comparison is not possible without first determining the amount by which diffusion has depleted the atmosphere of any star. It should be kept in mind that the abundances of other stars are determined by using 1D stellar atmosphere models and these too could change if abundance calculations with 3D models are done.

6. Consequences of the new abundances

Chemical composition enters the equations of stellar structure through input physics like the opacity, equation of state and nuclear energy generation rate. In studies of stellar evolution, it has been found that stars that have lower heavy-element abundances are bluer (higher effective temperature) and more luminous than higher-metallicity stars of the same mass and helium abundance (see e.g., Salaris and Cassisi (2005)). The Sun, however, has a known effective temperature, luminosity and age, and hence whatever the metallicity, a solar model has to have the same effective temperature and luminosity as the Sun at the same age. This usually implies a change in the helium abundance (one of the unknown parameters of the system as described in Section 2.3). Low-metallicity solar models, therefore, generally have lower helium abundances in order to have the correct luminosity at the solar age. Thus solar models with different metallicities have different evolutionary histories that intersect in the HR diagram at the solar age, and the models also have different structures. In this section we examine the consequences of the lowered solar heavy-element abundance on the structure of solar models. Prior to that we discuss why and how heavy-element abundances affect solar structure. It should be noted that spectroscopy measures the photospheric abundance of the Sun. However, the convection-zone

abundances are believed to be the same as the photospheric abundances because of constant convective overshoot into the photosphere. Moreover, the convection zone is believed to be chemically homogeneous because convective turn-over time-scales are much shorter than evolutionary and diffusion time-scales. We should keep in mind that the composition of the solar surface today is not the composition with which the Sun was formed since helium and heavy elements diffuse out of the convection zone to the layers below.

Even before the current revision of heavy-element abundances, solar models with low Z were examined to explore the possibility of reducing neutrino fluxes. Although helioseismic data were not very precise at that point, they did not favor these models (e.g., Christensen-Dalsgaard and Gough (1980)). Much more seismic data have become available since this early work and solar models have also improved through advances in our understanding of input physics. However, the conclusion still remains valid. Of course, as we know today, the solution of the solar neutrino problem lies in non-standard properties of neutrinos rather than non-standard processes in solar models.

The primary effect of the heavy-element abundance on solar structure is through its effect on opacity. Opacity mainly affects the structure of the radiative interior and the position of the base of the convection zone. The structure of the convection zone itself is independent of opacity, except for a thin layer near the surface where convection is inefficient. Of course, there are some indirect effects of Z on the convection zone since conditions at the convection-zone base determine the adiabat that defines the structure of the lower-convection zone. While hydrogen and helium, the main constituents of the Sun, are completely ionized in the deeper parts of the solar interior, some of the heavy elements, such as iron, silicon, sulfur, etc. are only partially ionized. These elements contribute to opacity in these regions through different atomic transitions.

The effect of heavy-element abundances on the equation of state is smaller. The equation of state mainly depends on the number of particles per unit volume. The number density of heavy elements is two orders of magnitude smaller than that of hydrogen or helium, as a result they only have a small effect on pressure. However, the process of ionization of the elements causes the adiabatic index Γ_1 to decrease in the ionization zones. The magnitude of the dip in Γ_1, though small for heavy-element ionization, depends on the abundance of these elements. The structure of most of the convection zone is essentially independent of opacity and is dominated by the equation of state. Thus the effect of heavy-element abundances on the structure of the solar convection zone is due to their effect on the equation of state. The convection zone is also the region where helioseismic inversions are very reliable and hence the equation of state effect is detectable.

Nuclear energy generation in the solar core occurs primarily through the p–p chain, which depends only on the abundance of hydrogen and not that of heavy elements. However, a small fraction of the energy in the Sun is produced by the CNO cycle, which does depend on the abundance of C, N and O. Thus there is some effect of the new abundances on the nuclear energy generation rate too. Using the updated reaction rates for the $^{14}\mathrm{N}(p,\gamma)^{15}\mathrm{O}$ reaction (Runkle et al., 2005), it was found that models with the GS98 abundances produce 0.8% of their energy through the CNO cycle, while models with the AGS05 abundances produce 0.5% of their energy through the CNO cycle (Bahcall et al., 2006). Nuclear energy generation through the CNO cycle is effective only in the inner core. It is not clear whether the effect of the heavy elements on the structure of core is predominantly through their effect on the CNO reaction rate or through their effect on opacities. Most of the heavy elements are fully ionized in these regions, and hence their effect on opacity is small, but the CNO reactions' contribution to the total energy generated is small too. Thus it is not completely clear which effect dominates in the inner core. A related effect of heavy-element abundances on the CNO cycle is in the production of neutrinos. Since the nuclear reaction rates change with change of C, N, and O abundances, the neutrino fluxes from these reactions change too.

In Fig. 11 we show the sound-speed and density differences between a standard solar model constructed with the new AGS05 abundances and the Sun. For comparison, we also show the results for a comparable model constructed with the GS98 abundances. As can be seen from the figure, the new abundances result in a solar model that is much worse than the model with the older abundances in terms of agreement with seismically inferred solar sound-speed and density profiles. Thus it is clear that while solar models with old abundances are closer to the seismically inferred profiles of the Sun, the one using newer abundances differs significantly. The maximum difference in sound-speed and density increases by more than a factor of five when AGS05 abundances are used instead of the GS98 abundances. The root mean-square deviation in squared sound speed, $\langle(\delta c^2/c^2)^2\rangle^{1/2}$, between the solar models and the Sun increases from 0.0014 for the GS98 model to 0.0053 for the model with AGS05 abundances. Similarly the rms density difference, $\langle(\delta\rho/\rho)^2\rangle^{1/2}$, increases from 0.011 to 0.047 when AGS05 abundances are used instead of GS98 (Bahcall et al., 2005a). The model with the AGS05 abundances has a convection-zone helium abundance of

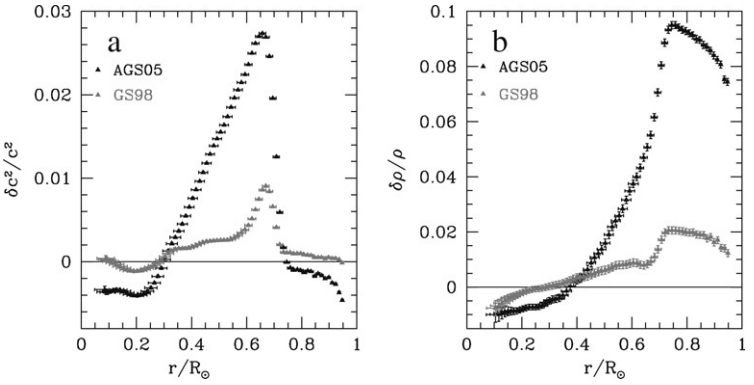

Fig. 11. The relative sound-speed (panel a) and density differences (panel b) between the Sun and a model constructed with the AGS05 abundances (Bahcall et al., 2005c). For comparison we also show the results for a model constructed with the GS98 abundances. MDI 360 day data have been used for the inversions.

$Y_s = 0.230$, much lower than the helioseismically determined value of Y_s. The position of the convection-zone base in that model is $r_b = 0.7289R_\odot$, again very different from the seismically determined value of r_b. We describe below in detail the changes in various parts of the solar model caused by the lowering of Z/X.

6.1. The base of the convection zone

The most easily detectable effect of the reduction of heavy-element abundances is a change in the position of the base of the convection zone. The temperature gradient in the radiative interior is determined by opacity, and hence, its structure is affected by the heavy-element abundances. The base of the convection zone occurs at a point where opacity is just small enough to allow the entire heat flux to be transported by radiation, and thus the location of this point depends on the abundance of those heavy elements that are the predominant sources of opacity in that region. If these abundances are reduced, opacity reduces, and the depth of the convection zone also reduces. Since the depth of the convection zone has been measured very accurately, it is the most sensitive indicator of opacity or heavy-element abundances.

After the revision of the solar heavy-element abundances was announced by Allende Prieto et al. (2001, 2002) and Asplund et al. (2004), Bahcall and Pinsonneault (2004) constructed a solar model with the reduced abundances and found that the depth of the convection zone in the model is reduced significantly with respect to a similar model with the GS98 abundances. The convection-zone base of that model was at $r_b = 0.726R_\odot$, which differs from the seismically determined value by 26σ. Bahcall et al. (2005a) also found a similar value. This solar model used $Z/X = 0.0176$ since some of the downward revisions of abundances found in the tables of AGS05 had not been determined at that stage. Using the same Z/X, Basu and Antia (2004) found $r_b = 0.732R_\odot$. Using a slightly different composition ($Z/X = 0.0172$), Turck-Chièze et al. (2004) found $r_b = 0.7285R_\odot$ for a standard model and $r_b = 0.7312R_\odot$ for a model that incorporates mixing below the convection zone. There is considerable variation in the location of r_b in different models and these arise because of differences in input physics used in calculating the models, but all these values are significantly different from the seismically determined value of r_b when low Z/X is used. The further lowering of Z/X to 0.0165 by AGS05 changed the position of the convection-zone base further, and Bahcall et al. (2005c) found that models constructed with these abundances have $r_b = 0.729R_\odot$, a difference of about 32σ from the seismically determined value. Table 3 lists r_b for several solar models, standard and non-standard, that have been published recently.

Bahcall et al. (2006) studied the consequences of the lowering of Z/X through a detailed Monte Carlo simulation of solar models where parameters controlling input physics were randomly drawn for each model from separate probability distributions for every parameter. The parameters varied include the rates of some of the nuclear reactions, age of the Sun, diffusion coefficients, luminosity, and most importantly the individual abundances of the elements that are used to calculate OPAL opacities. Two types of models were constructed, ones where the central value of the heavy-element abundances were obtained from the GS98 abundances, and another where they were drawn from the AGS05 abundances. Two types of error-distributions were considered for the heavy elements. The so-called

Table 3
The position of the base of the convection zone (r_b) and the helium abundance Y_s in the convection zone for different solar models

Reference	Z/X	r_b	Y_s	Remarks
Basu et al. (2000)	0.0245	0.7123	0.2453	GN93
Bahcall et al. (2001)	0.0229	0.7140	0.2437	GS98
Montalbán et al. (2004)	0.0245	0.714	0.246	GN93
Montalbán et al. (2004)	0.0177	0.727	0.243	
Montalbán et al. (2004)	0.0177	0.723	0.248	Enhanced opacity
Montalbán et al. (2004)	0.0177	0.718	0.249	Enhanced opacity
Montalbán et al. (2004)	0.0177	0.714	0.226	Enhanced diffusion
Montalbán et al. (2004)	0.0177	0.717	0.239	Enhanced diffusion & opacity
Turck-Chièze et al. (2004)	0.0172	0.7285	0.2353	
Turck-Chièze et al. (2004)	0.0172	0.7312	0.2407	Mixing in tachocline
Bahcall et al. (2005a)	0.0176	0.7259	0.238	
Bahcall et al. (2005a)	0.0176	0.7133	0.239	21% increase in opacity
Bahcall et al. (2005a)	0.0176	0.7162	0.243	11% increase in opacity
Bahcall et al. (2005b)	0.0192	0.7174	0.2411	OP, increased Ne
Bahcall et al. (2005b)	0.0207	0.7146	0.2439	OP, increased Ne, CNO
Bahcall et al. (2005c)	0.0229	0.7138	0.243	GS98, OP opacity
Bahcall et al. (2005c)	0.0165	0.7280	0.229	AGS05, OP opacity
Guzik et al. (2005)	0.0244	0.7133	0.2419	GN93
Guzik et al. (2005)	0.0196	0.7022	0.1926	Enhanced diffusion
Guzik et al. (2005)	0.0186	0.7283	0.2339	Enhanced Z diffusion
Guzik et al. (2005)	0.0206	0.7175	0.2269	Enhanced diffusion
Guzik et al. (2005)	0.0173	0.7406	0.2541	Enhanced diffusion
Yang and Bi (2007)	0.0174	0.7335	0.2294	
Yang and Bi (2007)	0.0176	0.7168	0.2225	Enhanced diffusion
Castro et al. (2007)	0.0164	0.730	0.223	
Castro et al. (2007)	0.0165	0.732	0.240	GS98 + low-Z accretion
Castro et al. (2007)	0.0165	0.712	0.249	GS98 + low-Z accretion & Mixing & overshoot

Unless mentioned otherwise, the models were calculated with OPAL opacities.

"optimistic" uncertainties corresponded to the error-bars in the composition tables of GS98 or AGS05; and the so-called "conservative" uncertainties, which assumes that the uncertainty in the abundance of a particular element is the difference in its abundance between the GS98 and the AGS05 tables. For all cases, Bahcall et al. (2006) found that the position of the base of the convection zone had a Gaussian distribution. The "conservative" distribution of the GS98 models shows that the convection-zone base at $r_b = (0.7154 \pm 0.0102)R_\odot$, while for the AGS05 models $r_b = (0.7296 \pm 0.0105)R_\odot$. The 'optimistic' AGS05 models fare worse, with the convection-zone base at $r_b = (0.7280 \pm 0.0037)R_\odot$, showing that changing other solar inputs within their errors do not bring the convection-zone base of any of these low-Z/X models in agreement with the Sun. For the 'optimistic' GS98 models on the other hand, $r_b = (0.7133 \pm 0.0035)R_\odot$, which is consistent with the seismic value.

The large difference in the sound speed between the Sun and the low-Z/X solar model shown in Fig. 11 is caused mainly by the difference in the position of the base of the convection zone. Since convection zones are adiabatically stratified, and thus have larger temperature gradients than radiatively stratified regions, a deeper convection zone results in higher temperatures at the base of the convection zone. The sudden increase in the sound-speed difference in Fig. 11 at the radius corresponding to the convection-zone base indicates that the Sun has a higher temperature than the model in that region which is a result of the deeper convection zone in the Sun. This sharp increase in the sound-speed differences with respect to the Sun is seen for other low-Z models too (see, e.g., Basu and Antia (2004), Turck-Chièze et al. (2004); Montalbán et al. (2004), Bahcall et al. (2005a) and Guzik et al. (2005), etc.). In their Monte Carlo study, Bahcall et al. (2006) too found that average rms sound-speed and density differences between the models and the Sun are much worse for the AGS05 models than the GS98 models.

Since the primary source of discrepancy in solar models is the reduction in opacity due to the lowering of Z/X, it is of interest to identify the elements that are responsible for the opacities in the radiative interior. Fig. 12 shows the logarithmic derivative of opacity with respect to abundances of individual elements. These derivatives are calculated for OPAL opacities at the GS98 abundances. Although the results are plotted as a function of temperature, the

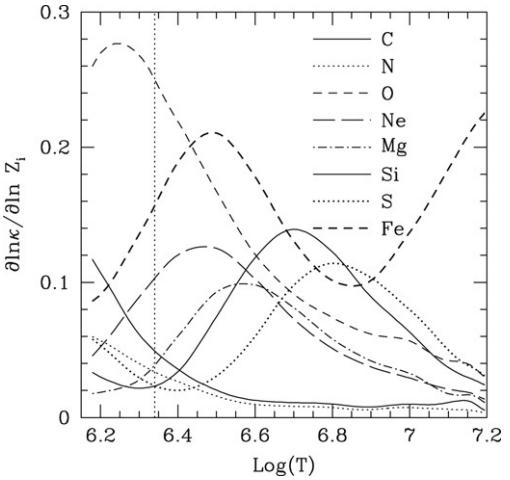

Fig. 12. The logarithmic gradient of opacity with respect to abundances of different heavy elements plotted as a function of temperature. The gradient is calculated at different points in a solar model, using the temperature, density and composition profiles of the solar model. The dotted vertical line in the figure marks the position of the base of the convection zone.

derivatives were calculated at temperature and density values for a solar model. The dashed vertical line in the figure marks the temperature corresponding to the base of the convection zone. It can be seen that elements that have low atomic number, such as C and N, that are more or less completely ionized inside the convection zone do not make a significant contribution to the opacity in the radiative interior. Oxygen, which is the most abundant among the heavy elements in the Sun, is the dominant source of opacity in the region near the base of the convection zone. In addition to O, Fe and Ne also contribute significantly to the opacities in this region. In the solar core, Fe, S, Si and O are the dominant sources of opacity. Thus it is not surprising that a reduction in oxygen abundance has a strong effect on the depth of the convection zone in a solar model.

6.2. *The convection-zone helium abundance*

The largest effect that the lowering of the heavy elements has within the convection zone is a change in the helium abundance Y_s. As mentioned earlier, the helium abundance of solar models needs to be changed in order to ensure that the models satisfy solar constraints at the current age of the Sun. The reduction of Z/X causes a reduction of Y_s in the calibrated solar models. This also implies that the initial helium abundance of the low-Z models at the zero-age main sequence is lower than the initial helium abundance for the higher-Z models. For a $Z/X = 0.0176$ model Basu and Antia (2004) found that helium abundance in the convection zone is 0.237, a difference of about 3σ from the seismically determined value. Similarly, for their $Z/X = 0.0176$ model, Bahcall et al. (2005a) found $Y_s = 0.238$. Turck-Chièze et al. (2004) found $Y_s = 0.235$ for their standard model, and $Y_s = 0.241$ for their model that incorporated mixing below the convection-zone base. All these results are lower than the seismic estimates, though as is evident, the exact value of Y_s in the models also depends on the other physical inputs of the model. The convection-zone helium abundance is lowered further when the AGS05 value of $Z/X = 0.0165$ is used, and Bahcall et al. (2005c) found that their models had $Y_s = 0.230$ when OPAL opacities were used, and $Y_s = 0.229$ when OP opacities were used. Table 3 also lists Y_s for several solar models that have been recently published.

From the results of their Monte Carlo simulations, Bahcall et al. (2006) found that the average Y_s for models with GS98 abundances with the "conservative" errors is $Y_s = 0.2420 \pm 0.0072$, while for the AGS05 models with conservative errors is $Y_s = 0.2285 \pm 0.0067$, i.e., marginally inconsistent with the seismic value. However, with optimistic errors, AGS05 models have $Y_s = 0.2292 \pm 0.0037$, which is more inconsistent. It should be noted that the optimistic uncertainties correspond to the uncertainties in the AGS05 table. The GS98 models with "optimistic" errors have $Y_s = 0.2425 \pm 0.0042$.

Fig. 13 shows the models from Monte Carlo simulations in the r_b–Y_s plane. It can be seen that many of the GS98 models fall in the region that is consistent with seismically determined values, while almost all the AGS05 models are outside the seismically accepted range. From a detailed analysis of the seismic constraints on Y_s and r_b, Delahaye

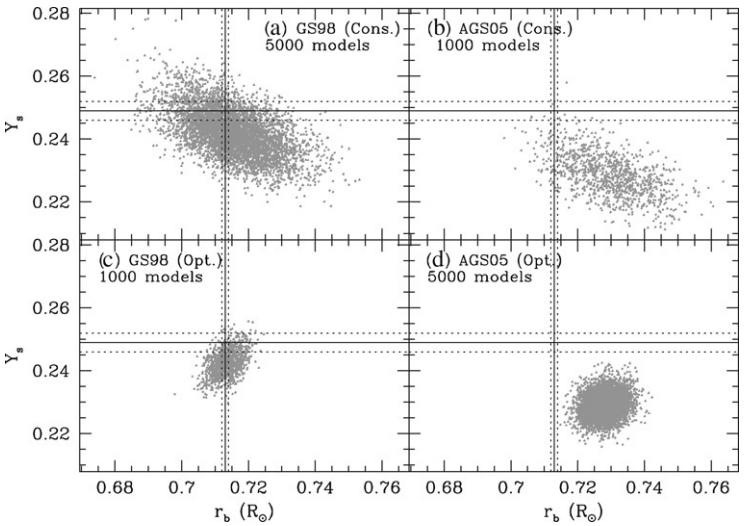

Fig. 13. The helium abundance in the convection zone, Y_s, plotted against r_b, the position of base of the convection zone, for the solar models from the Monte Carlo simulations of Bahcall et al. (2006). The horizontal and vertical lines respectively, show the seismically determined values of r_b and Y_s with dotted lines showing the 1σ error-bars. The labels "Cons." and "Opt." refer to conservative and optimistic errors respectively.

and Pinsonneault (2006) estimate that solar models with revised abundances disagree at the level of 15σ with seismic data, while models constructed with older solar abundances are consistent within 2σ with seismic data. Their analysis was mainly based on the seismic value of the depth of the convection zone and the helium abundance in convection zone. Using these constraints they also attempted to estimate the solar heavy-element abundances and obtained values close to the GS98 ones.

6.3. The radiative interior

The effect of the heavy elements on opacities implies that the structure of the radiative zone changes when the heavy-element abundance is changed. Both sound-speed and density profiles are significantly different, as can be seen from Fig. 11. The main difference between models using different composition is seen in regions just below the base of the convection zone. Since the equation of state is not very important in determining the structure of the solar radiative zone, the effect of Z on the equation of state does not affect the structure of the radiative zone significantly. Although, we can invert for $\Gamma_{1,\mathrm{int}}$ differences between models and the Sun in order to investigate signatures of differences in abundances, the errors in the results are large enough in these regions to make it difficult to detect any signatures of ionization of elements in the radiative zone.

Since solar models are constructed to produce the observed luminosity irrespective of composition, the structure of the inner core is less sensitive to opacity and Z variations than the rest of the radiative zone. Most of the reduction in abundances is for lighter elements like C, N, O, and Ne that are fully ionized in the core and hence, do not contribute significantly to the opacities (cf., Fig. 12). The main source of opacities in the core is the heavier elements like Fe, S, Si. Of these, only sulfur abundance has been reduced by a substantial amount (about a factor of 1.55), however, the small differences in these abundances do produce small differences in opacities. Although, the C, N and O abundances in the core do not affect opacities significantly, they affect the rates of the nuclear reactions involved in the CNO cycle. There are, therefore, noticeable differences between the models. For instance, the central temperature of model with GS98 abundances is 15.67×10^6 K, but that of a model with AGS05 abundances is 15.48×10^6 K (Bahcall et al., 2006). Also, for the models in the Monte Carlo study of Bahcall et al. (2006), it is found that the average mean molecular weight in the inner 20% of the Sun by radius is 0.7203 ± 0.0029 for models with GS98 composition and 0.7088 ± 0.0029 for models with the AGS05 composition (Chaplin et al., 2007b). Unfortunately, there are no direct seismic determinations of these quantities, though Chaplin et al. (2007b) have attempted to determine μ for the solar core (see Section 8.2). These differences affect the sound-speed profile of the core and hence, the frequency separations. Basu et al. (2007) examined the scaled small-frequency spacing and separation ratios of the low-degree modes, which are sensitive to conditions in the solar core and hence provide an independent test of solar models. They

Table 4
Neutrino fluxes at the Earth (in $cm^{-2}\ s^{-1}$) from solar models with GS98 and AGS05 abundances

Reaction/Detector	GS98	AGS05
pp	5.99×10^{10}	6.06×10^{10}
pep	1.42×10^{8}	1.45×10^{8}
hep	7.93×10^{3}	8.25×10^{3}
^{7}Be	4.84×10^{9}	4.34×10^{9}
^{8}B	5.69×10^{6}	4.51×10^{6}
^{13}N	3.05×10^{8}	2.00×10^{8}
^{15}O	2.31×10^{8}	1.44×10^{8}
^{17}F	5.83×10^{6}	3.25×10^{6}
Cl (SNU)	8.12	6.58
Ga (SNU)	126.08	118.88

Models are from Bahcall et al. (2006).

find that models with AGS05 abundances are not consistent with the observed frequency spacings and separation ratios as obtained from observations carried out by the BiSON network.

The change in the structure of the solar core caused by changes in the heavy-element abundance also affect the neutrino fluxes expected from a solar model. However, as explained above, the major changes are in the outer radiative zone, where the temperature is too low for nuclear reactions to take place. As a result, the neutrino fluxes are comparatively less affected by the changes in the abundances (e.g., Bahcall and Pinsonneault (2004), Turck-Chièze et al. (2004) and Bahcall et al. (2005c)). Neutrino fluxes for two models, one with GS98 and the other with AGS05 abundances are listed in Table 4. Bahcall and Serenelli (2005) have studied the effect of the abundance of each element separately on the neutrino fluxes to get a better estimate of uncertainties due to the uncertainties in the abundances of heavy elements. They find that the calculated uncertainties in neutrino fluxes are overestimated if Z, the total abundance of all elements is considered. This is a result of the fact that heavier elements like Fe and Si have the most effect on neutrino fluxes, but they do not contribute much to errors in Z since their abundances are believed to be more reliably determined. On the other hand, lighter elements like C, N, O, Ne have little effect on neutrino fluxes (except for those emitted by the CNO reactions), but their abundances are more uncertain in view of recent developments, and affect Z changes more. Thus errors in solar Z are more a result of changes in elements that do not affect neutrino emissions by much, rather than a result of changes in those elements that have a larger influence on the emitted neutrinos. Hence, Bahcall and Serenelli (2005) argue that more realistic estimate of uncertainties due to heavy-element abundances can only be calculated by examining the effect of each element separately. They also include the effects of correlations between the abundances of different elements. The flux of CNO neutrinos is significantly affected by the difference in GS98 and AGS05 abundances, but it is difficult to isolate these neutrino fluxes.

6.4. The ionization zones

There are other, more subtle, effects of the change in heavy-element abundances on the structure of the convection zone. These are caused by the effects heavy elements have on the equation of state, which in turn determines the structure of the convection zone. The convection zone essentially has an adiabatic temperature gradient, and that is determined by the equation of state. The effect of heavy-element abundances on the structure of the convection zone is usually too small to be seen directly in the sound-speed and density profiles. The effect is seen more clearly in the dimensionless sound-speed gradient $W(r)$ (cf., Eq. (39)) or the adiabatic index $\Gamma_{1,\mathrm{int}}$.

Both Γ_1 and $W(r)$ show dips or peaks at the ionization zones of different elements. In Fig. 8 we showed the fractional abundances of different ionization stages of various elements in a solar model. These ionization fractions were calculated for a solar model using the CEFF equation of state. The CEFF equation of state allows us to explicitly include different elements and to follow the ionization stages of the different elements. Since hydrogen and helium, which form the bulk of solar material, are ionized in the outer 5% of the Sun, $\Gamma_{1,\mathrm{int}}$ and $W(r)$ in these layers are dominated by these elements, making it difficult to discern the signatures of heavy elements. Below this depth one can expect to see features due to ionization of heavy elements. High ionization states of light elements like C, N, O and Ne have broad ionization regions, in particular C V, N VI, O VII, and Ne IX have ionization zones

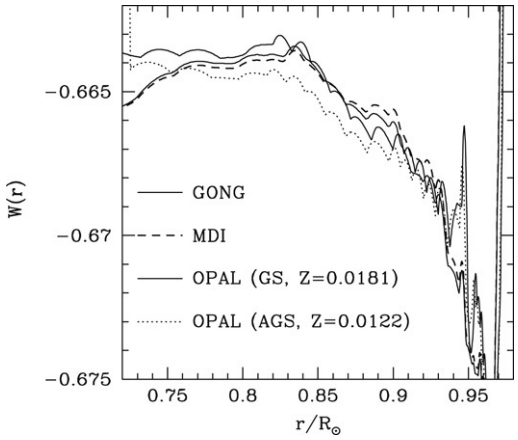

Fig. 14. The dimensionless sound-speed gradient, $W(r)$ in solar models with GS98 and AGS05 abundances are compared with those inferred from inverted sound-speed profiles obtained using GONG and MDI data.

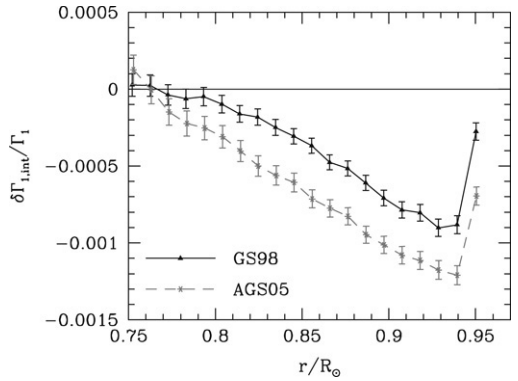

Fig. 15. The intrinsic Γ_1 differences between the Sun and two solar models, one with AGS05 abundances, the other with GS98 abundances.

around $(0.90–0.95)R_\odot$, $(0.87–0.93)R_\odot$, $(0.83–0.90)R_\odot$ and $(0.75–0.85)R_\odot$ respectively. There is considerable overlap between the different ionization zones of different elements and hence, unlike in the case of helium, it is difficult to isolate the signal from these elements in either Γ_1 or $W(r)$, but we should expect to see the cumulative effect of all the heavy elements.

Fig. 14 shows the function $W(r)$ for the Sun and two models, one with the GS98 abundances, and one with the AGS05 abundances. As can be seen, $W(r)$ for the low-Z model is consistently lower than the solar value of $W(r)$, while the higher Z model matches the solar value very well, at least below $0.9R_\odot$, where errors in the equation of state have a small effect. Fig. 15 shows the relative difference in $\Gamma_{1,\mathrm{int}}$ between two models with different Z and the Sun. It can be seen that although none of the models agree perfectly with the Sun, the low-Z model has a larger disagreement. Thus although the largest difference between models constructed with the AGS05 models and the Sun is at the base of the convection zone, the structure of the convection zone also shows considerable disagreement.

6.5. Some consequences for stellar models

The revision in solar metallicity also affects models for other stars. This is because the abundances of stars are often expressed relative to solar abundances. Very often stellar metallicity is expressed as [Fe/H], and translating this to Z assumes that solar metallicity is known. Furthermore, most evolutionary tracks and isochrones for population I stars are calculated assuming that they have the solar mixture of heavy elements. Thus using AGS05 mixture instead of GS98 would result in a lower value of Z, and also a different relative abundances of elements. Stellar models

with lower-Z but the same helium abundance are bluer and more luminous than their high-Z counterparts (Salaris and Cassisi, 2005). There have been a number of recent investigations examining the effects of the lowered solar abundances on models for other stars. The results do not clearly demonstrate whether or not the lower solar Z values are better for other stars. Some of these results are discussed below.

Degl'Innocenti et al. (2006) examined the effects of heavy-element abundances on the determination of the stellar cluster ages. They found that there are two ways in which the revised heavy-element abundances can affect the age calibration for globular clusters. First is the effect of the change in the heavy-element mixture, and second is the effect of the reduction of Z for the same value of [Fe/H]. They have examined the effect of updating the heavy-element mixture on theoretical evolutionary tracks and isochrones to find a maximum variation of the estimated age of order of 10%. They also found that when the Z values are adjusted from the observed [Fe/H] for solar like stars, the revised solar Z/X value leads to a disagreement between theoretical isochrones and the color-magnitude diagram of the Hyades cluster, although, the discrepancy is not large enough to rule out the revised solar abundances.

Piersanti et al. (2007) studied the effect of heavy-element abundance on stellar evolution calculations for low-mass stars. They found that the evolutionary tracks on the HR diagram are significantly affected when the lower abundances from Lodders (2003) were used instead of the GS98 abundances. They estimate that this leads to an increase in the estimated age of globular clusters by up to 0.7 Gyr.

VandenBerg et al. (2007) have studied the effect of heavy-element abundances on fits of isochrones to the color-magnitude diagram of M67. The open cluster M67 has an age of about 4 Gyr and was chosen since high-resolution spectroscopy indicates that this cluster has almost same heavy-element abundance as the Sun and its turn-off stars have masses just around the lower limit for sustained core convection on the main sequence. Using MARCS model atmospheres as boundary conditions, they constructed evolutionary models of stars in range of 0.6–1.4 $M_{\odot}$ to find that isochrones formed from models with AGS05 abundances predict a turn-off gap that does not match the observations. This difficulty does not arise when GS98 abundances are used.

Montalbán and D'Antona (2006) studied lithium depletion in pre-main-sequence stellar models with 2D radiative-hydrodynamical convection models. They found that with higher Z, lithium depletion in models is much higher than that expected from the observations of lithium in young open clusters. Reduction of heavy-element abundance as suggested by AGS05 significantly reduces the lithium depletion in pre-main-sequence stellar models, thus bringing them in better agreement with observations. Sestito et al. (2006) also found that lithium depletion increases with increase in Z in the pre-main-sequence stage, however, they conclude that none of the adopted solar mixtures and variations in the chemical composition appear to explain the very small amount of pre-main-sequence lithium depletion observed for solar-type stars.

Miglio et al. (2007a,b) have examined the effect of opacity and heavy-element abundances on the stability of slowly pulsating B stars and β Cephei stars. They have used both OP and OPAL opacities, and have used heavy-element mixtures from Grevesse and Noels (1993) or from AGS05 after enhancing the abundance of neon. The instability in these stars is believed to be due to an opacity bump which occurs at lower temperatures than those at the base of the solar convection zone. At these temperatures the difference between OP and OPAL opacities, as well as the contribution of heavy elements, is much larger and they find significant shifts in the instability strip due to both opacity and abundances. By comparing these models with observations it may be possible to test the opacities and heavy-element abundances. Unfortunately, they did not use the AGS05 mixture without neon enhancement and hence that mixture cannot be tested. Pamyatnykh and Ziomek (2007) find that the β Cephei instability domain in the HR diagram when computed with AGS05 abundances and OP opacities is very similar to the instability domain calculated earlier with OPAL opacities and the higher abundances. Looking at the stability of beat Cepheids, Buchler and Szabó (2007) favor the lower solar abundances. They found that the stability of beat Cepheid models depends sensitively on Z as well as the mixture of heavy elements. They showed that with reduced Z the galactic beat Cepheid models are in better agreement with observations as compared to models with Grevesse and Noels (1993) mixture.

Alecian et al. (2007) have investigated the impact of the new solar abundances on the calibration of the pre-main-sequence binary system RS Cha to find that it is possible to reproduce the observational data of the RS Cha stars with models based on AGS05 mixture using standard input physics. On the other hand, using GN93 mixture it is not possible to find such models. The difference presumably arises from the relative abundance of Fe and C, N, O in the two mixtures. They have not used GS98 abundances.

7. Attempts to reconcile low-Z solar models with the Sun

The large discrepancies between models constructed with the AGS05 abundances and the Sun have resulted in numerous attempts to change the inputs to solar models in order to reconcile the models with the helioseismic data. The proposals generally fall into four categories or combinations thereof. These are: (1) increasing input opacities, (2) increasing the heavy-element abundance of the radiative interior through increased diffusion, or alternatively, decreasing the heavy-element abundance of the convection zone through the accretion of low-Z material, (3) increasing the abundance of other elements to compensate for the reduction in oxygen abundance, (4) other processes such as mixing, or the deposition of energy by gravity waves which effectively changes opacity. We consider each of these in the following subsections. It should be noted that all these proposals only address the effect of abundances on the structure of solar models through opacity in the radiative interior. The discrepancy, if any, in equation of state is not addressed by these proposals. Guzik (2006) has reviewed some of the proposed modifications. Of course, increasing the oxygen abundance to its old value will resolve all discrepancies. As it happens, none of the proposed changes resolve the discrepancy fully, but it is possible that some combination of these will fare better depending on how much the inputs are changed compared to their expected values.

7.1. Increasing input opacities

Since the primary effect of reducing Z/X is to reduce opacity, an obvious possibility is to increase the opacities. Near the base of the convection zone $\partial \ln \kappa / \partial \ln Z$ is about 0.7 (Bahcall et al., 2004) and hence, opacity reduces by about 25% when Z/X is changed from the GS98 value to the AGS05 value. The actual change is slightly different since the relative abundances of the heavy elements in the AGS05 table is different from that in the GS98 tables. If the available opacity tables underestimate the opacity of solar material, then the effect of the reduction of Z/X on the opacities may be compensated to some extent. Opacities are theoretically calculated for a given composition, temperature and density, and hence, it is possible that some opacity sources, such as weak lines, are missed. The fact that there are no laboratory measurements of opacities also makes it difficult to estimate the errors in these computations. The only way that is available for estimating the errors in the computed opacities is through comparison with other, independent calculations. However, the extent of opacity modifications required to restore agreement between solar convection-zone model and seismic data can be estimated by looking at the changes in the position of the convection-zone base in models constructed with different opacities.

Using low-Z solar-envelope models constructed with specified helium abundance and convection-zone depth, Basu and Antia (2004) estimated that the opacity near the convection-zone base needs to be increased by about 20% to restore agreement with the seismically inferred density profile. Basu and Antia (2004) also calculated the extent of the opacity increase required to match the convection-zone model for different mixtures of heavy elements as a function of Z/X. From that they could estimate the value of Z/X, or alternatively the opacity, required to match the seismic model of the convection zone. Since the contribution to opacity from oxygen and neon fall-off with temperature above a temperature of about 3×10^6 K (Fig. 12), it would be necessary to taper-off the required increase in opacity beyond this point.

Montalbán et al. (2004) constructed a model in fairly good agreement with the solar sound-speed profile with a 14% opacity increase in region near the convection-zone base. Bahcall et al. (2005a) estimated that increases in opacity ranging from 11% to 21% may be needed to reconcile the low-Z models with helioseismology, the exact increase depends on the temperature-dependence of the opacity increase. They found that a localized increase in opacity near the base of the convection zone improves the agreement with the depth of the convection zone, but the sound-speed profile in deeper layers is significantly different (see Fig. 16). Hence it is necessary to modify the opacity over a wide range of temperature to compensate for the reduction in Z. They find that an increase in opacity by 11% in the temperature range of 2–5 $\times 10^6$ K, which in a solar model corresponds to a radius in the range of $(0.4–0.7)R_\odot$, can restore agreement in sound-speed and density profiles of the solar models. The helium abundance in this model is 0.243, which is within 2σ of the seismically estimated value. From these experiments it appears that an opacity increase of at least 10% is required to resolve the discrepancy in solar models caused by reduced Z. Bahcall et al. (2005a) also compared the opacities in solar models constructed using GS98 and AGS05 abundances. After accounting for density differences between the models, they find an opacity difference of 15% near the base of the convection zone, but the difference falls sharply to about 5% around $T = 5 \times 10^6$ K. For $T > 9 \times 10^6$ K or $r < 0.2R_\odot$, the

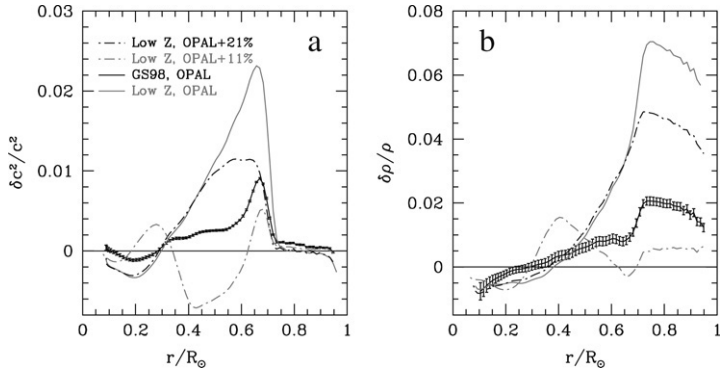

Fig. 16. The relative sound-speed and density differences between the Sun and several models with modified opacities. The models marked "Low Z" have $Z/X = 0.0176$. The model "Low Z" was constructed with unmodified OPAL opacities. Model "Low Z + 21%" had OPAL opacities increased by 21% near the base of the convection zone, and model "Low Z + 11%" had OPAL opacities increased by 11% for temperatures ranging from 2×10^6 to 5×10^6 K. For comparison a model with GS98 abundances and unmodified OPAL opacities is also shown. Details of these models can be found in Bahcall et al. (2005a).

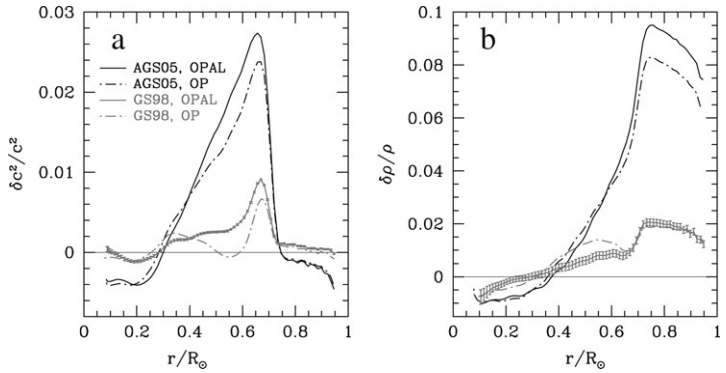

Fig. 17. The relative sound-speed and density differences between the Sun and models constructed with OPAL and OP opacities. Models with both GS98 and AGS05 abundances are shown. These models are described by Bahcall et al. (2005c).

opacity difference is less than 3%. This is expected from what is seen in Fig. 12, and is a result of the fact that most of the elements are fully ionized in this temperature range, and as a result the difference in opacities due to difference in abundances is not significant.

Earlier, Bahcall et al. (2004) had done a detailed study of uncertainties in determining opacities for conditions in stars using stellar evolution codes, in particular they looked at what happens to position of the base of the convection zone. They found that different interpolation techniques used to calculate opacities from OPAL tables give results which can differ by up to 4%. They stressed the need for improved opacity tables with finer grid spacings to reduce interpolation errors. Nevertheless, these errors do not explain the discrepancy caused by the reduction of Z/X.

At around the time that the implications of the low-Z/X solar models were being discussed, Seaton and Badnell (2004) presented the results of independent opacity calculations made by the OP project, and showed that OP opacities were larger than OPAL values by about 5% in the region near the base of the convection zone. This comparison was for opacities calculated with a mixture of only six elements, H, He, C, O, S and Fe. These initial results raised hopes that opacity errors could, at least partially, account for the discrepancy caused by the reduction in Z. The expectations, however, were not fulfilled. Badnell et al. (2005) calculated OP opacities with more elements in the heavy-element mixture, and a comparison between models constructed with these OP opacities and those constructed with OPAL opacities showed that the difference between OP and OPAL opacities near the base of the convection zone is less than 2.5%. As can be seen from Fig. 17, OP opacities do not solve the problem with the low-Z/X models (Bahcall et al., 2005c). Guzik et al. (2005) also compared different opacity calculations, including the LANL LEDCOP opacities (Neuforge-Verheecke et al., 2001a), to find that these agree within about 3%. Thus the estimated error in opacities near the base of the convection zone is 2%–4%. As the temperature increases, the difference between

different opacity estimates generally reduces. Thus, although improvements in low-Z solar models can be made by ad hoc opacity increases, there appears to be little justification for doing so, at least if OP, OPAL and LEDCOP opacities are compared. The difference between OP, OPAL and LEDCOP opacities could be considered to be an estimate of uncertainties in the computed opacities, and this does not seem to be large enough. Thus increasing opacities within reasonable limits is unlikely to explain the discrepancy between low-Z solar models and helioseismology.

Primary inversions for sound-speed and density are independent of opacity, however estimating temperature and composition profile in radiative interior needs the equations of thermal equilibrium, which requires opacity. Antia and Basu (2005) have investigated the effect of opacity on these inversions using models with both OPAL and OP opacity for calculations. They find that the difference between OPAL and OP opacity does not affect the results for temperature and hydrogen-abundance profiles significantly. Using reduced heavy-element abundances in these calculations will certainly have significant effects on the result, but since these abundances are not consistent with the primary seismic constraints, the solar T and X profiles obtained with these abundances will not be meaningful.

It may be possible to get better agreement between solar models and helioseismology by combining a modest increase in opacity with an increase in Z at the convection-base by increasing diffusion. This option is discussed in the next subsection.

7.2. *Increasing diffusion*

Since only convection-zone abundances are measured, one way to improve the agreement of the models with helioseismic data is to somehow increase the heavy-element abundance at the base of the convection zone and the radiative interior. This can be done relatively easily if it is assumed that diffusion and gravitational settling of helium and heavy elements is more efficient than what is normally assumed. This was indeed suggested as a possibility by Asplund et al. (2004). Increased diffusion would lead to higher helium and heavy-element abundance in the radiative interior, thereby increasing opacities and thus bringing the structure of radiative interior closer to that in the Sun.

Basu and Antia (2004) constructed models with increased diffusion to find that although, the convection zone became deeper, the helium abundance in the convection zone reduced further to 0.225. Thus increasing diffusion in the radiative interior increases the discrepancy with the seismically inferred helium abundance. This has also been reported by Montalbán et al. (2004) and Guzik et al. (2005). Guzik et al. (2005) also tried to enhance diffusion separately for helium and heavy elements to find that although the agreement between solar models and seismically inferred profiles improves to some extent, the required increases in thermal diffusion rates are unphysically large. None of the variations that they tried completely restored the good agreement obtained using earlier abundances. They found that depending on how the diffusion rate is enhanced, it may be possible to improve the agreement with either the convection zone depth or the helium abundance in the convection zone, but it is difficult to restore both to the seismically measured values. They did find that a combination of modest opacity increases, diffusion enhancements and abundance increases at the level of their respective uncertainties may be able to restore agreement with helioseismology, however, they admit that the solution is rather contrived. Montalbán et al. (2004) too tried a combination of increased opacity and increased diffusion. They found that they were able to restore most of the sound-speed profile agreement by e.g., a 50% increase in diffusion velocities combined with a 7% increase in opacities. However, the helium abundance in the convection zone in this model, $Y_s = 0.239$, is still significantly lower than the seismic value. Yang and Bi (2007) also tried to resolve the discrepancy between low-abundance models and seismology by enhancing diffusion. They too find that diffusion coefficients have to be increased by a factor of two in order to construct models with convection-zone depths that are closer to the seismic value. They found that the inclusion of mixing below the convection-zone base helps in improving the agreement with helium abundance in the convection zone. However, Yang and Bi (2007) do not give any physical justification of why diffusion needs to be enhanced by such a large amount. Moreover, the sound-speed and density profiles of the resulting models still disagree considerably with the seismically obtained solar profiles, unless Z is increased to 0.0154, a value that lies between the AGS05 and GS98 abundances.

Guzik et al. (2005) suggested that considering later accretion of low-metallicity material onto the solar surface that keeps a high-metallicity interior may resolve the discrepancy. They assumed that the Sun had 98% of its current mass in its pre-main-sequence stage and had metallicities like the GS98 metallicities and accreted the last 2% of material after it was no longer fully convective. This material was assumed to be low-Z. The accretion model has an acceptable value of Y_s (0.2407), but it still has a shallow convection zone ($r_b = 0.7235 R_\odot$). Castro et al. (2007) too invoked accretion of low-metallicity material in the early-main-sequence phase of the Sun to explain the observed

low abundances of heavy elements in the current solar atmosphere. They too found that these models have better agreement with helioseismology, as compared to normal AGS05 models, but they find a spike in $\delta c^2/c^2$ just below the convection zone that is as large as 3.4%. Furthermore, both the convection-zone depth and the helium abundance in this model are lower than the corresponding seismically determined values. Castro et al. (2007) also found that the agreement with the solar sound-speed profile could be improved by invoking mixing in the region just below the convection zone, however, the sound-speed profile remains significantly different.

7.3. Increasing the abundance of neon and other elements

Since the errors in opacity calculations are unlikely to be large enough to resolve the discrepancy caused by reduction in oxygen abundance, and since increasing diffusion does not help either, the next possibility that was explored was increasing the abundance of some other element to compensate for the decrease in the oxygen abundance.

Antia and Basu (2005) examined this issue and found that the convection-zone depth is sensitive to the abundances of O, Fe and Ne. Other elements have little influence on the convection-zone models. They suggested that the neon abundance may be increased to compensate for the reduction in oxygen abundance. Iron would work as well as neon in providing opacity at the base of the convection zone, however, it is believed that the solar iron abundance is known reasonably well. Besides, iron is also an important source of opacity in the solar core and thus increasing iron abundance could have adverse effects on the structure there. Neon is an ideal candidate. It cannot be detected in the solar photosphere since it does not form lines at photospheric temperature. Thus usually neon abundance is determined from lines formed in the solar corona. It is assumed that the abundance ratio of neon to oxygen in the solar corona and the photosphere is the same, and hence the photospheric oxygen abundance, along with the coronal Ne/O ratio (0.15) is often used to determine the photospheric abundance of neon. Since coronal models are uncertain, the abundance of neon is quite uncertain, justifying models with increased neon abundance.

It can be seen from Fig. 12 that the logarithmic opacity gradient with respect to the abundance of oxygen is about 2.5 times that with neon near the base of the convection zone. This implies that to compensate for a reduction in the oxygen abundance by a factor of 1.48 we need to increase the neon abundance by almost a factor of 4 (an additional factor of 1.48 was included to take into account the fact that the reduction of the oxygen abundance in the AGS05 table automatically led to the reduction of the neon abundance). Since this increase is probably larger than the expected uncertainties and hence may be unacceptable, Antia and Basu (2005) also explored the option of increasing the abundances of C, N, and O by 1σ of their tabulated uncertainty, and then increasing the Ne abundance to restore agreement with the seismically determined structure of the convection zone. They found that in this case the neon abundance needs to be increased by a factor of 2.5, which is more acceptable.

Fig. 12 shows that the contributions of oxygen and neon to opacity have rather different temperature-dependences and hence just increasing the neon abundance cannot compensate for the reduction of the oxygen abundance throughout the radiative interior. It may also be necessary to adjust the diffusion coefficient or other factors to construct models whose structure is in better agreement with the seismically inferred solar structure. Antia and Basu (2005) used models of only the solar envelope and hence, could not examine the effects of neon enhancement in the deep interior. Bahcall et al. (2005b) examined the issue of neon in more detail using full solar models evolved from the zero-age main-sequence stage. They found that increasing the neon abundance by 0.4–0.5 dex (i.e., factors of about 2.5–3) over the AGS05 values improves agreement with helioseismology in that the position of the convection-zone base and the convection-zone helium abundance are then within a few σ (rather that 26σ) of the respective helioseismic estimates. However, the sound-speed and density profiles do not match the seismic estimates very well (see Fig. 18). Nevertheless, they did get an overall good match to the seismic profiles when they considered simultaneous increases in Ne and Ar, as well as a 1σ increase in C, N, O and some of the heavy elements whose meteoritic abundances have been well determined. The sound-speed and density results for some of these models are shown in Fig. 19.

Zaatri et al. (2007) examined the effect that increasing the abundance of neon has on the core of solar models. They compared the scaled small-frequency spacings and the separation ratio (cf., Eqs. (35) and (36)) on the low-degree modes of the models with the observed small-frequency spacing derived from GOLF data (Gelly et al., 2002) to test the models, and like Basu et al. (2007) found that the small frequency separations are extremely sensitive to the metallicity of the models. They found that increasing neon can reduce the discrepancy between the frequency spacings of the solar models and those of the Sun. In addition to examining frequency spacings, they also did the usual helioseismic tests of comparing the position of the convection-zone base, the convection-zone helium abundance, and the sound-speed

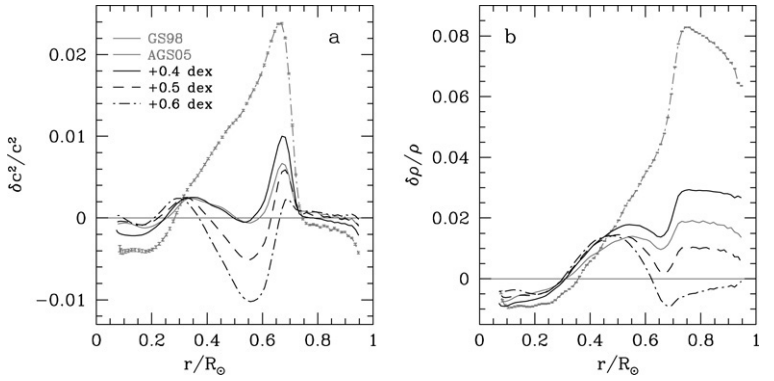

Fig. 18. The relative sound-speed and density differences between the Sun and several neon-enhanced models. The amount by which the abundance of neon is enhanced over the AGS05 values is mentioned in the legend. For comparison a model with normal AGS05 abundances and one with GS98 abundances are also shown. All models are from Bahcall et al. (2005b) and were constructed with OP opacities.

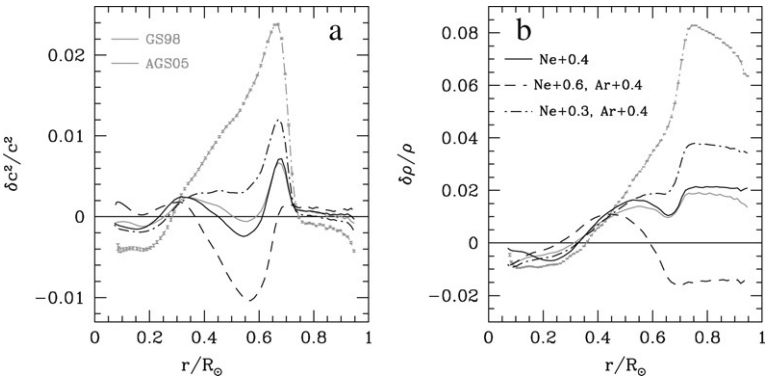

Fig. 19. The relative sound-speed and density differences between the Sun and several models with neon and other abundances increased over the AGS05 values. The amount by which the neon abundance is increased is shown in the figure. The CNO abundances in all models have been increased by 0.05 dex, and the abundances of meteoritic elements have been increased by 0.02 dex. In addition, two models have the argon abundance increased by 0.4 dex. For comparison a model with normal AGS05 abundances and one with GS98 abundances are also shown. All models are from Bahcall et al. (2005b) and were constructed with OP opacities.

profile. They found that an increase in neon abundance by 0.5 ± 0.05 dex can bring the model in reasonably good agreement with observations, particularly if in addition to enhancing the neon abundance, they slightly modified the solar age and the CNO abundances. Zaatri et al. (2007) also pointed out that the abundance of sulfur also plays a role in the discrepancy. Sulfur primarily contributes to opacity in core and its abundance affects the helium abundance required by a solar model to match solar luminosity and radius constraints.

It is by no means clear that increasing the solar neon abundance is justified. Soon after Antia and Basu (2005) and Bahcall et al. (2005b) suggested neon-abundance enhancement as a means of reducing the discrepancy between the AGS05 models and the Sun, Drake and Testa (2005) claimed that twenty one solar neighborhood almost Sun-like stars seem to have a Ne/O ratio of 0.41 which is much higher than 0.15, the accepted value of the Ne/O ratio for the Sun which is also what was used by AGS05. These results were based on the study of X-ray spectra from Chandra. If this higher ratio is adopted for the Sun, then the solar neon abundance will increase by a factor of 2.7, and thus, would be of some help in resolving the discrepancy between solar models and helioseismology. However, Schmelz et al. (2005) and Young (2005) reanalyzed solar X-ray and ultraviolet data respectively to find that the Ne/O ratio of the Sun is indeed consistent with the old lower value. Young (2005) used an emission-measure method applied to extreme ultraviolet emission lines of Ne IV– VI and O III– V ions observed by the Coronal Diagnostic Spectrometer on board SOHO to find the abundance ratio Ne/O to be 0.17 ± 0.05 which is consistent with the value used by AGS05. Schmelz et al. (2005) analyzed solar active-region spectra from the archives of the Flat Crystal Spectrometer on the

Solar Maximum Mission to find that the data are consistent with the standard Ne/O abundance ratio of 0.15. They explain the higher ratio found by Drake and Testa (2005) as being due to the higher activity level in the stars studied.

Bochsler et al. (2006) examined the abundances in solar winds and found that the neon abundance is $\log\epsilon(\mathrm{Ne}) = 8.08 \pm 0.12$, i.e., consistent with the value in the GS98 tables, but lower by about a factor of 1.5 than the neon abundance of $\log\epsilon(\mathrm{Ne}) = 8.29 \pm 0.05$ proposed by Bahcall et al. (2005c) to bring the AGS05 solar models back into agreement with the Sun. Bochsler (2007b) extended this work to determine the absolute abundances of Ne and O. After accounting for fractionation in the solar wind, he finds $\log\epsilon(\mathrm{O}) = 8.87 \pm 0.11$ and $\log\epsilon(\mathrm{Ne}) = 7.96 \pm 0.13$. These values are closer to those listed in the GS98 table, though their large errors mean that they are also within 2σ of the AGS05 values. Landi et al. (2007) used the ultraviolet spectrum of a solar flare obtained with the SUMER instrument on board SOHO to measure the absolute abundance of neon in the solar atmosphere. They find $\log\epsilon(\mathrm{Ne}) = 8.11 \pm 0.12$, which is much higher than the neon abundance in the AGS05 tables (7.84 ± 0.06), but somewhat lower than the abundance proposed by Bahcall et al. (2005c)

The situation of the solar neon abundance remains confusing, particularly since measurements of other stars seems to yield high Ne/O ratios. Cunha et al. (2006) measured the abundance of neon in B stars in the Orion association and found $\log\epsilon(\mathrm{Ne}) = 8.11 \pm 0.04$, about twice the value of AGS05, and they found $\mathrm{Ne/O} = 0.25$, higher than what is assumed for the Sun. Using X-ray spectra obtained with XMM-Newton, Liefke and Schmitt (2006) determined Ne/O for α Cen, and found a value that is twice the usual adopted value for the Sun. Using Chandra X-ray spectra again, Maggio et al. (2007) studied the chemical composition of 146 X-ray-bright pre-main-sequence stars in the Orion nebula cluster, and found an Ne/O ratio which is a factor of 2.2 higher than that used by AGS05. However, their error-bars are large. Planetary nebulae at solar galactic distances appear to have high neon abundances too. Pottasch and Bernard-Salas (2006) determined abundances in planetary nebulae using infrared lines. They find a higher (by about a factor of 2) neon abundance at solar distances from the galactic center. Their neon-abundance result is consistent with that of Feldman and Widing (2003) who used the Ne/Mg ratio to determine the solar neon abundance rather than the Ne/O ratio used by GS98 and AGS05. Stanghellini et al. (2006) also examined neon abundances in planetary nebulae and obtained $\mathrm{Ne/O} = 0.26$. Ignace et al. (2007) attempted to estimate Ne abundances from a Spitzer/IRAS survey of Wolf-Rayet stars and obtained results that are consistent with the old solar neon abundances listed by Cox (2000). Wang and Liu (2007) studied elemental abundances of Galactic bulge planetary nebulae from optical recombination lines and found a value of Ne/O which is much higher than that used by AGS05. Similarly, Lanz et al. (2007) studied Argon abundance in a sample of B main-sequence stars in the Orion association to find a value $\log\epsilon(\mathrm{Ar}) = 6.66 \pm 0.06$ which is about a factor of 3 higher than that obtained by AGS05. Lodders (2007) has tried to estimate solar Argon abundance using variety of techniques, including solar wind, solar flares, solar energetic particles as well as from Jupiter, B stars, H II regions etc. to find that all these are higher than the estimated value by AGS05. She has proposed a mean value of $\log\epsilon(\mathrm{Ar}) = 6.50 \pm 0.10$ for the current photospheric abundance and 6.57 ± 0.10 for the protosolar abundance after taking into account diffusion of Argon in solar interior.

As is evident from the discussion above, it is not clear whether an increase in the adopted solar neon abundance is justified. Increasing the neon abundance does bring models with low C, N, and O abundances in better agreement with the Sun. However, the main reason for this is the increased opacities at the base of the convection zone. Lin et al. (2007) investigated the consequences of increased neon abundances in the ionization zones by looking at $\Gamma_{1,\mathrm{int}}$ in those regions. They found that increasing neon abundances alone does not help in resolving the discrepancy in the ionization zones, it actually increases the discrepancy in the region 0.75–0.9 $R_\odot$. Better results are obtained only if C, N and O abundances are raised simultaneously. Thus, the improvement appears to be a result of increased Z/X rather than a result of the increased neon abundance. Although they could not rule out increased neon abundances, they showed that an increased neon abundance does not resolve the discrepancy between solar models with AGS05 abundances and seismic data. Thus while increasing neon abundance reduces the discrepancy at the convection-zone base, it does not reduce the discrepancy in the ionization zones within the convection zone. This can be seen from Fig. 20.

7.4. Other processes

Several other processes have been tried to bring low-Z/X solar models in agreement with the helioseismic data. Given that there is evidence of mixing below the convection-zone base, Turck-Chièze et al. (2004) tried models with mixing in the tachocline region. They found that mixing raised the convection-zone helium abundance to acceptable

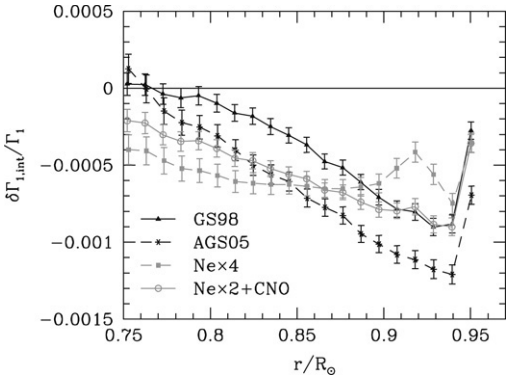

Fig. 20. The intrinsic Γ_1 differences between the Sun and neon-enhanced solar models. Unmodified GS98 and AGS05 models are also shown for comparison. Model Ne×4 has neon increased by a factor of 4 over the AGS05 abundances, and Ne × 2 + CNO has neon abundance increased by a factor of 2 and CNO abundances increased by 1σ of observed errors.

levels, however, the convection zone itself became shallower. Montalbán et al. (2006) explored the role of overshoot below the convection-zone base. They assumed an overshoot of order $0.15H_p$, and by increasing the opacity by ≈7% they were able to reproduce the position of the convection-zone base and the convection-zone helium abundance. However, the discrepancy of the sound-speed profile in the radiative zone remained quite large.

Arnett et al. (2005) and Young and Arnett (2005) following Press (1981) and Press and Rybicki (1981) have tried models in which internal gravity waves deposit energy in the radiative zone. These waves are assumed to be excited and launched inwards at the convection-zone base. The radiative damping of these waves, as they travel inwards, deposits energy and changes the structure in a manner similar to opacity enhancements. Young and Arnett (2005) use inertial wave-driven mixing as formulated by Young et al. (2001). Their models have mixed success with some being able to reproduce the position of the convection-zone base and convection-zone helium abundance. However, none of the models has a radius that is exactly $1R_\odot$ and in that sense these are not really solar models. An alternate mechanism for energy transfer in the solar interior is the role of dark matter particles like the Weakly Interacting Massive Particles (WIMP). Although there are no published studies investigating role of these particles in low-Z models, solar models with dark matter have been studied in other contexts (e.g., Däppen et al. (1986), Faulkner et al. (1986), Giraud-Heraud et al. (1990), Christensen-Dalsgaard (1992) and Lopes et al. (2002)). These models generally show large effects in the core, and hence may not explain the departures between the Sun and low-Z solar models in the region below the base of the convection zone. Whether or not WIMPs with different characteristics can give the required differences in the right region has not been studied.

8. Seismic estimates of solar abundances

Even before the current controversy over solar abundances started, there had been attempts to infer the heavy-element abundance of the Sun using helioseismic data, as was done for determining the abundance of helium, as an independent test of solar abundances. The efforts gained urgency once it was clear that solar models with the AGS05 abundances did not match helioseismic constraints, and that none of the changes made to bring the models back in concordance with helioseismology worked.

Like helium, heavy elements affect oscillation frequencies indirectly, and hence, one cannot determine Z directly through inversions. One depends on the effect of Z on different inputs to the solar models. Unlike the helium abundance in the Sun, the abundance of heavy elements is small, as a result, attempts to "invert" for Z in a manner similar to that for Y_s (cf., Eqs. (38) and (40)) have not been very successful and have given results that have very large errors and are somewhat unstable (e.g., Takata and Shibahashi (2001)).

Attempts to determine the solar heavy-element abundance can be grouped into three categories: (1) Studying the regions where opacity plays a role and depends on the heavy-element abundance. The base of the convection zone is the most obvious region. (2) Using information about core structure, which depends predominantly on the mean molecular weight of material there (which in turn depends on the abundances) and to a smaller extent on opacities. (3) Looking at the ionization zone where ionization causes changes in the adiabatic index and sound speed. The equation

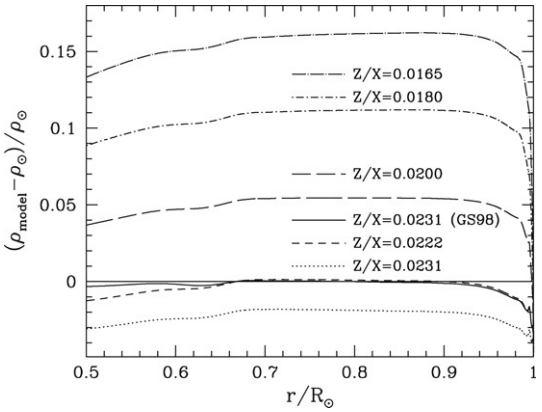

Fig. 21. The relative density difference between the Sun and solar-envelope models constructed with different values of Z/X. All models, except the one marked GS98, have AGS05 relative abundances. All models were constructed with OPAL opacities, and have the seismic values of r_b and Y_s.

of state plays a role here. We describe below how different regions of the Sun have been used in attempts to determine the heavy-element abundance of the Sun.

8.1. Results that depend on the Z-dependence of opacity

The depth of the solar convection zone is determined by the opacity at that position, which in turn depends on the solar heavy-element abundances. Basu and Antia (1997) found that the density profiles of solar-envelope models constructed to have the correct convection-zone depth and helium abundance is extremely sensitive to the heavy-element abundance. They looked at the possible sources of systematic error in the determination of the position of the convection-zone base, and concluded that if the OPAL opacity tables constructed with the then standard heavy-element abundances (i.e., those of Grevesse and Noels (1993)) were valid, then the heavy-element abundance in the solar envelope should be $Z/X = 0.0245 \pm 0.0008$, consistent with the then accepted value of Z/X. Basu (1998) repeated the exercise with different data and obtained the same result. Subsequently, GS98 revised the value of Z/X to 0.0231, which is within 2σ of the seismic value. However, the latest revision of Z/X by AGS05 makes it 10σ different from the seismically estimated value. Of course, the seismic estimate of Z/X obviously depends on the mixture of heavy element used to calculate the opacity. Basu and Antia (2004) repeated the exercise for a mixture similar to that of AGS05 to get a seismic estimate of $Z/X = 0.0214$, which still differs by about 6σ from the AGS05 value. This exercise can be repeated using the AGS05 mixture. Fig. 21 shows density differences between the Sun and solar-envelope models that have the seismically estimated values of the convection-zone helium abundance and the position of the convection-zone base, but have different values of Z/X. Most of the models were constructed with the AGS05 mixture. An analysis of the figure will show that for $Z/X = 0.0222 \pm 0.0008$ the models with AGS05 mixture are consistent with the seismic density profile. It is possible to estimate the extent of opacity modification required to get the correct density profile in the lower part of the convection zone for other values of Z/X. The results are shown in Fig. 22, where the shaded regions show the allowed region in the opacity–Z/X plane where the envelope models are consistent with seismic data within estimated errors. It is clear that the AGS05 abundance with OPAL opacity is well outside the allowed region, while the Z/X value of GS98 is consistent with OPAL opacities. For $Z/X = 0.0165$, the value obtained by AGS05, the required opacity modification is $26.8 \pm 3.5\%$. It is also clear that the seismic estimate of Z/X depends rather sensitively on the relative mixture of heavy elements, though the AGS05 abundances are well below the seismic estimates using any of the mixtures. OP opacities were not available when the work of Basu and Antia (2004) was done. Since the OP opacities are somewhat larger than OPAL opacities at conditions near the base of the solar convection zone, the seismic estimate of Z/X will decrease slightly. If OP opacities are used instead of OPAL, then the allowed region in the Fig. 22 shifts downwards by about 1.7% and for AGS05 mixture, the models are consistent with seismic data when $Z/X = 0.0218 \pm 0.0008$.

Delahaye and Pinsonneault (2006) did a detailed analysis of seismic constraints, in particular the convection-zone depth and the convection-zone helium abundance, in order to try and estimate the heavy-element abundance in

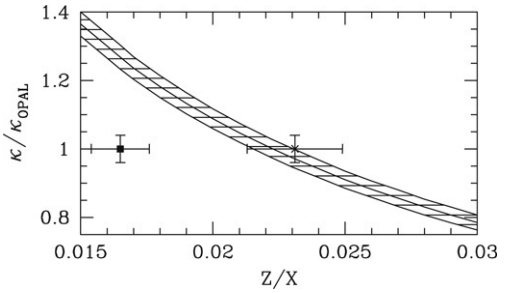

Fig. 22. The shaded area shows the allowed region in the Z/X–opacity plane that is consistent with seismic constraints when OPAL opacities with AGS05 mixture is used. The points with error-bars show current value of opacity and abundances from AGS05 and GS98. The solid square on the left side marks the AGS05 abundances, while the cross on the right side marks the Z/X value in GS98.

the convection zone. For their study they assumed reasonable errors on input physics and other parameters such as opacities, diffusion coefficients, nuclear reaction rates, and the equation of state. They estimated that the theoretical error in the values of r_b in solar models is about $0.0027\,R_\odot$ and that in Y_s is about 0.0031. These values are consistent with those found by Bahcall et al. (2006). They found that the depth of the convection zone is primarily determined by abundances of lighter elements like C, N, O and Ne, while the helium abundance is more sensitive to abundances of heavier elements like Fe. Thus, they separated the heavy elements in two groups, one consisting of the lighter elements (C, N, O, Ne) which they refer to as "photospheric" since the abundances of these elements are determined spectroscopically; and another group with heavier elements like Fe, which they refer to as "meteoritic" since the abundances of these elements are primarily determined from meteorites. Since these two groups of elements have different influences on the depth of convection zone and its helium abundance, Delahaye and Pinsonneault (2006) argue that it is, in principle, possible to determine their abundances independently. Using the seismic constraints on r_b and Y_s, they attempted to estimate solar heavy-element abundances and found that $\log\epsilon(\mathrm{O}) = 8.87$ dex and $\log\epsilon(\mathrm{Fe}) = 7.51$ dex, which are values very similar to those in the GS98 tables.

8.2. Results from the core

Basu et al. (2007) used very precise frequencies of low-degree solar-oscillation modes measured from 4752 days of data collected by the Birmingham Solar-Oscillations Network (BiSON) to determine the degree of agreement between the cores of solar models constructed with different values of Z and the Sun. They examined the scaled small-frequency spacings (cf., Eq. (35)) and separation ratios (cf., Eq. (36)) of the low-degree modes — these are sensitive to conditions in the solar core and hence provide an independent test of solar models. Basu et al. (2007) showed that the small spacings and separation ratios of models constructed with the old GS98 composition match the observed BiSON spacings and ratios much more closely than do the spacings and ratios of models with the lower AGS05 composition. In short, models constructed with higher metallicities compare better with the BiSON data than do models constructed with lower metallicities. The level of agreement deteriorates when the metallicity becomes very large, indicating that one should be able to determine solar metallicity using the spacing and ratio data. They showed that the separation ratios depend predominantly on the mean-molecular weight of the core.

Chaplin et al. (2007b) expanded on the work of Basu et al. (2007) to try and determine the average mean molecular weight of the core of the Sun. Since the mean molecular weight of the core is related to the metallicity of the outer layers, they also put constraints on Z. They used the average difference in separation ratios between models and the Sun. Thus if the separation ratios of the BiSON data are $r_{\ell,\ell+2}(n)$ and model ratios are $r'_{\ell,\ell+2}(n)$, then the difference of the two is

$$\Delta r_{\ell,\ell+2}(n) = r_{\ell,\ell+2}(n) - r'_{\ell,\ell+2}(n). \tag{41}$$

These differences were then averaged over n, for each of the $\Delta r_{02}(n)$ and $\Delta r_{13}(n)$, to yield weighted mean differences, $\langle\Delta r_{\ell,\ell+2}\rangle$:

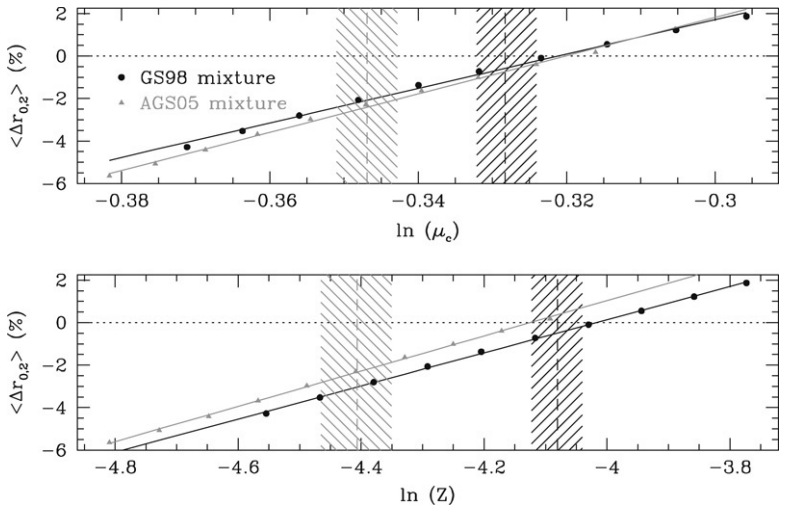

Fig. 23. The relation between the averaged difference of the frequency separation ratios between a solar model and that obtained from BiSON data, and the average mean molecular weight in the core of solar models as well as Z for the models. Only results for the (0,2) separation ratios are shown, results for the (1,3) ratios are similar. The best-fit straight lines are also shown. Results are shown for models with both GS98 relative heavy-element abundances and AGS05 relative heavy-element abundances. The two vertical lines mark the models with GS98 and AGS05 abundances. The hashed region around these lines represent uncertainties in μ_c and Z. Errors in $\langle \Delta r_{0,2} \rangle$ are of the size of the points. In the case of the μ_c plot, the errors represent the range of μ_c for a given Z caused by differences in relative composition, errors in the diffusion rate, etc. The errors were obtained from the Monte Carlo simulations of Bahcall et al. (2006).

$$\langle \Delta r_{\ell,\ell+2} \rangle = \frac{\sum_n \Delta r_{\ell,\ell+2}(n)/\sigma^2_{r_{\ell,\ell+2}}(n)}{\sum_n 1/\sigma^2_{r_{\ell,\ell+2}}(n)}. \tag{42}$$

The formal uncertainties of the BiSON spacings, $\sigma_{r_{\ell,\ell+2}}(n)$, were used to weigh the averages. The data were averaged over the radial-order ranges where good determinations of the separation ratios were available, which for the data set used was $n = 9$ to 25. While Basu et al. (2007) had shown that the separation ratios depend on the molecular weight, they did not determine the exact dependence of the separation ratios on the average mean molecular weight of the core. To do so, Chaplin et al. (2007b) constructed two sets of test models. The models in each set had different values of Z/X, but one sequence of models was constructed with the relative heavy-element abundances of GS98, while the second sequence was made with the relative heavy-element abundances of AGS05. To fix the Z/X of a given model in either sequence, the individual relative heavy-element abundances of GS98 (or AGS05) were multiplied by the same constant factor. The models otherwise had identical physical inputs. Chaplin et al. (2007b) found that $\langle \Delta r_{\ell,\ell+2} \rangle$, the mean difference of the separation ratios between the Sun and the models was a linear function of $\ln \mu_c$ and $\ln Z$, where μ_c is the mean molecular weight in the inner 20% (by radius) of the Sun, and Z is the metallicity in the convection zone. This relation can be seen in Fig. 23. This monotonic relationship led the authors to argue that $\ln \mu_c$ and $\ln Z$ for the model that lead to perfect match between the separation ratios of the model and the Sun would be a good estimate of $\ln \mu_c$ and $\ln Z$ of the Sun. The quantities μ_c and Z are related — higher Z results in a higher μ_c. Two models with the same Z, nuclear reaction rates, opacities and equation of state can have different values of μ_c only if the diffusion rates are different in the two models. It is, however, not surprising that the dependence of the separation ratios on the two parameters is somewhat different given that μ_c also depends heavily on the helium abundance in the core. Since all the models were calibrated to have the same radius and luminosity at the solar age, differences in Z generally gave rise to differences in the core helium abundance.

The value of μ_c for which $\langle \Delta r_{\ell,\ell+2} \rangle = 0$ is almost independent of the heavy-element mixture used in the model, but the value of Z for which $\langle \Delta r_{\ell,\ell+2} \rangle = 0$ depends on the mixture. This is not difficult to understand. For the calibrated solar models used by Chaplin et al. (2007b), the dominant contribution to the Z and μ_c of each model comes from different elements. For Z, the dominant elements, in order of importance, are oxygen, carbon, neon and iron. The value of μ_c is determined by the mass fractions of helium and hydrogen in the core. The abundances of hydrogen and

helium in the core depend strongly on the abundances of heavy elements that contribute to the opacity in the core. These elements, again in order of importance, are iron, sulfur, silicon and oxygen. The difference between the GS98 and AGS05 mixture lies predominantly in the relative abundances of oxygen, carbon, nitrogen and neon, less so in sulfur, and much less so in the abundances of iron and silicon. This explains why for the same Z, μ_c is different for the GS98 and AGS05 models. From the calibration curves shown in Fig. 23, Chaplin et al. (2007b) determined the solar μ_c and Z to be 0.7248 ± 0.0008 and 0.01785 ± 0.00007 respectively using GS98 models, and $\mu_c = 0.7258 \pm 0.0008$ and $Z = 0.01611 \pm 0.00008$ using AGS05 models. The errors here are caused by errors in the BiSON frequencies alone and do not have any contribution from errors in inputs to the two sets of models.

Since μ_c for a model depends on other input physics Chaplin et al. (2007b) used the large set of solar models of Bahcall et al. (2006) that were obtained from a Monte Carlo simulation (see Section 6) to actually determine μ_c and Z for which $\langle \Delta r_{\ell,\ell+2} \rangle = 0$. These models take into account the relevant uncertainties in standard solar model calculations, and hence, the spread in the results will give the uncertainty in the results. Since the Monte Carlo results did not take into account the error due to the input opacity tables, these were determined separately and added to the uncertainties. From the results obtained using the Monte Carlo models, Chaplin et al. (2007b) found that the error on μ_c is about 0.5%. The uncertainty in Z is larger and is in the range 12%–19%. Because of the indirect dependence of the separation ratios on Z, it is difficult to obtain a more precise result. The main source of uncertainty in the Z results is the relative abundance of the heavy elements, and not any of the other physical inputs used to make solar models. The solar results indicate that the AGS05 models do not satisfy seismic constraints even in the core. The average μ_c for the AGS05 models in the Monte Carlo simulation was 0.7088 ± 0.0029. The GS98 models had an average μ_c of 0.7203 ± 0.0029. Thus the results of Chaplin et al. (2007b) indicate that the discrepancies between the solar models constructed with low metallicity and the helioseismic observations extend to the solar core and thus cannot be attributed to the deficiencies in the modelling of the solar convection zone.

8.3. Results that depend on the Z-dependence of the equation of state

The results mentioned in Sections 8.1 and 8.2 exploited the effect of heavy-element abundances on opacity. Such estimates are sensitive to other uncertainties in input physics, like errors in the opacity table, diffusion coefficients, etc., and it is quite difficult to estimate the effect of these on the derived abundances. As a result, it is necessary to use seismic techniques that do not depend on opacity, but on some other input physics. In the case of determining the helium abundance, one used the dimensionless sound-speed gradient $W(r)$ (see Eq. (39), and also Section 3.3, Section 4.1) or the adiabatic index, Γ_1. These two functions are determined by the equation of state rather than opacity. There have been attempts to determine Z using $W(r)$ and Γ_1 (e.g., Elliott (1996)). The main problem with these techniques is that the effect of heavy-element abundances on $W(r)$ or Γ_1 is rather small because of the low abundances of heavy elements. The typical ratio of an heavy element to hydrogen abundance by number is of the order of 10^{-4}. It is this quantity, rather than the mass ratio, that is the relevant measure needed to quantify the effect of heavy elements on the equation of state. Hence the expected effect of the heavy-element abundance on $W(r)$ or Γ_1 in the lower convection zone is of this order. This is just about the accuracy of the inversion techniques in this region.

The dimensionless gradient of squared sound speed, $W(r)$ shows peaks in the ionization zones of various elements. As mentioned in Section 4.1, The peak due to the He II ionization zone around $r = 0.98 R_\odot$ has been successfully used to determine the helium abundance. The height of this peak is about 0.1, which is roughly the relative abundance of He by number. Thus the bumps due to heavy elements are expected to be of the order of 10^{-4}. Furthermore, as can be seen from Fig. 8 the ionization zones of different elements overlap and hence it is difficult to isolate the signal from each heavy element, making it difficult to measure the abundances of individual elements using this technique. However, Antia and Basu (2006) showed that it is possible to determine the total heavy-element abundance, Z, using $W(r)$.

Antia and Basu (2006) used the RLS inversion technique to estimate the solar sound-speed profile using observed frequencies. The RLS technique was used because it gives the sound speed in a form that can be easily differentiated to calculate $W(r)$. The acceleration due to gravity, $g(r)$, was estimated from the inverted density profile. Before applying this technique to observed frequencies, they tested it by using frequencies of known solar models to infer the Z for these models. They found that it is indeed possible to reliably determine $W(r)$ for the Sun to sufficient accuracy and precision to determine Z, and obtained $Z = 0.0172 \pm 0.002$ in the solar convection zone.

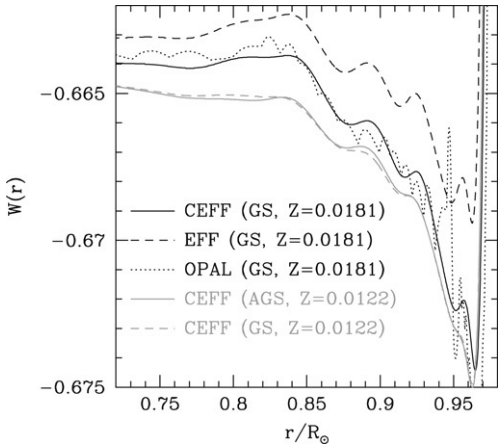

Fig. 24. The dimensionless sound-speed gradient, $W(r)$ in solar models with different equations of state and heavy-element abundances.

The main source of uncertainty in the determination of Z from $W(r)$ is the equation of state, since in addition to abundances, $W(r)$ depends on the equation of state. The more sophisticated equations of state like OPAL and MHD are tabulated for a fixed mixture of heavy elements that is quite different from the solar abundances mixture. For example, the OPAL equation of state is calculated for a mixture consisting of only C, N, O and Ne, while the MHD equation of state only uses C, N, O and Fe. Hence, it is not possible to use these equations of state for determining solar Z. As a result, Antia and Basu (2006) had to use the CEFF equation of state for their work. They calculated this equation of state using a mixture of 20 elements (which includes almost all elements used in OPAL or OP opacity calculations). The advantage of using CEFF equation of state was that they could change the mixture of heavy elements (and Z) as per requirements.

Fig. 24 shows $W(r)$ for a few solar models using different equations of state and heavy-element abundances. The peak due to the He II ionization zone extends till $0.96R_\odot$, and hence one can only look for signatures from heavy elements below this region. The broad peak in $W(r)$, which extends till the convection-zone base, is caused by the combined effects of all heavy elements. Its height, of the order of 10^{-3}, is comparable to the total relative heavy-element abundance by numbers. The curve for the model constructed using the CEFF equation of state shows small peaks that modulate the general peak, and these are caused by the ionization zones of the individual elements. The curve for the model with OPAL equation of state shows some additional fluctuations that are caused by interpolations needed to use the OPAL tables. These errors are magnified when derivatives are calculated. The numerical errors arise from the interpolation in the grid of tabulated values and from the finite accuracy to which the entries in tables are stored. The CEFF equation of state and the derivatives are calculated analytically, and hence does not suffer from this problem. It is clear that tables with higher accuracy are needed to calculate thermodynamic quantities using OPAL equation of state to sufficient accuracy. However, for the same heavy-element abundances, there is not much difference between $W(r)$ using CEFF and OPAL equation of state in the radius range of interest in this study. Thus CEFF is more useful than OPAL equation of state in determining Z. It is clear from Fig. 24 that $W(r)$ depends on total heavy-element abundance Z, and that its dependence on the mixture of heavy elements is more subtle. Although, the exact shape of the curve also depends on the equation of state, the results for OPAL and CEFF models that have the same value of Z are very similar.

In order to get a quantitative estimate of $W(r)$, Antia and Basu (2006) proposed to use the average value of $W(r)$, $\langle W(r)\rangle$, calculated over different radius ranges. They used three different radius intervals, 0.75–$0.95R_\odot$, 0.80–$0.95R_\odot$ and 0.85–$0.95R_\odot$. They examined the behavior of $\langle W(r)\rangle$ with Z using solar-envelope models with fixed X_s and r_b but different Z. The dependence was found to be almost linear in the expected range of Z. This can be seen in Fig. 25. These calibration curves can be used to estimate Z from measured $\langle W(r)\rangle$. The calibration curve, of course, depends on the equation of state, but the difference between the OPAL and CEFF equation of state is not very large. The calibration curve also depends on the mixture of heavy elements used, but the difference between the mixtures obtained by GS98 and AGS05 is very small hence the effect is not large. Antia and Basu (2006) have estimated the systematic errors expected from these and other sources of uncertainties. The largest source of systematic errors are

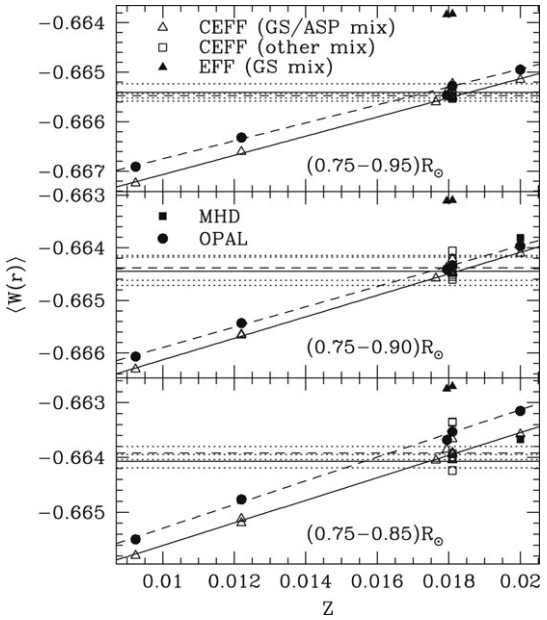

Fig. 25. The average value of $W(r)$ in different radius intervals is shown as a function of Z for different solar models. The horizontal lines in each panel shows $\langle W(r)\rangle$ inferred through inversions of observed solar frequencies. The dotted lines showing the 1σ error limits on the helioseismic results. The solid horizontal lines are for GONG data and dashed for MDI.

the equation of state and the depth of the convection zone. The difference between OPAL and CEFF equations of state leads to an error of 0.0015 in Z, while a variation of $0.01R_\odot$ in the depth of the convection zone results in an error of 0.0012 in Z.

Using different data sets of observed frequencies obtained from GONG and MDI observations, and calibration models constructed with CEFF and OPAL equations of state, Antia and Basu (2006) found $Z = 0.0172 \pm 0.002$. The error-bars include systematic errors caused by uncertainties in the equation of state, heavy-element mixture and other uncertainties in the solar models. As can be seen from Fig. 14, the function $W(r)$ in models constructed with AGS05 abundances is inconsistent with that for the Sun as derived from observed frequencies. Models with GS98 abundances on the other hand, fare much better. It should be noted that the discrepancy between solar models and seismic data is essentially independent of opacities and will not be improved by increasing the opacity or diffusion coefficients as described in the last section. Increasing Ne abundance will change the equation of state and this option too can be examined using $W(r)$.

The total heavy-element abundance obtained by Antia and Basu (2006) using $W(r)$ is consistent with the GS98 abundances. Basu and Antia (2006) examined whether or not one could determine the abundances of individual elements. For this purpose they looked at $W(r)$ of models constructed with different heavy-element mixtures but with the same value of Z. Thus when the relative abundance of one element was increased, the actual abundances of other elements were scaled down appropriately. Fig. 26 shows the results obtained for models where abundances of some elements are enhanced by a factor of two. It can be seen that increasing carbon abundance leads to a small peak in $W(r)$ around $r = 0.9R_\odot$ which is probably due to the C V ionization zone. Similarly, increasing the oxygen abundance gives a broad peak around $r = 0.85R_\odot$ that is probably the ionization zone for O VII, while increasing the neon abundance gives a peak around $r = 0.92R_\odot$. The main peak, caused by Ne IX, occurs at the lower end of the convection zone and is not in the radius-range where the solar $W(r)$ can be determined to the required precision. All these peaks, however, are fairly small and it is difficult to identify them in the solar $W(r)$ profile obtained from sound-speed inversions, and hence, cannot be used directly to determine the abundances of individual elements.

Although, it may be difficult to isolate the peaks due to individual elements from $W(r)$ obtained from inversions, it is clear from Fig. 26 that the average value of $W(r)$, $\langle W(r)\rangle$, calculated over different radius ranges changes by different amounts when the mixture of elements is changed. If the calibration models are constructed using the same mixture of heavy elements as that of the Sun, and if the equation of state of the models also correctly represents the

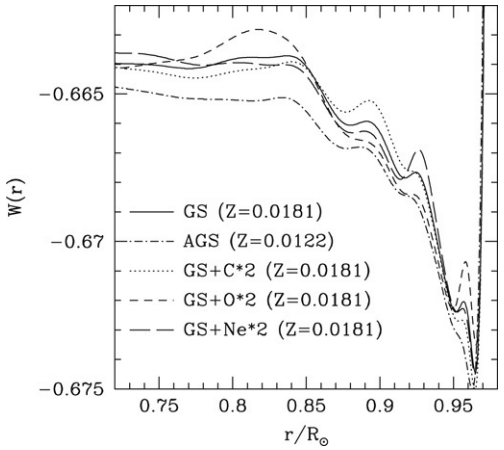

Fig. 26. The dimensionless sound-speed gradient, $W(r)$, of solar models with different heavy-element abundances and mixtures. Some of these models were constructed by enhancing the abundance of an individual element by a factor of 2. All models were constructed with the CEFF equation of state.

solar equation of state, then the estimated value of Z using $\langle W(r)\rangle$ calculated over the three radius ranges will be identical. Thus, the differences in these estimates would imply a difference in the mixture, differences in the equation of state, or some other errors in the solar models. Basu and Antia (2006) found that $\langle W(r)\rangle$ calculated between 0.75–$0.95R_\odot$ is fairly insensitive to differences in the mixture of heavy elements and is essentially determined by the total value of Z. Thus if Z_1,Z_2 and Z_3 represent the values of Z obtained using $\langle W(r)\rangle$ over the radius ranges 0.75–$0.85R_\odot$, 0.75–$0.90R_\odot$, and 0.75–$0.95R_\odot$, respectively, then the differences $Z_1 - Z_3$ and $Z_2 - Z_3$ will contain some signature of the difference of the heavy-element mixture. For example, when oxygen abundance is increased by a factor of 2, $Z_1 - Z_3 = 0.0025$, but $Z_2 - Z_3 = 0.0010$. Basu and Antia (2006) found using CEFF calibration models constructed with GS98 heavy-element mixture that for solar data $Z_1 - Z_3 = 0.00036 \pm 0.00088$ and $Z_2 - Z_3 = 0.00013 \pm 0.00135$. Thus it again appears that the solar heavy-element abundances are consistent with GS98.

In principle, one can parameterize the heavy-element mixture using three parameters that can be determined from the three estimates Z_1, Z_2, Z_3. For example, if we assume that these values are mainly determined by abundances of C, O and Ne, then:

$$\frac{\partial(Z_1 - Z_3)}{\partial \ln Z_C}\frac{\delta Z_C}{Z_C} + \frac{\partial(Z_1 - Z_3)}{\partial \ln Z_O}\frac{\delta Z_O}{Z_O} + \frac{\partial(Z_1 - Z_3)}{\partial \ln Z_{Ne}}\frac{\delta Z_{Ne}}{Z_{Ne}} = Z_1 - Z_3, \tag{43}$$

$$\frac{\partial(Z_2 - Z_3)}{\partial \ln Z_C}\frac{\delta Z_C}{Z_C} + \frac{\partial(Z_2 - Z_3)}{\partial \ln Z_O}\frac{\delta Z_O}{Z_O} + \frac{\partial(Z_2 - Z_3)}{\partial \ln Z_{Ne}}\frac{\delta Z_{Ne}}{Z_{Ne}} = Z_2 - Z_3, \tag{44}$$

$$\delta Z_C + \delta Z_O + \delta Z_{Ne} = \delta Z = 0. \tag{45}$$

For the last equation we have assumed that the value of Z is determined from some average of Z_1, Z_2, and Z_3. Using solar-oscillation frequencies, Basu and Antia (2006) found that

$$\frac{\delta Z_C}{Z_C} = 0.37 \pm 0.86, \qquad \frac{\delta Z_O}{Z_O} = 0.04 \pm 0.31, \qquad \frac{\delta Z_{Ne}}{Z_{Ne}} = -0.62 \pm 2.75. \tag{46}$$

It is clear that the estimated errors in the determination of individual elements are rather large. In particular, the error in the estimated neon abundance is extremely large because of the relative insensitivity of $W(r)$ to the neon abundance in the radius range that is used. The oxygen abundance has the least errors, which is to be expected since it is the most abundant of the heavy elements and it also has a significant influence in the convection zone. The estimated oxygen abundance is consistent with GS98 abundance. However, it has an error of about 31%, which is about a factor of 2 larger than the quoted uncertainties in the spectroscopic estimates listed in GS98 and AGS05, however the uncertainty is about a factor of 1.5 smaller than the difference between the GS98 and AGS05 abundances.

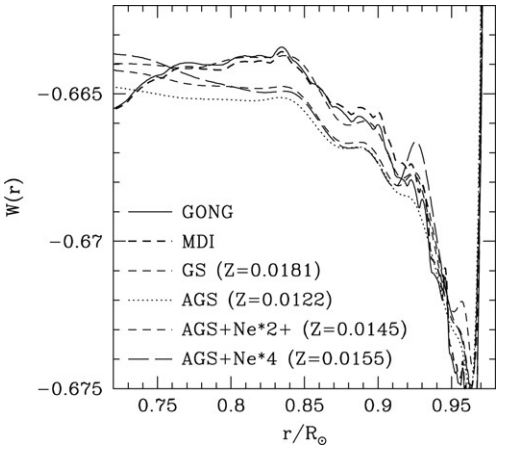

Fig. 27. The dimensionless sound-speed gradient, $W(r)$, of solar models with different different heavy-element abundances and mixtures compared with $W(r)$ obtained from inversions of GONG and MDI data. The model labeled as Ne*2+ was constructed by enhancing the abundance of Ne by a factor of 2 and increasing the C, N, O abundance by 1σ of AGS05 abundances. All models, including the neon-enhanced ones, were constructed with the CEFF equation of state.

Basu and Antia (2006) also examined the issue of the solar neon abundance. From Fig. 26 it is clear that the effect of increasing neon abundance on $W(r)$ is quite different from that of increasing oxygen abundance. Hence, the reduction in the oxygen abundance cannot be compensated by increasing the neon abundance, at least as far as $W(r)$ is concerned. Fig. 27 compares $W(r)$ of models with increased neon abundance with those of models with GS98 and AGS05 abundances. It is clear that increasing the abundance of neon does not bring the $W(r)$ of the models close to the solar $W(r)$, though it is better than the model with normal AGS05 abundances. Interestingly, increasing the neon abundance in the GS98 mixture may still be consistent with observations. Thus, although, increasing neon abundance with the other abundances at the AGS05 level does not work, one cannot rule out an increased neon abundance beyond the GS98 value. Such an increase will also be consistent with other seismic constraints.

In addition to $W(r)$, one can also use the adiabatic index, Γ_1, to constrain solar heavy-element abundances, since, like $W(r)$, Γ_1 is also affected in the ionization zones of heavy elements. The advantages of using Γ_1 are two-fold. First is that unlike $W(r)$, which requires calculation of a derivative with r, Γ_1 can be directly inferred from seismic inversions. The second advantage is that using the equation of state, we can calculate the dependence of Γ_1 on structure variables such as P and ρ, and this can be subtracted to calculate the intrinsic difference in Γ_1 as explained in Section 3.3. This intrinsic difference, $\delta\Gamma_{1,\mathrm{int}}/\Gamma_1$, depends only on the equation of state and heavy-element abundances. Thus the structure-dependence is explicitly filtered out, something that cannot be done for $W(r)$. While $W(r)$ shows a mild dependence on opacities because of the effect of opacities on the density profile, $\delta\Gamma_{1,\mathrm{int}}/\Gamma_1$ does not show that. Since $\delta\Gamma_{1,\mathrm{int}}/\Gamma_1$ is independent of differences in solar structure and depends only on equation of state and the heavy-element abundances, any discrepancy in Γ_1 between solar models and the Sun will not be resolved by increasing opacity or diffusion coefficients.

As mentioned in Section 6.4, Lin et al. (2007) showed that $\delta\Gamma_{1,\mathrm{int}}/\Gamma_1$ can be used to distinguish between the models with different values of Z/X (see Fig. 15). They found that models constructed with AGS05 heavy-element abundances have larger $\delta\Gamma_{1,\mathrm{int}}/\Gamma_1$ with respect to the Sun than models with GS98 abundances. It is clear from Fig. 15 that in the region where reliable inversions are possible, $\delta\Gamma_{1,\mathrm{int}}/\Gamma_1$ has essentially a uniform shift with change in Z, and, in principle, by measuring this shift one can estimate Z. However, differences in the equation of state between the models and the Sun makes it difficult to get a perfect match with the Sun.

Lin et al. (2007) also looked at the effect of different heavy-element mixtures and found peaks and dips at different positions when various elements were enhanced separately. But the peaks and dips for different elements often overlap and in some cases it is possible to nearly cancel the effect of changes in the abundance of one element by adjusting the abundances of other elements suitably. Thus it may not be possible to determine the abundances of individual elements using this technique, though one may get a good estimate of total heavy element abundance, and it appears that the heavy-element abundance is close to the GS98 value.

If the AGS05 abundances are applicable in the convection zone, then the discrepancy in $W(r)$ and Γ_1 can only be attributed to errors in the equation of state. It is difficult to estimate the possible errors in equations of state since these are theoretically calculated and not obtained from laboratory measurements. If we assume that the differences between independently calculated equations of state like OPAL and CEFF, or OPAL and MHD are a measure of the error in the equation of state, we find that the differences are not sufficient to explain the discrepancy in $\Gamma_{1,\mathrm{int}}$ between models with AGS05 abundances and the seismic data. Thus in addition to opacity, and diffusion coefficient etc., the equation of state too will have to be modified to resolve the discrepancy between the AGS05 models and seismic data.

9. Possible causes for the mismatch between seismic and spectroscopic abundances

Since attempts to modify low-metallicity solar models to bring them in agreement with seismic inferences have failed, and furthermore since seismic determinations of heavy-element abundances consistently yield higher values in agreement with GS98, it is worthwhile to examine the spectroscopic determinations that lowered the solar abundances in some detail. The problems could lie with the solar-atmosphere model used by AGS05, or perhaps with the abundance of any one of the elements, or perhaps in the physics inputs to stellar models and those need to be re-examined. In this section, we discuss attempts to check the AGS05 abundances and what needs to be done for that purpose.

It should be recalled that the lowered C, N and O abundances listed in AGS05 were obtained using a 3D simulation of a small region of the lower solar atmosphere instead of the semi-empirical 1D atmospheric models used for earlier abundance determinations. Asplund et al. (2006) claim to be convinced that their results are correct for a number of different reasons. These include the fact that they have used a full NLTE analysis. However, more important is the fact that they believe the 3D simulation they use is more realistic than the 1D empirical model atmosphere because the 3D model includes the effects of turbulence. As a result of this, they could match the line profiles without using any free parameters for micro- and macro-turbulence and they could match the line-bisectors too. Another reason for their confidence in the results is that the 3D models fit the line profiles better than 1D models. More importantly, the abundances obtained from different lines are more consistent with each other than those obtained with a similar 1D analysis. In addition to all these reasons, Grevesse et al. (2007) also claim that the AGS05 abundances are more believable since the lower abundances make solar abundances consistent with the abundances of the surrounding interstellar medium and nearby B stars. While these are powerful arguments, the correctness of the abundance results depends crucially on whether or not the density and thermal structure of the simulations used is indeed the density and thermal structure of the Sun. And although 3D models give similar results using different lines for C and O, the same is not true for N, where the 1D Holweger and Müller (1974) model actually gives more consistent results using both the N I and NH lines and these values agree with GS98. Furthermore, the AGS05 abundance for Na is about 0.1 dex lower than the meteoritic abundance, while for Ne the abundances obtained from Ne/O ratio in corona does not match with that obtained using Ne/Mg ratio. It is difficult to explain these discrepancies. Thus it is clear that more work is needed to calculate all heavy-element abundances consistently.

Since the publication of the Allende Prieto et al. (2001, 2002) and Asplund et al. (2004) papers and the AGS05 table, there have been some attempts to independently derive the solar oxygen abundance. Meléndez (2004) determined the solar oxygen abundance using infrared OH lines. He used a number of model atmospheres, such as a Kurucz model (Kurucz, 1970; Sbordone et al., 2004; Kurucz, 2005a,b) with convective overshooting, a temporally and spatially averaged version of the Asplund et al. (2004) model that he calls ⟨3D⟩, the MARCS model of Asplund et al. (1997), and the Holweger and Müller (1974) model. He used non-LTE corrections from Asplund et al. (2004). The results obtained by Meléndez (2004) varied according to the model atmosphere used. The ⟨3D⟩ model yielded an abundance of 8.59 dex, the MARCS, Kurucz and Holweger and Müller (1974) models give 8.61, 8.71 and 8.80 dex respectively. However, since this work basically uses the 3D model of AGS05, it cannot be considered to be an independent determination of the abundances.

Socas-Navarro and Norton (2007) used spatially resolved spectropolarimetric observations of the O I infrared triplet around 777.4 nm. They used Fe I lines at 630.2 nm to reconstruct the 3D thermal and magnetic structure of the atmosphere. They used a 1.5D approach which neglects lateral radiative transfer. They claim $\log\epsilon(\mathrm{O}) = 8.93$ for an LTE calculation and $\log\epsilon(\mathrm{O}) = 8.63$ for a non-LTE calculation using the code of Socas-Navarro et al. (2000). Their error estimate is 0.1 dex. But the most disconcerting feature of their results is that they find that the oxygen abundance they obtain, whether LTE or non-LTE, is not constant across the solar surface, with magnetic features showing higher

abundances, by as much as 0.3 dex. Their LTE results range for $\log \epsilon(\mathrm{O}) = 8.7$–$9.3$, and non-LTE results vary from somewhat less than $\log \epsilon(\mathrm{O}) = 8.5$ to somewhat more than 8.9. Since there is no physical reason to expect spatially varying abundances, the authors conclude that this variation must be an artifact of the analysis, probably caused by imperfect modelling, especially in the presence of magnetic fields.

Ayres et al. (2006) did a photospheric "thermal profiling" analysis using rotational-vibrational bands of carbon monoxide as observed with the McMath–Pierce Fourier Transform Spectrometer at Kitt peak, and from the space shuttle-borne ATMOS experiment. They find a high oxygen abundance, $\log \epsilon(\mathrm{O}) = 8.85$, which is consistent with GS98 value, but larger than AGS05. They point out that this discrepancy may be because the 3D model of Asplund et al. (2000b) has too steep a temperature gradient in the visible continuum forming layers. It is possible that the 3D atmospheric models reproduce the velocity field in the solar atmosphere reasonably well and hence they are able to predict correct line shapes, but the thermal structure in these models may not match the solar atmosphere. The 1D model perhaps represent the thermal structure of the solar atmosphere better because of the adjustable parameters used in 1D model calculations. Ayres et al. (2006) admit that there are considerable uncertainties in deriving oxygen abundance using CO lines and more work is required to get a reliable estimate of the oxygen abundance. These results are now disputed by Scott et al. (2006), who used the same lines as Ayres et al. (2006) but the simulations of Asplund et al. (2000b) to get a lower abundance. Scott et al. (2006) find low abundances, consistent with AGS05, using the weak lines, and they also find that the abundance is independent of the equivalent width when the 3D model is used. However, when using the low-excitation lines, they find that the determined abundance does depend on the equivalent width and the mean value is somewhat larger. This discrepancy is likely to be due to the deficiency in modelling higher layers in the solar atmosphere. They also compared the results using different 1D models and found that in all cases 1D models yield significantly larger abundances. Thus all recent investigations show that there are large discrepancies in the solar oxygen abundance obtained from spectroscopy.

The simulations used by Allende Prieto et al. (2001, 2002) and Asplund et al. (2004, 2005a) were obtained using the code of Nordlund and Stein, which had been developed to study solar and stellar surface convection (see e.g., Nordlund and Stein (1990) and Stein and Nordlund (1989, 1998)), which has been described in Section 5. It should be noted that the purpose of simulations done with this code was to study the properties of solar convection, not abundances. While there have been some tests of the simulations against the velocity spectrum obtained at the solar surface, there are no direct tests to examine whether or not the density and the vertical thermal structure obtained from the simulations matched that of the Sun. The influence of magnetic fields that permeate the solar photosphere has also not been properly estimated. Borrero (in press) has attempted to estimate the effect of magnetic fields on abundance estimates, to find that although Fe abundance can be affected by up to 0.1 dex, the effect on oxygen abundance is small.

There are two important tests available for validating models of the solar photosphere that can be performed on the 3D model — one is the center-to-limb variation and the other are the absolute fluxes (Allende Prieto, 2007). Preliminary results of Asplund et al. (1999) and Allende Prieto et al. (2004) on center to limb variation were encouraging. Koesterke et al. (submitted for publication), using a different spectral-synthesis code, found that for many wavelengths, the center-to-limb variation in abundances obtained from these 3D models are comparable to that for theoretical 1D models. They did not test the 3D models against semi-empirical 1D models since the latter show the correct center-to-limb variation by design. Another powerful diagnostic that can be applied to test the 3D models is an analysis of spatially resolved solar spectra. The line profiles in the granules would be different from that in the inter-granular regions and if these are compared with model predictions, it can provide an independent test of the models (Asplund, 2005).

A hint that the thermal structure of the simulations do not exactly match that of the Sun comes from the fact that hydrogen Balmer-line profiles and the cores of strong lines do not match, and there is too little flux in the ultraviolet (Trampedach and Asplund, 2003). While Koesterke et al. (submitted for publication) found that the center-to-limb variation of the 3D models are not worse than those of the theoretical 1D models, they however, find that the models have temperature gradients that are too steep around $\tau = 2/3$. Ayres et al. (2006) too have argued that it is important to calibrate all photospheric models against the center-to-limb behavior since this quantity is a measure of the temperature gradients of the regions from which emission occurs. They also claim that the temperature gradient of the averaged simulation used by Asplund et al. is too steep in the layers that form the visible continuum, however Koesterke et al. (submitted for publication) argue that the arguments are not valid. Scott et al. (2006) examined the line shapes of the strongest CO lines, which form high in the solar photosphere to find some discrepancy which probably implies that temperature is overestimated in the highest layers of the simulation. Ayres et al. (2006) point out that the

discrepancy between their estimate of the solar oxygen abundance and those obtained with the 3D model could be a result of the fact that the 3D model of Asplund et al. (2000b) has too steep a temperature gradient in the visible continuum forming layers.

One possible reason for an incorrect thermal structure of the 3D models is the treatment of radiative transfer in the simulations. Because of the two extra dimensions in the horizontal direction, it is not possible to perform the radiative-transfer calculations with the same level of details as for the 1D stellar-atmosphere models (Trampedach, 2006). Trampedach and Asplund (2003) showed that the use of the multigroup method, i.e., opacity binning, leads to systematic differences in radiative heating compared with monochromatic opacities. There are efforts underway to improve the radiative transfer in the Nordlund–Stein simulation code (Trampedach, 2006). In addition to assumptions used in the calculation of radiative transfer, all convection simulations have some "hidden" parameters. These include some type of numerical viscosity to keep the code stable. Solar plasma on the other hand, has very small molecular viscosity. Also given that turbulence can occur on scales much smaller than what the simulations usually resolve, a sub-grid scale model of the quantities must be specified. Uncertainties in sub-grid scale physics can also give rise to uncertainties in the thermal structure. The effect of larger scales of convection, like supergranulation is also not included in these simulations. All these can lead to differences in simulation results obtained by different codes. It is not clear yet how these factors affect abundance determinations using these simulations. The results of AGS05, therefore, need to be verified using simulations obtained from other codes that use different models of viscosity and sub-grid scale physics, as well as different assumptions to do the radiative transport. It would, therefore, be very valuable if different groups would analyze the solar abundances using different simulations. The comparison between the results of different groups would permit a more robust estimation of the systematic uncertainties.

Although, the use of 3D atmospheric models is an improvement in stellar abundance calculations, it should be noted that even the highest resolution simulations available today are many orders of magnitude away from being able to reproduce the characteristic Reynolds number in the Sun. Scott et al. (2006) found significant changes in the line-bisectors high in the atmosphere as they changed their resolution. Asplund et al. (2000a) found sensitivity of up to 0.10 dex for abundances derived from intermediate strong lines with significant non-thermal broadening. Thus numerical tests with substantially increased resolution are required to test abundance results obtained with 3D hydrodynamical models. In addition to the use of 3D models, two other factors have played a role in the reduction of the oxygen abundance, atomic physics (including non-LTE effects), and problems with blended lines. These issues also need to be examined critically. In particular, a quantum mechanical treatment of cross-section for inelastic electron and hydrogen collision is required to calculate the NLTE corrections. Presently, NLTE calculations have not been performed for all lines and a systematic study of these for all lines and elements is required.

In Section 7 we discussed attempts to modify solar interior models with low abundances to bring them in agreement with seismic data. The same exercise needs to be done with solar atmospheric models used in spectroscopic determination of abundances to check how robust the results are. Just like the standard solar models, the 3D atmospheric models do not have any explicit free parameters, but the input physics, and the treatment of radiative transfer can be modified to test the sensitivity of these models. The atmospheric models depend on input physics like the opacity, equation of state and other atomic data. Opacities at these temperatures and densities are more uncertain than opacities in the solar interior and their effect on the atmospheric models and the inferred abundances needs to be studied. The equation of state may also play an important role in atmospheric model since at these temperatures most of the free electrons are contributed by heavy elements with low ionization potential and the electron pressure plays an important role in line formation. The MHD equation of state used in simulations of AGS05 probably does not use the correct mixture of heavy elements. Thus it is necessary to use equation of state with correct mixture of heavy elements to get the correct electron pressure. These models also depend on how radiative transfer is handled. Owing to the extremely time-consuming nature of radiative-transfer calculations, simplified assumptions are used to solve the relevant equations.

In the absence of extensive tests it is difficult to estimate systematic errors in these abundance calculations. We think that it is necessary to do a Monte Carlo simulation for atmospheric models, of the kind done by Bahcall et al. (2006) for solar interior models, to get a realistic estimate of errors in abundance calculations. To a first approximation, the difference between results obtained by 1D and 3D atmospheric models may be considered to be an estimate of the errors caused by uncertainties in the atmospheric models. The difference in abundances between the GS98 and AGS05 tables are generally of the order of 2σ and as such we can conclude that there is no serious disagreement.

However, the precision of helioseismic data are much higher, and hence the relatively small changes in the heavy-element abundances (compared to their error estimates) result in changes that are much larger than the errors in seismic inferences.

It is heartening to note that there are at least some efforts to determine solar abundances using the same technique as Asplund et al. (2004) etc., but using simulations obtained by different codes. Ludwig and Steffen (2007) report a preliminary estimate of $\log \epsilon(\mathrm{O}) = 8.72 \pm 0.06$ which is consistent with 8.66 ± 0.05 determined by AGS05, and somewhat lower than the GS98 value of 8.83 ± 0.06. However, Ludwig and Steffen (2007) also used opacity binning in their simulations and hence the results probably have uncertainties related to the thermal structure. Caffau et al. (2007) have used 3D atmospheric models to find phosphorus abundance using the P I multiplet at 1051–1068 nm to find $\log \epsilon(\mathrm{P}) = 5.46 \pm 0.04$, which is consistent with the GS98 value but higher than the AGS05 estimate. They used 3D models computed with CO^{5}BOLD code (Freytag et al., 2002; Wedemeyer et al., 2004). They find that the corrections due to use of 3D models is small for these lines. It is not clear why their results are about 0.1 dex higher than AGS05. Thus much more work needs to be done to understand the results.

Assuming that the 3D solar atmosphere models have the correct thermal structure, and that the NLTE corrections have been applied correctly and hence the new C, N, and O abundances are correct, the possibility still remains that the abundance of one key element is incorrect. As discussed in Section 7.3, judiciously increasing the abundance of neon can bring models with low C, N and O abundances in better agreement with seismic data. There still is considerable uncertainty in the abundance of neon, which is an important source of opacity in solar interior. Photospheric models are not relevant for determining neon abundance since there are no photospheric lines of neon, good coronal models are needed for this purpose. More work is needed to understand the abundance variations in the solar corona, solar energetic particles and solar wind to identify the various processes giving rise to fractionation in the upper solar atmosphere. Similar problems were encountered in determining the solar helium abundance, which is now measured seismically. Determining neon abundance seismically is more difficult because of its low abundance, though the possibility should be explored.

There is, of course, also a need for more detailed (and independent) studies of systematic errors involved in seismic determination of the solar heavy-element abundance. Opacity effects have been studied by different investigators independently using independent solar models, and there is good agreement between the results. However, the more subtle effects caused by the equation of state have not been studied independently. This is particularly important since these effects are the ones that can rule out most of the input-physics modifications that have been suggested to resolve the discrepancy between AGS05 models and the Sun. Current seismic studies in this direction are based on the CEFF equation of state, which is not the best that is available, but is the best that can be used for these studies. Much better results could be obtained if tables for more sophisticated equations of state like MHD or OPAL are available with different mixtures of heavy elements so that these studies can be repeated with these equations of state. This, coupled with improved understanding of systematic errors should lead to improved seismic estimates of heavy-element abundances.

10. Concluding thoughts

The discussions presented in the previous sections clearly indicate that there is a large discrepancy between the heavy-element abundances needed to make solar models consistent with helioseismic data and the lowered solar heavy-element abundances as compiled by AGS05. The disagreement between the models and the Sun, as determined from helioseismology, covers almost the whole of the solar interior. As discussed in Section 6, the most obvious discrepancies between these models and the Sun are the position of the base of the convection zone and the helium abundance in the convection zone. Careful investigations, however, have shown that the models are discrepant in the ionization zones in the upper part of the convection zone, and in the core as well. Various suggestions have been put forward to bring the models using reduced abundances back in concordance with helioseismic data, none of the suggestions however, seem to work very well.

Since the publication of the AGS05 abundances, there have been attempts to determine solar abundances from helioseismic data, as has been discussed in Section 8. All the seismic estimates point towards a high solar Z compared with AGS05. Since the Z-dependence of solar oscillations frequencies is not direct, but occurs through the influence of Z on input microphysics such as opacities, equation of state, nuclear reaction rates etc., it is possible, in principle, that the errors in the input physics results in discrepant values of Z obtained from helioseismology on one hand and

the analysis technique used by Allende Prieto et al. (2001, 2002) and Asplund et al. (2004, 2005a) on the other. However, the seismic Z determinations have been done using techniques that depend on different inputs, and despite the differences in techniques and dependences on different inputs, all seismic estimates of Z/X are consistent with the higher GS98 abundances, and they agree with each other as well. Thus the question arises as to what could be causing the discrepancy between the seismic abundances on one hand and the abundances determined from spectral lines listed in AGS05.

If the convection-zone abundances of the Sun are indeed consistent with the low abundances compiled by AGS05, then almost all the input physics that goes into construction of stellar models are much more uncertain than they are normally assumed to be. On the other hand, if the GS98 abundances are correct then the currently known input physics is consistent with seismic data. Thus it is either a sheer coincidence that the errors in the input physics cancel each other when GS98 abundances are used, or the recently revised abundances due to AGS05 need to be revised upwards. The only other option is that some fundamental process is missing in the theory of stellar structure and evolution, but it is difficult to speculate what that could be. It is easier to find reasons that could cause the thermal stratification of the new 3D model atmospheres to be modified and give results different from that of AGS05.

The serious disagreements between helioseismic estimates and recent spectroscopic estimates of the solar heavy-element abundance requires a careful examination of solar atmospheric models, and also models of the solar interior. This is important not only to resolve the discrepancy, but also because solar abundances are used as the scale for abundances of other astronomical objects. A lot of improvements in solar models during the last three decades of the previous century were fueled by the solar neutrino problem. The discrepancy between the observed neutrino fluxes and those predicted by the solar models led to critical examination of all input physics that goes in the construction of solar models. These developments, including the seismic studies, finally led to confirmation of new physics beyond the standard model of particle physics. We can expect that the discrepancy caused by revision of solar heavy-element abundances will lead to further improvements in models of the solar atmosphere and perhaps of the solar interior as well.

Acknowledgments

The authors thank the referee for the comments on the first version of this review. They would like to thank the OPAL project for making it possible to calculate the opacities for different relative abundances. The authors would also like to thank Profs. Pierre Demarque and Sabatino Sofia for their comments on this article. Most of the results quoted in this work and the figures shown were obtained using data from the GONG and MDI projects. MDI is an instrument on board the Solar and Heliospheric Observatory (SOHO). SOHO is a project of international cooperation between ESA and NASA. MDI is supported by NASA grant NAG5-8878 to Stanford University. The GONG Program is managed by the National Solar Observatory, which is operated by AURA, Inc. under a cooperative agreement with the National Science Foundation. The data were acquired by instruments operated by the Big Bear Solar Observatory, High Altitude Observatory, Learmonth Solar Observatory, Udaipur Solar Observatory, Instituto de Astrofisica de Canarias, and Cerro Tololo Interamerican Observatory. Some of the figures use data from the Birmingham Solar Oscillations Network (BiSON) which is funded by the UK Science and Technology Facilities Council (STFC). SB acknowledges NSF grant ATM 0348837 for the partial support.

Appendix. Supplementary data

Supplementary data associated with this article can be found, in the online version, at doi:10.1016/j.physrep.2007.12.002.

References

Adelberger, E.G., et al., 1998. Rev. Modern Phys. 70, 1265–1291.
Aellig, M.R., Lazarus, A.J., Steinberg, J.T., 2001. Geophys. Res. Lett. 28, 2767–2770.
Ahmad, Q.R., et al., 2002. Phys. Rev. Lett. 89, 011301.
Alecian, E., Lebreton, Y., Goupil, M.-J., Dupret, M.-A., Catala, C., 2007. Astron. Astrophys. 473, 181–184.
Allen, C.W., 1973. Astrophysical Quantities. Athlone Press, London.
C. Allende Prieto, 2007. In: Van Belle, G. (Ed.), Proc. 14th Cambridge Workshop on Cool Stars, Stellar Systems, and the Sun. arXiv:astro-ph/0702429.

Allende Prieto, C., Lambert, D.L., Asplund, M., 2001. Astrophys. J. 556, L63–L66.
Allende Prieto, C., Lambert, D.L., Asplund, M., 2002. Astrophys. J. 573, L137–L140.
Allende Prieto, C., Asplund, M., Fabiani Bendicho, P., 2004. Astron. Astrophys. 423, 1109–1117.
Anders, E., Ebihara, M., 1982. Geochimica et Cosmochimica Acta 46, 2363–2380.
Anders, E., Grevesse, N., 1989. Geochimica et Cosmochimica Acta 53, 197–214.
Ando, H., Osaki, Y., 1975. Publ. Astron. Soc. Japan 27, 581–603.
Angulo, C., Arnould, M., Rayet, M. et al., The NACRE collaboration, 1999. Nuclear Phys. A 656, 3–183.
Antia, H.M., 1998. Astron. Astrophys. 330, 336–340.
Antia, H.M., Basu, S., 1994a. Astron. Astrophys. Suppl. Ser. 107, 421–444.
Antia, H.M., Basu, S., 1994b. Astrophys. J. 426, 801–811.
Antia, H.M., Basu, S., 2005. Astrophys. J. 620, L129–L132.
Antia, H.M., Basu, S., 2006. Astrophys. J. 644, 1292–1298.
Antia, H.M., Chitre, S.M., 1995. Astrophys. J. 442, 434–445.
Antia, H.M., Chitre, S.M., 1997. Mon. Not. Roy. Astron. Soc. 289, L1–L4.
Antia, H.M., Chitre, S.M., 1998. Astron. Astrophys. 339, 239–251.
Antia, H.M., Chitre, S.M., 1999. Astron. Astrophys. 347, 1000–1004.
Antia, H.M., Chitre, S.M., 2002. Astron. Astrophys. 393, L95–L98.
Antia, H.M., Basu, S., Hill, F., Howe, R., Komm, R.W., Schou, J., 2001. Mon. Not. Roy. Astron. Soc. 327, 1029–1040.
Arnett, D., Meakin, C., Young, P.A., 2005. In: Barnes III, T.G., Bash, F.N. (Eds.), Cosmic Abundances as Records of Stellar Evolution and Nucleosynthesis. In: ASP Conference Series, vol. 336. pp. 235–246.
Asplund, M., 2000. Astron. Astrophys. 359, 755–758.
Asplund, M., 2005. Ann. Rev. Astron. Astrophys. 43, 481–530.
Asplund, M., Gustafsson, B., Kiselman, D., Eriksson, K., 1997. Astron. Astrophys. 318, 521–534.
Asplund, M., Nordlund, Å., Trampedach, R., 1999. In: Gimenez, A., Guinan, E.F., Montesinos, B. (Eds.), Stellar Structure: Theory and Test of Convective Energy Transport. In: ASP Conf. Ser., vol. 173. pp. 221–224.
Asplund, M., Ludwig, H.-G., Nordlund, Å., Stein, R.F., 2000a. Astron. Astrophys. 359, 669–681.
Asplund, M., Nordlund, Å., Trampedach, R., Allende Prieto, C., Stein, R.F., 2000b. Astron. Astrophys. 359, 729–742.
Asplund, M., Carlsson, M., Botnen, A.V., 2003. Astron. Astrophys. 399, L31–L34.
Asplund, M., Grevesse, N., Sauval, A.J., Allende Prieto, C., Kiselman, D., 2004. Astron. Astrophys. 417, 751–768;
Asplund, M., Grevesse, N., Sauval, A.J., Allende Prieto, C., Kiselman, D., 2005. Astron. Astrophys. 435, 339–340 (erratum).
Asplund, M., Grevesse, N., Sauval, A.J., Allende Prieto, C., Blomme, R., 2005a. Astron. Astrophys. 431, 693–705.
Asplund, M., Grevesse, N., Sauval, A.J., 2005b. In: Barnes, T.G., Bash, F.N. (Eds.), Cosmic Abundances as Records of Stellar Evolution and Nucleosynthesis. In: ASP Conf. Ser., vol. 336. pp. 25–38. AGS05.
Asplund, M., Grevesse, N., Sauval, A.J., 2006. Commun. Asteroseismology 147, 76–79.
Ayres, T.R., Plymate, C., Keller, C.U., 2006. Astrophys. J. Suppl. Ser. 165, 618–651.
Backus, G.E., Gilbert, J.F., 1968. Geophys. J. Roy. Astron. Soc. 16, 169–205.
Badnell, N.R., Bautista, M.A., Butler, K., Delahaye, F., Mendoza, C., Palmeri, P., Zeippen, C.J., Seaton, M.J., 2005. Mon. Not. Roy. Astron. Soc. 360, 458–464.
Bahcall, J.N., Peña-Garay, C., 2004. New J. Phys. 6, 63.
Bahcall, J.N., Pinsonneault, M.H., 2004. Phys. Rev. Lett. 92, 121301.
Bahcall, J.N., Serenelli, A.M., 2005. Astrophys. J. 626, 530–542.
Bahcall, J.N., Pinsonneault, M.H., Wasserburg, G.J., 1995. Rev. Modern Phys. 67, 781–808.
Bahcall, J.N., Pinsonneault, M.H., Basu, S., Christensen-Dalsgaard, J., 1997. Phys. Rev. Lett. 78, 171–174.
Bahcall, J.N., Basu, S., Pinsonneault, M.H., 1998. Phys. Lett. B 433, 1–8.
Bahcall, J.N., Pinsonneault, M.H., Basu, S., 2001. Astrophys. J. 555, 990–1012.
Bahcall, J.N., Serenelli, A.M., Pinsonneault, M., 2004. Astrophys. J. 614, 464–471.
Bahcall, J.N., Basu, S., Pinsonneault, M., Serenelli, A.M., 2005a. Astrophys. J. 618, 1049–1056.
Bahcall, J.N., Basu, S., Serenelli, A.M., 2005b. Astrophys. J. 631, 1281–1285.
Bahcall, J.N., Serenelli, A.M., Basu, S., 2005c. Astrophys. J. 621, L85–L88.
Bahcall, J.N., Serenelli, A.M., Basu, S., 2006. Astrophys. J. Suppl. Ser. 165, 400–431.
Balmforth, N., 1992. Mon. Not. Roy. Astron. Soc. 255, 603–649.
Bandyopadhyay, A., Choubey, S., Goswami, S., Roy, D.P., 2002. Phys. Lett. B 540, 14–19.
Baschek, B., Garz, T., Holweger, H., Richter, J., 1970. Astron. Astrophys. 4, 229–233.
Basu, S., 1997. Mon. Not. Roy. Astron. Soc. 288, 572–584.
Basu, S., 1998. Mon. Not. Roy. Astron. Soc. 298, 719–728.
Basu, S., Antia, H.M., 1994. J. Astrophys. Astron. 15, 143–156.
Basu, S., Antia, H.M., 1995. Mon. Not. Roy. Astron. Soc. 276, 1402–1408.
Basu, S., Antia, H.M., 1997. Mon. Not. Roy. Astron. Soc. 287, 189–198.
Basu, S., Antia, H.M., 2001. Mon. Not. Roy. Astron. Soc. 324, 498–508.
Basu, S., Antia, H.M., 2004. Astrophys. J. 606, L85–L88.
Basu, S., Antia, H.M., 2006. In: Fletcher, K., Thompson, M.J. (Eds.), Proc. SOHO 18/GONG 2006/HELAS I. In: Beyond the spherical Sun, ESA SP-624, p. 80.

Basu, S., Christensen-Dalsgaard, J., 1997. Astron. Astrophys. 322, L5–L8.
Basu, S., Thompson, M.J., 1996. Astron. Astrophys. 305, 631–642.
Basu, S., Antia, H.M., Narasimha, D., 1994. Mon. Not. Roy. Astron. Soc. 267, 209–224.
Basu, S., Christensen-Dalsgaard, J., Schou, J., Thomson, M.J., Tomczyk, S., 1996. Bull. Astron. Soc. India 24, 147–150.
Basu, S., Christensen-Dalsgaard, J., Chaplin, W.J., Elsworth, Y., Isaak, G.R., New, R., Schou, J., Thompson, M.J., Tomczyk, S., 1997. Mon. Not. Roy. Astron. Soc. 292, 243–251.
Basu, S., Däppen, W., Nayfonov, A., 1999. Astrophys. J. 518, 985–993.
Basu, S., Pinsonneault, M.H., Bahcall, J.N., 2000. Astrophys. J. 529, 1084–1100.
Basu, S., Chaplin, W.J., Elsworth, Y., New, R., Serenelli, A.M., Verner, G.A., 2007. Astrophys. J. 655, 660–671.
Berthomieu, G., Provost, J., Rocca, A., Cooper, A.J., Gough, D.O., Osaki, Y., 1980. In: Hill, H.A., Dziembowski, W. (Eds.), In: Nonradial and Nonlinear Stellar Pulsation, LNP 125. Springer-Verlag, Berlin, pp. 307–312.
Biermann, L., 1951. Z. Astrophys. 28, 304–309.
Bochsler, P., 2007a. Astron. Astrophys. Rev. 14, 1–40.
Bochsler, P., 2007b. Astron. Astrophys. 471, 315–319.
Bochsler, P., Auchère, F., Skoug, R.M., 2006. In: Lacoste, H., Ouwehand, L. (Eds.), Proc. SOHO 17, 10 Years of SOHO and Beyond. In: ESA SP-617, p. 28.
Böhm-Vitense, E., 1958. Z. Astrophys. 46, 108–143.
Boothroyd, A.I., Sackmann, I.-J., 2003. Astrophys. J. 583, 1004–1023.
Borrero, J.M., 2007. Astrophys. J., in press (arXiv:0709.3809).
Botnen, A. 1997. Master's Thesis, Inst. Theor. Astrophys. Oslo.
Botnen, A., Carlsson, M., 1999. In: Miyama, S.M., Tomisaka, K., Hanawa, T. (Eds.), Proc. Int. Conf. on Numerical Astrophysics. In: Astrophysics and Space Science Library, vol. 240. Kluwer Academic, Boston, pp. 379–382.
Bowen, I.S., 1935. Astrophys. J. 81, 1–16.
Brown, H., 1949. Rev. Modern Phys. 21, 625–634.
Brown, T.M., Christensen-Dalsgaard, J., 1998. Astrophys. J. 500, L195–L198.
Brun, A.S., Turck-Chièze, S., Morel, P., 1998. Astrophys. J. 506, 913–925.
Brun, A.S., Turck-Chièze, S., Zahn, J.-P., 1999. Astrophys. J. 525, 1032–1041.
Brun, A.S., Antia, H.M., Chitre, S.M., Zahn, J.-P., 2002. Astron. Astrophys. 391, 725–739.
Buchler, J.R., Szabó, R., 2007. Astrophys. J. 660, 723–731.
Caffau, E., Steffen, M., Sbordone, L., Ludwig, H.-G., Bonifacio, P., 2007. Astron. Astrophys. 473, L9–L12.
Cameron, A.G.W., 1982. In: Barnes, C.A., Clayton, D.D., Schramm, D.N. (Eds.), Essays in Nuclear Astrophysics. Cambridge University Press, Cambridge, pp. 23–43.
Canuto, V.M., Mazzitelli, I., 1991. Astrophys. J. 370, 295–311.
Carlsson, M., 1986. Uppsala Astronomical Observatory Report, No. 33.
Castellani, V., Degl'Innocenti, S., Fiorentini, G., Lissia, M., Ricci, B., 1997. Phys. Rep. 281, 309–398.
Castro, M., Vauclair, S., Richard, O., 2007. Astron. Astrophys. 463, 755–758.
Chaboyer, B., Deliyannis, C.P., Demarque, P., Pinsonneault, M.H., Sarajedini, A., 1992a. Astrophys. J. 388, 372–382.
Chaboyer, B., Sarajedini, A., Demarque, P., 1992b. Astrophys. J. 394, 515–522.
Chandrasekhar, S., 1964. Astrophys. J. 139, 664–674.
Chaplin, W.J., Elsworth, Y., Isaak, G.R., McLeod, C.P., Miller, B.A., New, R., 1997. Astrophys. J. 480, L75–L78.
Chaplin, W.J., Elsworth, Y., Miller, B.A., Verner, G.A., New, R., 2007a. Astrophys. J. 659, 1749–1760.
Chaplin, W.J., Serenelli, A.M., Basu, S., Elsworth, Y., New, R., Verner, G.A., 2007b. Astrophys. J. 670, 872–884.
Christensen-Dalsgaard, J., 1992. Astrophys. J. 385, 354–362.
Christensen-Dalsgaard, J., 2002. Rev. Modern Phys. 74, 1073–1129.
Christensen-Dalsgaard, J., Berthomieu, G., 1991. In: Cox, A.N., Livingston, W.C., Matthews, M. (Eds.), Solar Interior and Atmosphere. In: Space Science Series, University of Arizona Press, pp. 401–478.
Christensen-Dalsgaard, J., Däppen, W., 1992. Astron. Astrophys. Rev. 4, 267–361.
Christensen-Dalsgaard, J., Gough, D.O., 1980. Nature 288, 544–547.
Christensen-Dalsgaard, J, Pérez Hernández, F., 1991. In: Gough, D.O., Toomre, J. (Eds.), In: Challenges to Theories of the Structure of Moderate Mass Stars, LNP 388. Heidelberg, Springer, pp. 43–50.
Christensen-Dalsgaard, J., Duvall Jr., T.L., Gough, D.O., Harvey, J.W., Rhodes Jr., E.J., 1985. Nature 315, 378–382.
Christensen-Dalsgaard, J., Thompson, M.J., Gough, D.O., 1989. Mon. Not. Roy. Astron. Soc. 238, 481–502.
Christensen-Dalsgaard, J., Gough, D.O., Thompson, M.J., 1991. Astrophys. J. 378, 413–437.
Christensen-Dalsgaard, J., Proffitt, C.R., Thompson, M.J., 1993. Astrophys. J. 403, L75–L78.
Christensen-Dalsgaard, J., et al., 1996. Science 272, 1286–1292.
Christensen-Dalsgaard, J., Di Mauro, M.P., Schlattl, H., Weiss, A., 2005. Mon. Not. Roy. Astron. Soc. 356, 587–595.
Claverie, A., Isaak, G.R., McLeod, C.P., van der Raay, H.B., Cortes, T.R., 1979. Nature 282, 591–594.
Cohen, E.R., Taylor, B.N., 1987. Rev. Modern Phys. 59, 1121–1148.
Conrath, B.J., Gautier, D., 2000. Icarus 144, 124–134.
Conrath, B.J., Gautier, D., Hanel, R.A., Honstein, J.S., 1984. Astrophys. J. 282, 807–815.
Conrath, B.J., Hanel, R.A., Gautier, D., Marten, A., Lindal, G., 1987. J. Geophys. Res. 92, 15003–15010.
Couvidat, S., Turck-Chièze, S., Kosovichev, A.G., 2003. Astrophys. J. 599, 1434–1448.

Cox, A.N. (Ed.), 2000. Allen's Astrophysical Quantities. 4th ed., AIP Press, New York.
Cox, A.N., Tabor, J.E., 1976. Astrophys. J. Suppl. Ser. 31, 271–312.
Cox, A.N., Guzik, J.A., Kidman, R.B., 1989. Astrophys. J. 342, 1187–1206.
Cox, J.P., 1980. Theory of Stellar Pulsation. Princeton University Press, Princeton.
Craig, I.J.D., Brown, J.C., 1986. Inverse Problems in Astronomy: A Guide to Inversion Strategies for Remotely Sensed Data. Adam Hilger, Bristol.
Cunha, K., Lambert, D.L., 1992. Astrophys. J. 399, 586–598.
Cunha, K., Hubeny, I., Lanz, T., 2006. Astrophys. J. 647, L143–L146.
Däppen, W., Gough, D.O., 1986. Seismology of the Sun and The Distant Stars. In: Proc. NATO Advanced Research Workshop, D. Reidel, Dordrecht, pp. 275–280.
Däppen, W., Gilliland, R.L., Christensen-Dalsgaard, J., 1986. Nature 321, 229–231.
Däppen, W., Anderson, L., Mihalas, D., 1987. Astrophys. J. 319, 195–206.
Däppen, W., Mihalas, D., Hummer, D.G., Mihalas, B.W., 1988a. Astrophys. J. 332, 261–270.
Däppen, W., Gough, D.O., Thompson, M.J., 1988b. Seismology of the Sun and Sun-like stars, ESA SP 286, pp. 505–510.
Däppen, W., Gough, D.O., Kosovichev, A.G., Thompson, M.J., 1991. In: Gough, D.O., Toomre, J. (Eds.), Challenges to Theories of The Structure of Moderate-Mass Stars. In: Lecture Notes in Physics, vol. 388. Springer, Heidelberg, pp. 111–120.
Degl'Innocenti, S., Fiorentini, G., Ricci, B., 1998. Phys. Lett. B 416, 365–368.
Degl'Innocenti, S., Prada Moroni, P.G., Ricci, B., 2006. Astrophys. Space Sci. 305, 67–72.
Delahaye, F., Pinsonneault, M.H., 2006. Astrophys. J. 649, 529–540.
Demarque, P., Guenther, D.B., 1988. In: Christensen-Dalsgaard, J., Frandsen, S. (Eds.), Proc. IAU Symp. 123. In: Advances in helio- and Asteroseismology, pp. 91–94.
Deubner, F.-L., 1975. Astron. Astrophys. 44, 371–375.
Di Mauro, M.P., Christensen-Dalsgaard, J., Rabello-Soares, M.C., Basu, S., 2002. Astron. Astrophys. 384, 666–677.
Drake, J.J., Testa, P., 2005. Nature 436, 525–528.
Drake, J.J., Ercolano, B., 2007. Astrophys. J. 665, L175–L178.
Durney, B.R., Hill, F., Goode, P.R., 1988. Astrophys. J. 326, 486–489.
Duvall Jr., T.L., Harvey, J.W., 1983. Nature 302, 24–27.
Duvall Jr., T.L., Harvey, J.W., Pomerantz, M.A., 1986. Nature 321, 500–501.
Dziembowski, W.A., Goode, P.R., 1991. Astrophys. J. 376, 782–786.
Dziembowski, W.A., Goode, P.R., 1992. Astrophys. J. 394, 670–687.
Dziembowski, W.A., Pamyatnykh, A.A., Sienkiewicz, R., 1990. Mon. Not. Roy. Astron. Soc. 244, 542–550.
Dziembowski, W.A., Pamyatnykh, A.A., Sienkiewicz, R., 1991. Mon. Not. Roy. Astron. Soc. 249, 602–605.
Eddington, A.S., 1926. The Internal Constitution of the Stars. Cambridge University Press, Cambridge.
Edvardsson, B., Andersen, J., Gustafsson, B., Lambert, D.L., Nissen, P.E., Tomkin, J., 1993. Astron. Astrophys. 275, 101–152.
Eggleton, P.P., Faulkner, J., Flannery, B.P., 1973. Astron. Astrophys. 23, 325–330.
Elliott, J.R., 1996. Mon. Not. Roy. Astron. Soc. 280, 1244–1256.
Elliott, J.R., Kosovichev, A.G., 1998. Astrophys. J. 500, L199–L202.
Elsworth, Y., Howe, R., Isaak, G.R., McLeod, C.P., New, R., 1990. Nature 347, 536–539.
Elsworth, Y., Howe, R., Isaak, G.R., McLeod, C.P., New, R., 1991. Mon. Not. Roy. Astron. Soc. 251, 7P–9P.
Evans, J.W., Michard, R., 1962. Astrophys. J. 136, 493–506.
Faulkner, J., Gough, D.O., Vahia, M.N., 1986. Nature 321, 226–229.
Feldman, U., Widing, K.G., 2003. Space Sci. Rev. 107, 665–720.
Feldman, U., Landi, E., Laming, J.M., 2005. Astrophys. J. 619, 1142–1152.
Ferguson, J.W., Alexander, D.R., Allard, F., Barman, T., Bodmarik, J.G., Hauscildt, P.H., Heffner-Wong, A., Tamanai, A., 2005. Astrophys. J. 623, 585–596.
Formicola, A., et al., 2004. Phys. Lett. B 591, 61–68.
Frazier, E.N., 1968. Z. Astrophys. 68, 345–356.
Freytag, B., Steffen, M., Dorch, B., 2002. Astron. Nacht. 323, 213–219.
Fröhlich, C., Lean, J., 1998. Geophys. Res. Lett. 25, 4377–4380.
Gabriel, A.H., et al., 1995a. Solar Phys. 162, 61–99.
Gabriel, A.H., Culhane, J.L., Patchett, B.E., Breeveld, E.R., Lang, J., Parkinson, J.H., Payne, J., Norman, K., 1995b. Adv. Space Res. 15 (7), 63–67.
Garz, T., Kock, M., 1969. Astron. Astrophys. 2, 274–279.
Garz, T., Holweger, H., Kock, M., Richter, J., 1969. Astron. Astrophys. 2, 446–450.
Gautier, D., Conrath, B., Flasar, M., Hanel, R., Kunde, V., Chedin, A., Scott, N., 1981. J. Geophys. Res. 86, 8713–8720.
Gelly, B., Lazrek, M., Grec, G., Ayad, A., Schmider, F.X., Renaud, C., Salabert, D., Fossat, E., 2002. Astron. Astrophys. 394, 285–297.
Giraud-Heraud, Y., Kaplan, J., de Volnay, F.M., Tao, C., Turck-Chièze, S., 1990. Solar Phys. 128, 21–33.
Goldberg, L., Muller, E.A., Aller, L.H., 1960. Astrophys. J. Suppl. Ser. 5, 1–137.
Goldreich, P., Keeley, D.A., 1977. Astrophys. J. 212, 243–251.
Goldreich, P., Norman, M., Kumar, P., 1994. Astrophys. J. 424, 466–479.
Goldschmidt, V.M., 1937. In: Skrifter utgit av det Norske Videnskaps-Akademi I Oslo, vol. 4. I. Math-Naturv, Klasse, 1–148.
Gong, Z., Däppen, W., Zejda, L., 2001. Astrophys. J. 546, 1178–1182.
Gough, D.O., 1984. Mem. Soc. Astron. Ital. 55, 13–35.
Gough, D.O., 1986. Seismology of the Sun and the Distant Stars. D. Reidel, Dordrecht, 125–140.

Gough, D.O., 1990. In: Osaki, Y., Shibahashi, H. (Eds.), Progress of Seismology of the Sun and Stars. In: Lecture Notes in Physics, vol. 367. Springer, Berlin, pp. 281–318.
Gough, D.O., 1993. In: Zahn, J.-P., Zinn-Justin, J. (Eds.), Astrophysical Fluid Dynamics, Les Houches Session XLVII. Elsevier, Amsterdam, pp. 399–560.
Gough, D.O., Kosovichev, A.G., 1988. Seismology of the Sun and Sun-Like Stars, ESA, pp. 195–201.
Gough, D.O., Kosovichev, A.G., 1990. In: Berthomieu, G., Cribier, M. (Eds.), Inside the Sun. In: IAU Colloquium, vol. 121. Kluwer, Dordrecht, pp. 327–340.
Gough, D.O., Thompson, M.J., 1990. Mon. Not. Roy. Astron. Soc. 242, 25–55.
Gough, D.O., Thompson, M.J., 1991. In: Cox, A.N., Livingston, W.C., Matthews, M. (Eds.), Solar Interior & Atmosphere. In: Space Science Series, University of Arizona Press, pp. 519–561.
Gough, D.O., et al., 1996. Science 272, 1296–1300.
Gray, D.F., 2005. The Observation and Analysis of Stellar Photospheres. 3rd ed., Cambridge University Press, Cambridge.
Grevesse, N., 1984a. In: Pallavacini, R. (Ed.), Frontiers of Astronomy and Astrophysics. Italian Astronomical Society, Florence, pp. 71–82.
Grevesse, N., 1984b. Phys. Scripta T8, 49–58.
Grevesse, N., Noels, A., 1993. In: Prantzos, N., Vangioni-Flam, E., Cassè, M. (Eds.), Origin and Evolution of the Elements. Cambridge Univ. Press, pp. 14–25.
Grevesse, N., Sauval, A.J., 1998. Space Sci. Rev. 85, 161–174. GS98.
Grevesse, N., Sauval, A.J., 1999. Astron. Astrophys. 347, 348–354.
Grevesse, N., Asplund, M., Sauval, A.J., 2007. Space Sci. Rev. 130, 105–114.
Guenther, D.B., Demarque, P., 1997. Astrophys. J. 484, 937–959.
Guenther, D.B., Demarque, P., Kim, Y.-C., Pinsonneault, M.H., 1992. Astrophys. J. 387, 372–393.
Gustafsson, B., 1998. Space Sci. Rev. 85, 419–428.
Gustafsson, B., Bell, R.A., Eriksson, K., Nordlund, Å., 1975. Astron. Astrophys. 42, 407–432.
Guzik, J.A., 2006. In: Fletcher, K., Thompson, M.J. (Eds.), Proc. SOHO 18/GONG 2006/HELAS I. In: Beyond the spherical Sun, ESA SP-624, p. 17.
Guzik, J.A., Cox, A.N., 1991. Astrophys. J. 381, 333–340.
Guzik, J.A., Cox, A.N., 1992. Astrophys. J. 386, 729–733.
Guzik, J.A., Swenson, F.J., 1997. Astrophys. J. 491, 967–979.
Guzik, J.A., Watson, L.S., Cox, A.N., 2005. Astrophys. J. 627, 1049–1056.
Hansen, C.J., Kawaler, S.D., Trimble, V., 2004. Stellar Interiors: Physical Principles, Structure, and Evolution. Springer-Verlag, New York.
Hansen, P.C., 1992. Inv. Prob. 8, 849–872.
Hata, N., Bludman, S., Langacker, P., 1994. Phys. Rev. D 49, 3622–3625.
Haxton, W.C., 1995. Ann. Rev. Astron. Astrophys. 33, 459–504.
Heasley, J., Milkey, R.W., 1978. Astrophys. J. 221, 677–688.
Heeger, K.M., Robertson, R.G.H., 1996. Phys. Rev. Lett. 77, 3720–3723.
Hill, F., et al., 1996. Science 272, 1292–1295.
Hirayama, T., 1979. In: Jensen, E., Maltby, P., Orrall, F.Q. (Eds.), Physics of Solar Prominences. In: IAU Colloq, vol. 44. pp. 4–32.
Holweger, H., Müller, E.A., 1974. Sol. Phys. 39, 19–30.
Huang, R.Q., Wu, K.N., 1998. Stellar Astrophysics. Springer-Verlag, Singapore.
Hummer, D.G., Mihalas, D., 1988. Astrophys. J. 331, 794–814.
Iglesias, C.A., Rogers, F.J., 1996. Astrophys. J. 464, 943–953.
Ignace, R., Cassinelli, J.P., Tracy, G., Churchwell, E.B., Lamers, H.J.G.L.M., 2007. Astrophys. J. 669, 600–605.
Johansson, S., Litzén, U., Lundberg, H., Zhang, Z., 2003. Astrophys. J. 584, L107–L110.
Johnson, J.A., 2002. Astrophys. J. Suppl. Ser. 139, 219–247.
Kippenhahn, R., Weigert, A., 1990. Stellar Structure and Evolution. Springer-Verlag, Berlin.
Kiselman, D., Nordlund, Å., 1995. Astron. Astrophys. 302, 578–586.
Koesterke, L., Allende Prieto, C., Lambert, D.L., 2007. In: van Belle, G. (Ed.), Proc. 14th Cambridge Workshop on Cool Stars, Stellar Systems, and the Sun. poster CD-ROM.
Koesterke, L., Allende Prieto, C., Lambert, D.L., 2008. Astrophys. J. (submitted for publication).
Korzennik, S.G., Ulrich, R.K., 1989. Astrophys. J. 339, 1144–1155.
Kosovichev, A.G., 1996. Bull. Astron. Soc. India 24, 355–358.
Kosovichev, A.G., Fedorova, A.V., 1991. Sov. Astron. 35, 507–514.
Kosovichev, A.G., Christensen-Dalsgaard, J., Däppen, W., Dziembowski, W.A., Gough, D.O., Thompson, M.J., 1992. Mon. Not. Roy. Astron. Soc. 259, 536–558.
Kosovichev, A.G., et al., 1997. Solar Phys. 170, 43–61.
Kuhn, J.R., Bush, R.I., Scheick, X., Scherrer, P., 1998. Nature 392, 155–157.
Kumar, P., Talon, S., Zahn, J.-P., 1999. Astrophys. J. 520, 859–870.
Kupka, F., Piskunov, N., Ryabchikova, T.A., Stempels, H.C., Weiss, W.W., 1999. Astron. Astrophys. Suppl. Ser. 138, 119–133.
Kurucz, R.L., 1970. Smithsonian Astrophysical Observatory Special Report No. 308, pp. 1–291.
Kurucz, R.L., 1991. In: Crivellari, L., Hubeny, I., Hummer, D.G. (Eds.), Stellar Atmospheres: Beyond Classical Models. In: NATO ASI Series, Kluwer, Dordrecht, p. 441.

Kurucz, R.L., 1995. In: Sauval, A.J., Blomme, R., Grevesse, N. (Eds.), Laboratory and Astronomical High Resolution Spectra. In: ASP Conf. Ser., vol. 81. pp. 17–31.
Kurucz, R.L., 2005a. Mem. Soc. Astron. Italy Supp. 8, 14–24.
Kurucz, R.L., 2005b. Mem. Soc. Astron. Italy Supp. 8, 73–75.
Kurucz, R.L., Furenlid, I., Brault, J., Testerman L., 1984. Solar flux atlas from 296 to 1300 nm, National Solar Observatory, Sunspot, New Mexico.
Landi, E., Feldman, U., Doschek, G.A., 2007. Astrophys. J. 659, 743–749.
Lanz, T., Cunha, K., Holtzman, J., Hubeny, I., 2007. arXiv:0709.2147.
Lefebvre, S., Kosovichev, A.G., Rozelot, J.P., 2007. Astrophys. J. 658, L135–L138.
Leibacher, J.W., Stein, R.F., 1971. Astrophys. Lett. 7, 191–192.
Leighton, R.B., Noyes, R.W., Simon, G.W., 1962. Astrophys. J. 135, 474–499.
Li, L.H., Ventura, P., Basu, S., Sofia, S., Demarque, P., 2006. Astrophys. J. Suppl. Ser. 164, 215–254.
Libbrecht, K.G., Woodard, M.F., Kaufman, J.M., 1990. Astrophys. J. Suppl. Ser. 74, 1129–1149.
Liefke, C., Schmitt, J.H.M.M., 2006. Astron. Astrophys. 458, L1–L4.
Lin, C.-H., Antia, H.M., Basu, S., 2007. Astrophys. J. 668, 603–610.
Lodders, K., 2003. Astrophys. J. 591, 1220–1247.
Lodders, K., 2007. arXiv:0710.4523.
Lopes, I.P., Bertone, G., Silk, J., 2002. Mon. Not. Roy. Astron. Soc. 337, 1179–1184.
Lubow, S.H., Rhodes Jr., E.J., Ulrich, R.K., 1980. In: Hill, H.A., Dziembowski, W. (Eds.), Nonradial and Nonlinear Stellar Pulsation. In: Lecture Notes in Physics, vol. 125. Springer-Verlag, Berlin, pp. 300–306.
Ludwig, H.-G., Steffen, M., 2007. In: Pasquini, L. Romaniello, M., Santos, N.C., Correia, A. (Eds.), Precision Spectroscopy in Astrophysics. arXiv: 0704.1176.
Maggio, A., Flaccomio, E., Favata, F., Micela, G., Sciortino, S., Feigelson, E.D., Getman, K.V., 2007. Astrophys. J. 660, 1462–1479.
Maltby, P., Avrett, E.H., Carlsson, M., Kjeldseth-Moe, O., Kurucz, R.L., Loeser, R., 1986. Astrophys. J. 306, 284–303.
Meléndez, J., 2004. Astrophys. J. 615, 1042–1047.
Mendoza, C., et al., 2007. Mon. Not. Roy. Astron. Soc. 378, 1031–1035.
Michaud, G., Fontaine, G., Charland, Y., 1984. Astrophys. J. 280, 247–254.
Miglio, A., Montalbán, J., Dupret, M.-A., 2007a. Mon. Not. Roy. Astron. Soc. 375, L21–L25.
Miglio, A., Montalbán, J., Dupret, M.-A., 2007b. Commun. Asteroseismology 151, pp. 48–56. arXiv:0706.3632.
Mihalas, D., Däppen, W., Hummer, D.G., 1988. Astrophys. J. 331, 815–825.
Mitler, H.E., 1977. Astrophys. J. 212, 513–532.
Meyer, J.-P., 1989. Cosmic abundances of matter. AIP Conf. Proc. 183, 245–303.
Montalbán, J., D'Antona, F., 2006. Mon. Not. Roy. Astron. Soc. 370, 1823–1828.
Montalbán, J., Miglio, A., Noels, A., Grevesse, N., di Mauro, M.P., 2004. In: Danesy, D. (Ed.), Proc. SOHO 14/GONG 2004 Helio- and Asteroseismology: Towards a Golden Future. In: ESA SP-559, pp. 574–576.
Montalbán, J., Miglio, A., Theado, S., Noels, A., Grevesse, N., 2006. Commun. Asteroseismology 147, 80–84.
Monteiro, M.J.P.F.G., Christensen-Dalsgaard, J., Thompson, M.J., 1994. Astron. Astrophys. 283, 247–262.
Morel, P., Provost, J., Berthomieu, G., 1997. Astron. Astrophys. 327, 349–360.
Neuforge-Verheecke, C., Guzik, J.A., Keady, J.J., Magee, N.H., Bradley, P.A., Noels, A., 2001a. Astrophys. J. 561, 450–454.
Neuforge-Verheecke, C., Goriely, S., Guzik, J.A., Swenson, F.J., Bradley, P.A., 2001b. Astrophys. J. 550, 493–502.
Nordlund, Å., 1982. Astron. Astrophys. 107, 1–10.
Nordlund, Å, Stein, R.F., 1990. Comput. Phys. Commun. 59, 119–125.
Otí Floranes, H., Christensen-Dalsgaard, J., Thompson, M.J., 2005. Mon. Not. Roy. Astron. Soc. 356, 671–679.
Palme, H., Beer, H., 1993. In: Voigt, H.H. (Ed.), In: Landolt-Börnstein, Group VI: Astronomy and Astrophysics: Instruments, Methods, Solar System, vol. 3a. Springer, Berlin, pp. 196–221.
Palme, H., Jones, A., 2005. In: Davis, A.M., Holland, H.D., Turekian, K.K. (Eds.), In: Meteorites, Comets and Planets: Treatise on Geochemistry, Vol. 1. Elsevier B. V., Amsterdam, pp. 41–61.
Pamyatnykh, A.A., Ziomek, W., 2007. In: Handler, G., Houdek, G. (Eds.), Proc. Vienna workshop in the Future of Asteroseismology. In: Communications in Asteroseismology, 150, pp. 207–208. arXiv:astro-ph/0703714.
Peimbert, M., Luridiana, V., Peimbert, A., Carigi, L., 2007. In: From Stars to Galaxies: Building the pieces to build up the Universe. arXiv:astro-ph/ 0701313.
Pérez Hernández, F., Christensen-Dalsgaard, J., 1994. Mon. Not. Roy. Astron. Soc. 269, 475–492.
Piersanti, L., Straniero, O., Cristallo, S., 2007. Astron. Astrophys. 462, 1051–1062.
Pijpers, F.P., 1997. Astron. Astrophys. 326, 1235–1240.
Pijpers, F.P., Thompson, M.J., 1992. Astron. Astrophys. 262, L33–L36.
Pijpers, F.P., Thompson, M.J., 1994. Astron. Astrophys. 281, 231–240.
Pottasch, S.R., Bernard-Salas, J., 2006. Astron. Astrophys. 457, 189–196.
Prandtl, L., 1925. Z. Agnew. Math. Mech. 5, 136.
Press, W.H., 1981. Astrophys. J. 245, 286–303.
Press, W.H., Rybicki, G.B., 1981. Astrophys. J. 248, 751–766.
Proffitt, C.R., Michaud, G., 1991. Astrophys. J. 380, 238–250.
Proffitt, C.R., Vandenberg, D.A., 1991. Astrophys. J. Suppl. Ser. 77, 473–514.
Rabello-Soares, M.C., Basu, S., Christensen-Dalsgaard, J., 1999. Mon. Not. Roy. Astron. Soc. 309, 35–47.

Reames, D.V., 1994. Adv. Space Res. 14 (4), 177–180.
Reames, D.V., 1998. Space Sci. Rev. 85, 327–340.
Reames, D.V., 1999. Space Sci. Rev. 90, 413–491.
Reetz, J., 1999. Astrophys. Space Sci. 265, 171–174.
Rentzsch-Holm, I., 1996. Astron. Astrophys. 305, 275–283.
Rhodes Jr., E.J., Ulrich, R.K., Simon, G.W., 1977. Astrophys. J. 218, 901–919.
Richard, O., Vauclair, S., Charbonnel, C., Dziembowski, W.A., 1996. Astron. Astrophys. 312, 1000–1011.
Richard, O., Dziembowski, W.A., Sienkiewicz, R., Goode, P.R., 1998. Astron. Astrophys. 338, 756–760.
Ritzwoller, M.H., Lavely, E.M., 1991. Astrophys. J. 369, 557–566.
Robinson, F.J., Demarque, P., Li, L.H., Sofia, S., Kim, Y.-C., Chan, K.L., Guenther, D.B., 2003. Mon. Not. Roy. Astron. Soc. 340, 923–936.
Rogers, F.J., Iglesias, C.A., 1992. Astrophys. J. Suppl. Ser. 79, 507–568.
Rogers, F.J., Nayfonov, A., 2002. Astrophys. J. 576, 1064–1074.
Rogers, F.J., Swenson, F.J., Iglesias, C.A., 1996. Astrophys. J. 456, 902–908.
Roxburgh, I.W., 2005. Astron. Astrophys. 434, 665–669.
Roxburgh, I.W., Vorontsov, S.V., 1994. Mon. Not. Roy. Astron. Soc. 268, 880–888.
Roxburgh, I.W., Vorontsov, S.V., 2003. Astron. Astrophys. 411, 215–220.
Runkle, R.C., Champagne, A.E., Angulo, C., Fox, C., Iliadis, C., Longland, R., Pollanen, J., 2005. Phys. Rev. Lett. 94, 082503.
Russell, H.N., 1929. Astrophys. J. 70, 11–82.
Saio, H., 1992. Mon. Not. Roy. Astron. Soc. 258, 491–496.
Salaris, M., Cassisi, S., 2005. Evolution of Stars and Stellar Populations. John Wiley and Sons, Chichester.
Salpeter, E.E., 1954. Australian J. Phys. 7, 373–388.
Santos, N.C., Israelian, G., Mayor, M., 2003. In: Brown, A., Harper, G.M., Ayres, T.R. (Eds.) Proc. The Future of Cool-Star Astrophysics: 12th Cambridge Workshop on Cool Stars, Stellar Systems, and the Sun, University of Colorado, pp. 148–157.
Santos, N.C., Israelian, G., Mayor, M., Bento, J.P., Almeida, P.C., Sousa, S.G., Ecuvillon, A., 2005. Astron. Astrophys. 437, 1127–1133.
Sbordone, L., Bonifacio, P., Castelli, F., Kurucz, R.L., 2004. Mem. Soc. Astron. Italy Supp. 5, 93–96.
Scherrer, P.H., et al., 1995. Solar Phys. 162, 129–188.
Schlattl, H., Bonanno, A., Paternò, L., 1999. Phys. Rev. D 60, 113002.
Schmelz, J.T., Nasraoui, K., Roames, J.K., Lippner, L.A., Garst, J.W., 2005. Astrophys. J. 634, L197–L200.
Schou, J., Christensen-Dalsgaard, J., Thompson, M.J., 1994. Astrophys. J. 433, 389–416.
Schou, J., Kosovichev, A.G., Goode, P.R., Dziembowski, W.A., 1997. Astrophys. J. 489, L197–L200.
Schou, J., Christensen-Dalsgaard, J., Howe, R., Larsen, R.M., Thompson, M.J., Toomre, J., 1998a. In: Structure and Dynamics of the Interior of the Sun and Sun-like Stars SOHO 6/GONG 98 Workshop, ESA SP-418, pp. 845–849.
Schou, J., et al., 1998b. Astrophys. J. 505, 390–417.
Schwarzschild, M., 1946. Astrophys. J. 104, 203–207.
Scott, P.C., Asplund, M., Grevesse, N., Sauval, A.J., 2006. Astron. Astrophys. 456, 675–688.
Seaton, M.J., Badnell, N.R., 2004. Mon. Not. Roy. Astron. Soc. 354, 457–465.
Sestito, P., Degl'Innocenti, S., Prada Moroni, P.G., Randich, S., 2006. Astron. Astrophys. 454, 311–319.
Shibahashi, H., 1993. In: Suzuki, Y, Nakamura, K. (Eds.), Frontiers of Neutrino Astrophysics. Universal Academy Press, Tokyo, p. 93.
Shibahashi, H., Takata, M., 1996. Publ. Astron. Soc. Japan 48, 377–387.
Socas-Navarro, H., Norton, A.A., 2007. Astrophys. J. 660, L153–L156.
Socas-Navarro, H., Trujillo, B.J., Ruiz Cobo, B., 2000. Astrophys. J. 530, 977–993.
Spergel, D.N., et al., 2007. Astrophys. J. Suppl. Ser. 170, 377–408.
Spiegel, E.A., Zahn, J.-P., 1992. Astron. Astrophys. 265, 106–114.
Stanghellini, L., Guerrero, M.A., Cunha, K., Manchado, A., Villaver, E., 2006. Astrophys. J. 651, 898–905.
Stein, R.F., Nordlund, Å., 1989. Astrophys. J. 342, L95–L98.
Stein, R.F., Nordlund, Å., 1998. Astrophys. J. 499, 914–933.
Stone, E.C., 1989. Cosmic abundances of matter. AIPC 183, 72–90.
Stringfellow, G.S., Bodenheimer, P., Noerdlinger, P.D., Arigo, R.J., 1983. Astrophys. J. 264, 228–236.
Strömgren, B., 1938. Astrophys. J. 87, 520–534.
Suess, H.E., Urey, H.C., 1956. Rev. Modern Phys. 28, 53–74.
Takata, M., Shibahashi, H., 1998. Astrophys. J. 504, 1035–1050.
Takata, M., Shibahashi, H., 2001. In: Brekke, P., Fleck, B., Gurman, J.B. (Eds.), Proc. IAU Symp. 203, Recent Insights into the Physics of the Sun and Heliosphere: Highlights from SOHO and Other Space Missions. pp. 43–45.
Tassoul, M., 1980. Astrophys. J. Suppl. Ser. 43, 469–490.
Thompson, M.J., et al., 1996. Science 272, 1300–1305.
Thoul, A.A., Bahcall, J.N., Loeb, A., 1994. Astrophys. J. 421, 828–842.
Trampedach, R., 2006. In: Leibacher, J., Stein, R.F., Uitenbroek, H. (Eds.), Solar MHD Theory and Observations: A High Spatial Resolution Perspective. In: ASP Conference Series, 354. pp. 103–108.
Trampedach, R., Asplund, M., 2003. In: Turcotte, S., Kellar, S.C., Cavallo, R.M. (Eds.), 3D Stellar Evolution. In: ASP Conference Series, vol. 293. pp. 209–213.
Trampedach, R., Däppen, W., Baturin, V.A., 2006. Astrophys. J. 646, 560–578.
Tripathy, S.C., Christensen-Dalsgaard, J., 1998. Astron. Astrophys. 337, 579–590.
Turck-Chièze, S., Däppen, W., Fossat, E., Provost, J., Schatzman, E., Vignaud, D., 1993. Phys. Rep. 230, 57–235.

Turck-Chièze, S., Couvidat, S., Piau, L., Ferguson, J., Lambert, P., Ballot, J., García, R.A., Nghiem, P., 2004. Phys. Rev. Lett. 93, 211102.
Ulrich, R.K., 1970. Astrophys. J. 162, 993–1002.
Ulrich, R.K., 1982. Astrophys. J. 258, 404–413.
Ulrich, R.K., Rhodes Jr., E.J., 1977. Astrophys. J. 218, 521–529.
Unno, W., Osaki, Y., Ando, H., Saio, H., Shibahashi, H., 1989. Nonradial Oscillations of Stars. 2nd ed., Tokyo University Press, Tokyo.
Unsöld, A., 1948. Z. Astrophys. 24, 306–329.
VandenBerg, D.A., Gustafsson, B., Edvardsson, B., Eriksson, K., Ferguson, J., 2007. Astrophys. J. 666, L105–L108.
Vauclair, S., 1998. Space Sci. Rev. 84, 265–271.
Vauclair, S., Vauclair, G., 1982. Ann. Rev. Astron. Astrophys. 20, 37–60.
Vernazza, J.E., Avrett, E.H., Loeser, R., 1973. Astrophys. J. 184, 605–632.
Vitense, E., 1953. Z. Astrophys. 32, 135–164.
von Steiger, R., Schweingruber, R.F.W., Geiss, J., Gloeckler, G., 1995. Adv. Space Res. 15 (7), 3–12.
von Zahn, U., Hunten, D.M., 1996. Science 272, 849–851.
Vorontsov, S.V., Baturin, V.A., Pamyatnykh, A.A., 1992. Mon. Not. Roy. Astron. Soc. 257, 32–46.
Wang, W., Liu, X.-W., 2007. Mon. Not. Roy. Astron. Soc. 381, 669–701.
Watanabe, S., Shibahashi, H., 2001. Publ. Astron. Soc. Japan 53, 565–575.
Wedemeyer, S., Freytag, B., Steffen, M., Ludwig, H.-G., Holweger, H., 2004. Astron. Astrophys. 414, 1121–1137.
Weiss, A., Schlattl, H., 1998. Astron. Astrophys. 332, 215–223.
Weiss, A., Keady, J.J., Magee Jr., N.H., 1990. Atomic Data and Nuclear Data Tables 45, 209–238.
Weiss, A., Hillebrandt, W., Thomas, H.-C., Ritter, H., 2004. Cox & Guili's Principles of Stellar Structure: Extended. 2nd ed., Cambridge Scientific Publishers, Cambridge.
Widing, K.G., 1997. Astrophys. J. 480, 400–405.
Wolff, C.L., 1972. Astrophys. J. 177, L87–L91.
Xiong, D.R., Chen, Q, L., 1992. Astron. Astrophys. 254, 362–370.
Yang, W.M., Bi, S.L., 2007. Astrophys. J. 658, L67–L70.
Young, P.R., 2005. Astron. Astrophys. 444, L45–L48.
Young, P.A., Arnett, D., 2005. Astrophys. J. 618, 908–918.
Young, P.A., Mamajek, E., Arnett, D., Liebert, J., 2001. Astrophys. J. 556, 230–244.
Zaatri, A., Provost, J., Berthomieu, G., Morel, P., Corbard, T., 2007. Astron. Astrophys. 469, 1145–1149.